Rapid Detection of the Severe Acute Respiratory Syndrome (SARS) Coronavirus by a Loop-Mediated Isothermal Amplification Assay, *Leo L.M. Poon,[1*] Cynthia S.W. Leung,[1] Masato Tashiro,[2] Kwok Hung Chan,[3] Bonnie W.Y. Wong,[1] Kwok Yung Yuen,[1] Yi Guan,[1] and Joseph S.M. Peiris[1]* ([1] Department of Microbiology, Queen Mary Hospital, University of Hong Kong, Hong Kong SAR; [2] Department of Viral Diseases and Vaccine Control, National Institute of Infectious Diseases, Musashi-Murayama, Tokyo, Japan; [3] Department of Microbiology, Queen Mary Hospital, Hong Kong SAR; * address correspondence to this author at: Department of Microbiology, University of Hong Kong, Queen Mary Hospital, Pokfulam, Hong Kong SAR; fax 852-2855-1241, e-mail llmpoon@hkucc.hku.hk)

Severe acute respiratory syndrome (SARS) is a newly emerging disease that first emerged in Guangdong Province, China in November 2002 *(1)*. The SARS coronavirus (SARS-CoV) was found to be the etiology of the disease *(2–4)*. Subsequent surveillance studies have indicated that this virus is of animal origin and have suggested that the source of the disease is still circulating in this geographic region *(5)*. Indeed, the potential risk of reemergence of SARS is further highlighted by a recent confirmed SARS case in January 2004 *(6)*. Therefore, the establishment of a rapid SARS diagnostic method is a high priority for control of the disease.

Currently, there are two major diagnostic approaches for SARS. Detection of antibodies against SARS-CoV is a sensitive and specific diagnostic approach, but serconversion can be detected only around day 10 of illness *(7)*. In contrast, PCR-based tests have been shown to be useful for early SARS diagnosis *(8)*. Quantitative PCR approaches are a powerful tool for identifying SARS-CoV early after disease onset *(4, 9–11)*. However, because of the requirements for sophisticated instrumentation and expensive reagents, these rapid molecular tests might not be the method of choice in basic clinical settings in developing countries or in field situations. It is therefore critical to develop simple and economical molecular tests for the above scenarios.

The invention of loop-mediated isothermal amplification (LAMP) has opened up a new horizon for molecular diagnosis *(12)*. This method depends on autocycling strand displacement DNA synthesis performed by a *Bst* DNA polymerase, and a detailed amplification mechanism has been described elsewhere *(12)*. The reaction relies on recognition of the DNA target by six independent sequences, making this kind of assay highly specific. This method is rapid and has a DNA amplification efficiency equivalent to that of PCR-based methods *(12–14)*. More importantly, this approach is inexpensive, and all reactions can be performed in an isothermal environment. The potential clinical applications of this method have been demonstrated recently *(13)*. Here we demonstrate the feasibility of using this technology for detection of SARS-CoV.

Thirty-one retrospective SARS samples collected between March 26, 2003, and April 9, 2003, were used in this study. All SARS patients in this study were confirmed to be seropositive for SARS-CoV by immunofluorescence assays *(2)*. The age range for these patients was 16–74 years (median, 45 years), and the M:F ratio was 16:15. The study was approved by our local clinical research ethics committee. Nasopharyngeal aspirate (NPA) samples were collected on days 1–15 after disease onset as described previously *(15)*. NPA samples from patients with other respiratory diseases (adenovirus, n = 8; respiratory syncytial virus, n = 10; human metapneumovirus, n = 10; influenza A virus, n = 20; influenza B virus, n = 4; rhinovirus, n = 6) and from healthy individuals (n = 30) were used as negative controls.

RNA from clinical samples was extracted, and cDNA was synthesized as described previously *(9, 15)*. In this study, the ORF1b region of SARS-CoV (nucleotides 17741–17984; accession no. AY274119; see Fig. 1S in the Data Supplement that accompanies the online version of this Technical Brief at http://www.clinchem.org/content/vol50/issue6/) was chosen for SARS diagnosis. DNA plasmids containing the target sequences were used as positive controls. To accelerate the amplification reaction, cDNA for the SARS-CoV ORF1b sequence was amplified by a modified LAMP reaction *(14)* in the presence of six primers: F3 (5′-CTTAGGATTGCCTACG-3′); B3c (5′-AGTCCAGTTACATTTTCT-3′); FIP (5′-AGTGTGCTGTTTCAGTAGTGATTCATCACAGGGTT-3′); BIP (5′-TGTAATGTCAACCGCTTTGCGACGTGGTATTTC-3′); Loop B (5′-TCTTTATGACAAACTGCAAT-3′); and Loop Fc (5′-TTTGTGTGAATATGACATAGTCATA-3′; see Fig. 1S in the online Data Supplement). In a typical LAMP reaction, 0.5–1 μL of heat-denatured cDNA was amplified in a 12.5-μL reaction containing 0.4 mM each of the deoxynucleotide triphosphates, 1.6 μM each of FIP and BIP, 0.2 μM each of F3 and B3c, 0.8 μM each of Loop F and Loop Fc, 4 U of *Bst* DNA polymerase (New England Biolabs), and 1× *Bst* polymerase buffer (New England Biolabs). Reaction mixtures were incubated at 60 °C for 1 h, followed by heat inactivation at 80 °C for 5 min. Amplified products were analyzed by gel electrophoresis.

In preliminary experiments, reactions were performed with different copy numbers of the positive control to determine the detection limit of the assay. Because the reaction products consist of stem-loop DNA structures with multiple inverted repeats of the target and cauliflower-like structures with multiple loop-stem-loops *(12, 14)*, the reaction would produce bands of different sizes in gel electrophoresis analyses. As shown in Fig. 1, a characteristic DNA ladder was observed in positive controls (lanes 1 and 26). The detection limit of the assay was 10 copies/reaction (see Fig. 2SA in the online Data Supplement), and positive signals were consistently observed in reactions containing ≥50 copies of the target sequence (data not shown).

Among 31 SARS samples, the SARS-CoV sequence could be detected in 20 cases (64%; Fig. 1, lanes 3–14). The detection rate for SARS-CoV in these samples increased as the disease progressed (Table 1). In the early stages after disease onset, 4 of 13 (31%) were positive in the assay. For

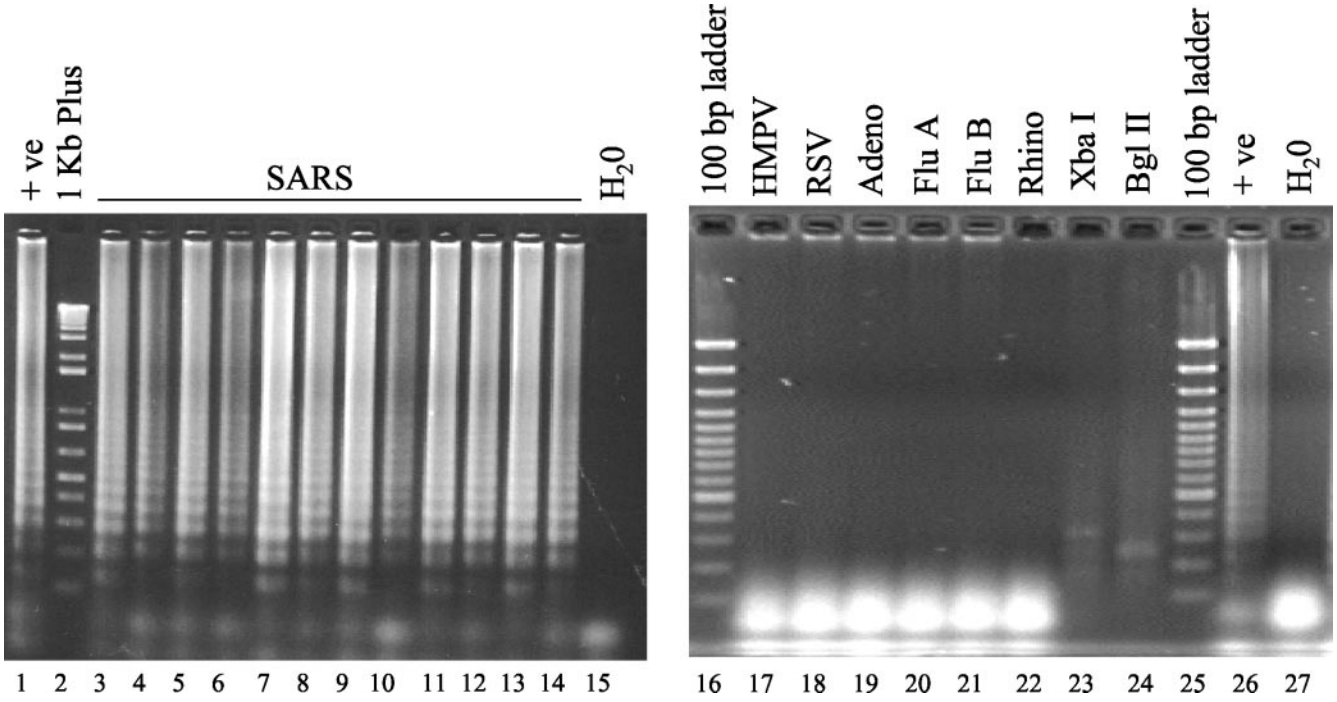

Fig. 1. LAMP assay for SARS.

Positive signals were observed in the positive control (+ *ve*; *lanes 1* and *26*) and SARS samples (*lanes 3–14*), but not in the water control (*lanes 15* and *27*) and non-SARS samples (*lanes 17–22*). *Lanes 23* and *24*, positive LAMP products digested with *Xba*I and *Bgl*II, respectively. *Lanes 2*, *16*, and *25*, DNA markers as indicated. *HMPV*, human metapneumovirus; *Adeno*, adenovirus; *RSV*, respiratory syncytial virus; *Flu A*, influenza A virus; *Flu B*, influenza B; *Rhino*, rhinovirus.

samples isolated from day 8 to day 15 after disease onset, positive signals were observed in all of the cases (n = 12). These results agreed with our previous findings that the viral load in SARS patients peaks at the second week of the disease *(7)*. Because the targeted sequence contains *Bgl*II and *Xba*I restriction sites (see Fig. 1S in the online Data Supplement), we also validated the identities of these positive signals by restriction enzyme digestion. All amplified products could be digested by these restriction enzymes as expected (Fig. 2SB in the online Data Supplement and Fig 1). By contrast, no positive signal was observed in healthy individuals (n = 30; data not shown), non-SARS patients (n = 58; Fig. 1, lanes 17–22), and water controls (Fig. 1, lanes 15 and 27).

In this study, we demonstrated the potential use of LAMP for early SARS diagnosis. Recently we also reported the use of a quantitative PCR method for SARS diagnosis *(9*, *16*, *17)*. Compared with quantitative PCR assays, the LAMP assay described in this study has two main shortcomings: (*a*) the LAMP assay does not allow quantification of SARS-CoV RNA; and (*b*) the LAMP assay is less sensitive than real-time PCR assays *(9)*. However, one should note that the detection rates for SARS in the LAMP assay (Table 1) are similar to those with our conventional PCR-based assays *(18)*. To confirm this observation, we further tested some of these clinical samples with a conventional PCR assay *(2)*. As shown in Table 1, the detection rate of the LAMP assay was similar to that of the reverse transcription-PCR assay. These results agree with previous findings that the sensitivities of LAMP assays are equivalent to those for conventional PCR-based methods *(12–14)*.

Table 1. Detection of SARS CoV by LAMP assay.

		Number positive, n (%)	
Day after onset	Sample size, n	LAMP assay	PCR[a]
1–3	13	4 (31%)	5 (38%)
4–7	6	4 (67%)	ND[b]
8–15	12	12 (100%)	12 (100%)

[a] Reverse transcription-PCR protocol adapted from Peiris et al. *(2)*.
[b] ND, not done.

Our LAMP reaction relies on recognition of viral sequences by six primers, potentially making this kind of assay more specific than conventional PCR assays. Indeed, none of the negative control samples (n = 88) was positive in our assay. Recently, Parida et al. *(19)* reported a real-time closed-tube detection method for West Nile virus in which the amounts of magnesium pyrophosphate precipitates generated in LAMP reactions are measured. This real-time approach for LAMP might further reduce the risk of cross-contamination problems.

The primary goal of this study was to develop a simple and inexpensive test for SARS diagnosis. Unlike the quantitative PCR-based detection approach, the LAMP assay does not require sophisticated instrumentation. Because reactions are performed in an isothermal environment (e.g., a water bath), there is no time loss from thermal changes during DNA amplification. The LAMP assay is rapid and does not require expensive reagents or

instruments. In a SARS outbreak, a diagnostic laboratory might routinely receive hundreds of clinical samples each day for SARS diagnosis. The application of this LAMP test might help to reduce the running cost for SARS diagnosis. From a practical point of view, highly sensitive quantitative reverse transcription-PCR assays should be used to test samples collected from patients within the first week of illness. For samples collected from patients after the first week of disease onset, the LAMP assay might be an inexpensive and accurate alternative for SARS diagnosis.

In conclusion, we report a simple LAMP assay for SARS diagnosis. We believe the inexpensive running costs of the assay make this technology very applicable to laboratories for SARS diagnosis in developing countries. The technique might have great potential to be used in field situations or at the bedside as a preliminary screening test. Regardless of the method used, testing in a suitably accredited laboratory is important, especially during an outbreak, when quality-assured diagnoses are essential. We expect that, with this rapid diagnostic method, prompt identification of this pathogen will facilitate control of the disease and provision of prompt treatment of patients.

This work was funded in part by the US National Institute of Allergy and Infectious Diseases (Public Health Research Grant A195357), the Research Grant Council of Hong Kong (HKU 7543/03M), The University of Hong Kong (HKU SARS Research Fund), and Funds for Promoting Science and Technology from the Ministry of Education, Culture, Sports, Science and Technology, Japan.

References

1. Zhong NS, Zheng BJ, Li YM, Poon LLM, Xie ZH, Chan KH, et al. Epidemiology and cause of severe acute respiratory syndrome (SARS) in Guangdong, People's Republic of China, in February, 2003. Lancet 2003;362:1353–8.
2. Peiris JSM, Lai ST, Poon LLM, Guan Y, Yam LYC, Lim W, et al. Coronavirus as a possible cause of severe acute respiratory syndrome. Lancet 2003; 361:1319–25.
3. Ksiazek TG, Erdman D, Goldsmith CS, Zaki SR, Peret T, Emery S, et al. A novel coronavirus associated with severe acute respiratory syndrome. N Engl J Med 2003;348:1953–66.
4. Drosten C, Gunther S, Preiser W, van der Werf S, Brodt HR, Becker S, et al. Identification of a novel coronavirus in patients with severe acute respiratory syndrome. N Engl J Med 2003;348:1967–76.
5. Guan Y, Zheng BJ, He YQ, Liu XL, Zhuang ZX, Cheung CL, et al. Isolation and characterization of viruses related to the SARS coronavirus from animals in southern China. Science 2003;302:276–8.
6. Cyranoski D. Swift response greets return of SARS in China. Nature 2004;427:89.
7. Peiris JSM, Chu CM, Cheng VCC, Chan KS, Hung IF, Poon LLM, et al. Clinical progression and viral load in a community outbreak of coronavirus-associated SARS pneumonia: a prospective study. Lancet 2003;361:1767–72.
8. Berger A, Drosten C, Doerr HW, Sturmer M, Preiser W. Severe acute respiratory syndrome (SARS)-paradigm of an emerging viral infection. J Clin Virol 2004;29:13–22.
9. Poon LLM, Chan KH, Wong OK, Yam WC, Yuen KY, Guan Y, et al. Early diagnosis of SARS coronavirus infection by real time RT-PCR. J Clin Virol 2003;28:233–8.
10. Ng EK, Ng PC, Hon KL, Cheng WT, Hung EC, Chan KC, et al. Serial analysis of the plasma concentration of SARS coronavirus RNA in pediatric patients with severe acute respiratory syndrome. Clin Chem 2003;49:2085–8.
11. Grant PR, Garson JA, Tedder RS, Chan PK, Tam JS, Sung JJ. Detection of SARS coronavirus in plasma by real-time RT-PCR. N Engl J Med 2003;349: 2468–9.
12. Notomi T, Okayama H, Masubuchi H, Yonekawa T, Watanabe K, Amino N, et al. Loop-mediated isothermal amplification of DNA. Nucleic Acids Res 2000;28:E63.
13. Enosawa M, Kageyama S, Sawai K, Watanabe K, Notomi T, Onoe S, et al. Use of loop-mediated isothermal amplification of the IS900 sequence for rapid detection of cultured *Mycobacterium avium* subsp. *paratuberculosis*. J Clin Microbiol 2003;41:4359–65.
14. Nagamine K, Hase T, Notomi T. Accelerated reaction by loop-mediated isothermal amplification using loop primers. Mol Cell Probes 2002;16: 223–9.
15. Poon LLM, Wong OK, Luk W, Yuen KY, Peiris JS, Guan Y. Rapid diagnosis of a coronavirus associated with severe acute respiratory syndrome (SARS). Clin Chem 2003;49:953–5.
16. Poon LLM, Chan KH, Wong OK, Cheung TK, Ng I, Zheng B, et al. Detection of SARS coronavirus in patients with severe acute respiratory syndrome by conventional and real-time quantitative reverse transcription-PCR assays. Clin Chem 2004;50:67–72.
17. Poon LLM, Wong BW, Chan KH, Leung CS, Yuen KY, Guan Y, et al. A one step quantitative RT-PCR for detection of SARS coronavirus with an internal control for PCR inhibitors. J Clin Virol (published online Feb 3, 2004; DOI accession number: doi:10.1016/j.jcv.2003.12.007; available at: http://dx.doi.org).
18. Chan KH, Poon LLM, Cheng VCC, Guan Y, Hung IFN, Kong J, et al. Detection of SARS coronavirus in patients with suspected SARS. Emerg Infect Dis 2004 (published online December 24, 2003; available at: http://www.cdc.gov/ncidod/EID/vol10no2/03-0610.htm).
19. Parida M, Posadas G, Inoue S, Hasebe F, Morita K. Real-time reverse transcription loop-mediated isothermal amplification for rapid detection of West Nile virus. J Clin Microbiol 2004;42:257–63.

DOI: 10.1373/clinchem.2004.032011

On-Site Quantification of Human Urinary Albumin by a Fluorescence Immunoassay, *Sunga Choi,*[1] *Eui Yul Choi,*[1,2] *Ha Suck Kim,*[3] *and Sang Wook Oh*[1*] ([1] Central Research Institute of BodiTech Inc., Chuncheon, South Korea; [2] Department of Genetic Engineering, Hallym University, Chuncheon, South Korea; [3] Department of Chemistry, Seoul National University, Seoul, South Korea; * address correspondence to this author at: Central Research Institute of BodiTech Inc., Chuncheon 200-160, South Korea; fax 82-33-258-6889, e-mail sangwoh@empal.com or sangwoh@boditech.co.kr)

Microalbuminuria (MAU), defined as a urinary albumin excretion of 30–300 mg/day, indicates a high probability of renal damage and is an accepted predictor for the early diagnosis of nephropathy in diabetic patients *(1, 2)*. In addition, MAU has diagnostic implications in pregnancy as a predictive marker of preeclampsia *(3, 4)* and may play a role in identifying high risk of developing complications from cardiovascular diseases even in nondiabetic patients *(5–7)*.

Dye-binding assays can measure serum albumin but are too insensitive for MAU testing, making immunochemical assays the most widely used MAU methods *(8)*. These immunoassays include immunoturbidimetry, immunofluorescence, ELISA, RIA, and zone immunoelectrophoresis. Recently, Kessler and coworkers *(9, 10)* introduced a laser-induced fluorescence system coupled to an automated centrifugal analyzer as a nonimmunologic assay for urinary albumin. Their system was based on the probe Albumin Blue 670/580, which becomes highly fluorescent on binding to albumin.

We report a fluorescence immunochromatography as-

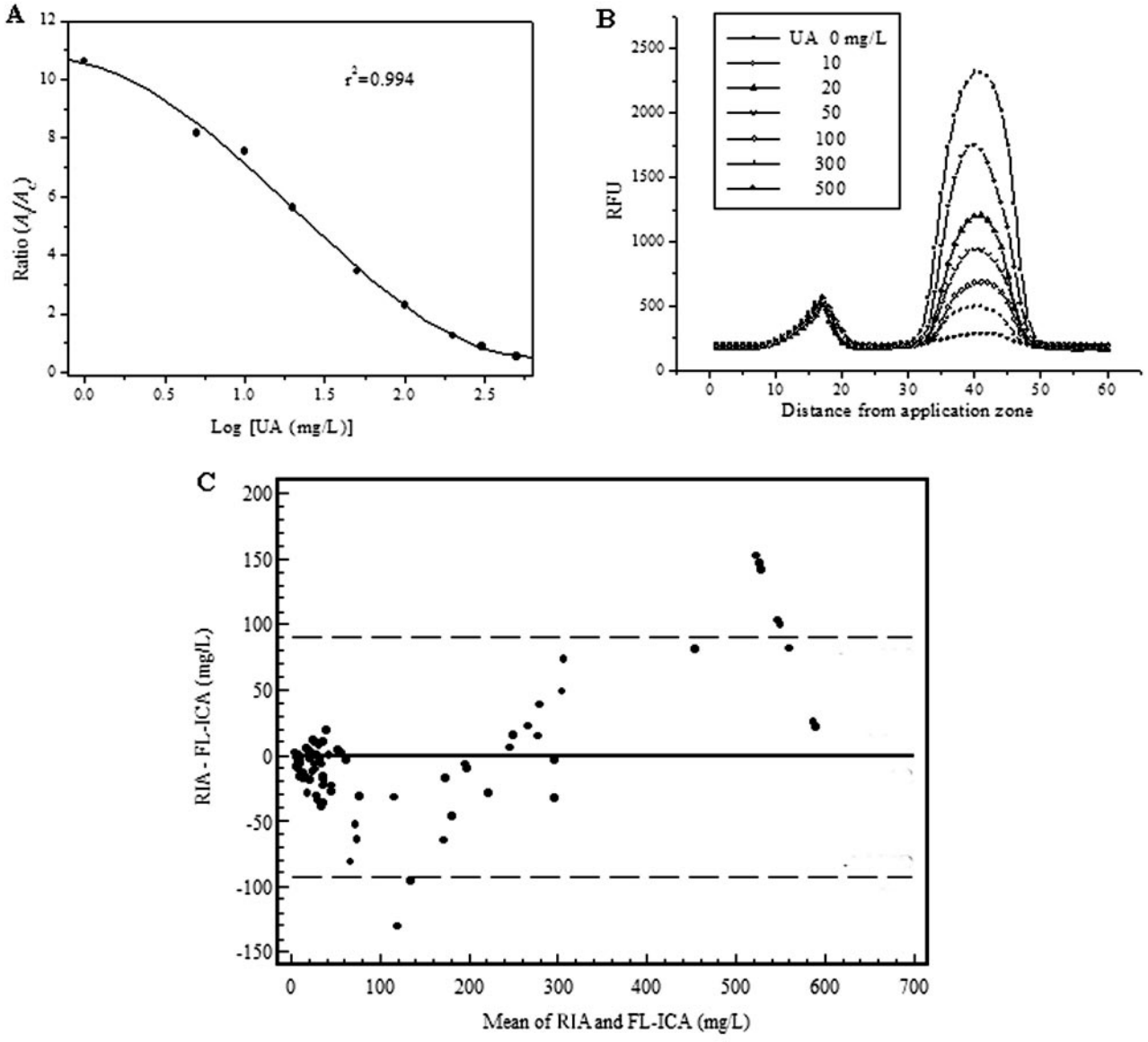

Fig. 1. Calibration curve for the ICA (*A*), scanning intensity profile for the competitive fluorescence ICA system (*B*), and Bland–Altman difference plot for urinary albumin results obtained with the ICA and a RIA (*C*).

(*A*), the area ratio (A_T/A_C) converted from RFU was plotted against the albumin concentration. The correlation between the area ratio and the albumin concentration is shown ($r^2 = 0.994$). The value for each point on the albumin calibration curve represents the mean value of eight independent experiments. (*B*), the first and second peaks indicated the RFUs for the control and the test line, respectively, depending on the albumin concentrations in the samples. (*C*), Bland–Altman difference plot comparing urinary albumin concentrations obtained with the fluorescence (*FL*) ICA system vs the RIA (Cobra 5010 II). The *solid line* represents the mean difference in measured urinary albumin concentration between the methods, and the *dashed lines* are ±1.96 SD. *UA*, urinary albumin.

say (ICA) for quantitative determination of albumin in urine. The assay system consists of an ICA test strip in a disposable cartridge, a fluorescently labeled detector, and a laser fluorescence reader. Basically, the assay system adopts the inherent simplicity of a lateral-flow ICA and uses a competitive immunoassay mode with a simple, one-step operation *(11)*. Briefly, fluorescently labeled albumin in the detector buffer competes with albumin in the sample for binding to an anti-albumin antibody immobilized on the test strip matrix. The more albumin is in the sample, the less the fluorescently labeled albumin reacts with the anti-albumin antibody and, thus, the lower the accumulation of fluorescence in the test line of a test strip.

We generated a monoclonal antibody against human albumin (Sigma A8763) as an immunogen and conducted immunizations, cell fusion, and screening of hybridoma cells according to a standard method *(12)*. Monoclonal antibody 22C5 was selected among the positive clones and used as the capture antibody (3 g/L) on the test line of a test strip for this study *(13)*. A control line was coated with anti-rabbit IgG (1 g/L; Sigma R4880) on nitrocellulose membrane by a BioJet dispenser (BioDot). We labeled the albumin competitor and rabbit IgG control with

activated Alexa Fluor 647 (Molecular Probes) in sodium bicarbonate buffer (pH 8.3) and made detector buffer by mixing two fluorescent conjugates in 0.1 mmol/L phosphate buffer (pH 6.0). The system components and the principle for the one-dimensional fluorescence reader for scanning of fluorescence intensity have been described in detail elsewhere *(14)*.

We tested the fluorescence ICA system at albumin concentrations of 0–600 mg/L. We mixed 10 μL of detector (2 μg of fluorescent competitor and 80 ng of fluorescent rabbit IgG control), 10 μL of 1 mol/L potassium phosphate buffer (pH 6.0), and 80 μL of urine sample in the test aliquot and loaded the mixture in the cartridge well. After the sample was allowed to react for 10 min, the cartridge was inserted in the laser fluorescence reader for scanning of fluorescence intensity.

Intensity profiles, in relative fluorescence units (RFUs), for the different albumin concentrations in the samples are shown in Fig. 1B. The first and second peaks represent the RFUs for the control line and the test line, respectively. Whereas the RFUs on the control lines were constant, the signals on the test lines changed dramatically depending on the albumin concentrations in the samples.

A commercially available multicalibrator set (Kamiya Biomedical) and a pure human albumin were used to construct a calibration curve. The albumin stock solution (1000 mg/L) was diluted with calibrator diluent to final concentrations of 5, 10, 20, 50, 100, 200, 300, 500, and 600 mg/L. The calibrator diluent contained, per liter, 2.7 g of KH_2PO_4, 0.9 g of K_2HPO_4, 4.5 g of NaCl, and 0.5 g of EDTA (pH 6.0) and was used as control material for all assays *(9)*. The RFUs recorded on the test and control lines at a given albumin concentration were converted into an area value (test, A_T, control, A_C) by a fitting algorithm. The calibration curve was obtained from the area ratios (A_T/A_C) and the albumin concentrations in the samples ($r^2 = 0.994$; Fig. 1A).

We next compared the fluorescence ICA system with a RIA (EURO Diagnostic Products Co.). The RIA was performed on a Cobra 5010 II analyzer (Quantum). Urine samples were collected from 81 patients who visited Hallym University Medical Center (Chuncheon, Korea). The results were compared by use of Medcalc, Ver. 6.12, software (Medcalc Inc.). A Bland–Altman difference plot analysis showed a mean (SD) difference of −1.2 (46.5) mg/L and little disagreement between the two assays at the mean urinary albumin concentration (Fig. 1C). However, the agreement between the two assays was lower in samples with concentrations >300 mg/L. The Passing–Bablok regression analysis yielded a slope of 1.06 (95% confidence interval, 0.988–1.153) and a *y*-intercept of −9.63 mg/L (95% confidence interval, −16.7 to −6.4 mg/L), indicating statistically good agreement between the two methods ($P < 0.05$).

We conducted precision studies to evaluate the analytical performance of the fluorescence ICA system with urine reference materials. We prepared four diluted control samples covering the albumin concentration range usually encountered in clinical practice (Table 1). The intra- and interassay CV for the new immunoassay system were, respectively, 7.2% and 7.7% at 15 mg/L, 4.5% and 7.1% at 92.3 mg/L, 5.2% and 3.6% at 180 mg/L, and 5.4% and 3.2% at 342 mg/L. The analytical precision was also calculated with 10 replicates in one analytical run from the same controls. The measured albumin values of 15, 92.3, 180, 342 mg/L were 100.1%, 108.5%, 112.8%, and 97.6%, respectively, of the expected values, with a mean measured value that was 105% of the expected. To confirm the reliability of the immunoassay, we also analyzed the parallelism in a series of twofold serial dilutions of the 600 mg/L albumin calibrator. The results obtained were compared with the expected results by linear regression and showed a slope (SD) of 1.026 (0.03) with correlation coefficient of 0.997 (see Fig. 1 in the Data Supplement that accompanies the online version of this Technical Brief at http://www.clinchem.org/content/vol50/issue6/).

We tested assay interference by adding to urine pools (20 mg/L albumin) urea (1 mol/L), creatinine (10 g/L), and human hemoglobin (10 mg/L). The concentrations added to the urine pools were well above the maximum concentrations encountered in clinical samples. The overall mean albumin concentration of 50 samples tested was 21.4 mg/L (CV = 7.2%). Because the albumin concentrations were all within 2 SD of the reference value, we considered that none of tested materials affected the assay. The limit of detection (3 SD above the value for the zero calibrator; n = 10) and limit of quantification (lowest concentration measured with a CV <10%) of the fluorescence ICA system were 1.6 and 4.65 mg/L, respectively. The developed assay system was sensitive to the pH of urine specimens and operated best at pH 6.0. Because the pH range of the collected urine specimens fell within the range typical of urine (pH 4.5–8.0), 1 mol/L potassium

Table 1. Imprecision and measured concentrations obtained in the fluorescence ICA system.

Urine albumin concentration, mg/L	Intraassay (n = 20)			Interassay (n = 10)[a]			Measured concentration as percentage of the expected (n = 10)
	Mean, mg/L	SD, mg/L	CV, %	Mean, mg/L	SD, mg/L	CV, %	
15	15.23	1.09	7.2	13.50	1.04	7.7	100.1%
92.3	89.75	4.05	4.5	94.21	6.66	7.1	108.5%
180	175.68	9.20	5.2	180.42	6.50	3.6	112.8%
342	327.46	17.75	5.4	324.16	10.33	3.2	97.6%

[a] Interassay studied was conducted on 10 sequential days, with 10 runs/day and with 10 replicate cartridges at each albumin concentration.

phosphate buffer (pH 6.0) was integrated into the assay component.

Fully automated immunoassay formats are available for quantification of urinary albumin in large numbers of samples. However, most of these methods are impractical or expensive. The criteria for point-of-care testing include affordable cost, a disposable device, and minimum maintenance/technical expertise required to perform tests *(15)*. The sample should be applied directly to the device, which should require only a small sample volume, and the assays should have a rapid turnaround time with good accuracy. There are some point-of-care devices for determination of MAU in urine, such as the ImmunoDip (Diagnostic Chemicals Limited) and Micral Urine Test Strip (Roche Diagnostics). Despite their many advantages, one drawback of these commercial test devices is that they give only negative, threshold, or positive results without displaying quantitative values for urinary albumin. Given the different principles of the assays compared, the results obtained with the fluorescence ICA agree well with the results obtained with the independent RIA. Considering the detection limit, imprecision, linearity, and working range, the fluorescent ICA is comparable to other, well-known immunoassays and appears to be suitable for determination of urinary albumin.

This study was supported by the Nano-Core Technology Development Program (M1-0213-05-0003) and the National Research Laboratory Program (M1-0104-00-0164) of the Korean Ministry of Science and Technology.

References

1. Rowe DJF, Dawnay A, Watts GF. Microalbuminuria in diabetes mellitus: review and recommendations for the measurement of albumin in urine. Ann Clin Biochem 1990;27:297–312.
2. Doumas BT, Peters T. Serum and urine albumin: a progress report on their measurement and clinical significance. Clin Chim Acta 1997;258:3–20.
3. Mogensen CE. Microalbuminuria, a marker for organ damage. London: Science Press, 1993:32–45.
4. Waugh J, Kilby M, Lambert P, Bell SC, Blackwell CN, Shennan A, et al. Validation of the DCA 2000 microalbumin:creatinine ratio urinanalyzer for its use in pregnancy and preeclampsia. Hypertens Pregnancy 2003;22:77–92.
5. Mogensen CE, Christensen CK. Predicting diabetic nephropathy in insulin dependent diabetes. New Engl J Med 1984;311:89–93.
6. Viberti GC, Hill RD, Jarrett RJ. Microalbuminuria as a predictor of clinical nephropathy in insulin dependent diabetes mellitus. Lancet 1982;I: 1430–2.
7. Mathiesesen ER, Ronn B, Jensen T, Deckert T. Relationship between blood pressure and urinary excretion in the development of microalbuminurea. Diabetes 1990;39:245–9.
8. Hill PG. The measurement of albumin in serum and plasma. Ann Clin Biochem 1985;22:565–78.
9. Kessler MA, Meinitzer A, Peter M, Wolfbeis OS. Microalbuminuria and borderline-increased albumin excretion determined with a centrifugal analyzer and the Albumin Blue 580 fluorescence assay. Clin Chem 1997;43: 996–1002.
10. Kessler MA, Hubmann MR, Dramel BA, Wolfbeis OS. Nonimmunological assay of urinary albumin based laser-induced fluorescence. Clin Chem 1992;38:2089–92.
11. Millipore Corp. A short guide: developing immunochromatographic test strips. Bedford, MA: Millipore, 1996.
12. Ha SG, Park JB, Ko KH, Choi EY. Production and characterization of isotype-specific monoclonal antibodies to bovine brain Rab GDI. Hybridoma 1999;18:371–6.
13. Choi S, Choi EY, Kim DJ, Kim JH, Kim TS, Oh SW. A rapid simple measurement of human albumin in whole blood using a fluorescence immunoassay (I). Clin Chim Acta 2004;339:147–56.
14. Kim BC, Jeong JH, Jeong DS, Choi EY, Kim JH, Nahm KB. Simplified laser fluorescence scanner for proteomics studies and early cancer diagnosis. SPIE Proc 2002;4916:103–8.
15. Brooks DE, Devine DV, Harris PC, Harris JE, Miller ME, Olal AD, et al. RAMP(TM): A rapid, quantitative whole blood immunochromatographic platform for point-of-care testing. Clin Chem 1999;45:1676–8.

DOI: 10.1373/clinchem.2004.032813

Evaluation of Human Chorionic Gonadotropin β-Subunit mRNA Concentrations in Maternal Serum in Aneuploid Pregnancies: A Feasibility Study, *Enders K.O. Ng,[1] Ahmad El-Sheikhah,[2] Rossa W.K. Chiu,[1] K.C. Allen Chan,[1] Matthew Hogg,[2] Renu Bindra,[2] Tse N. Leung,[3] Tze K. Lau,[3] Kypros H. Nicolaides,[2] and Y.M. Dennis Lo[1*]* (Departments of [1] Chemical Pathology and [3] Obstetrics & Gynaecology, The Chinese University of Hong Kong, Prince of Wales Hospital, Hong Kong SAR; [2] Harris Birthright Research Centre for Fetal Medicine, King's College Hospital, London, United Kingdom; * address correspondence to this author at: Department of Chemical Pathology, The Chinese University of Hong Kong, Room 38023, 1/F Clinical Sciences Bldg., Prince of Wales Hospital, 30-32 Ngan Shing St., Shatin, New Territories, Hong Kong Special Administrative Region, China; e-mail loym@cuhk.edu.hk)

The recent demonstration of detectable circulating fetal RNA in maternal plasma *(1, 2)* has led to the development of new, noninvasive prenatal diagnostic opportunities *(3, 4)*. Unlike fetal DNA measurements in maternal plasma/serum, quantitative analysis of circulating fetal RNA has the advantage of being applicable to all pregnant women irrespective of fetal gender and genetic polymorphism status. In addition, the unexpected stability of circulating RNA has enhanced the practicality of this approach *(2, 5, 6)*. Previously, we developed a real-time quantitative reverse transcription-PCR (RT-PCR) assay for measuring the concentration of human chorionic gonadotropin β-subunit (*βhCG*) mRNA in plasma samples from healthy pregnant women *(2)*. We conducted a case–control study to investigate whether abnormal concentrations of *βhCG* mRNA might be detectable in the serum of mothers carrying fetuses with trisomy 21 and trisomy 18.

We sought informed consent from pregnant women who presented for aneuploidy screening at the King's College Hospital London in the United Kingdom between January and August 2003. Ethics approval was obtained from the Institutional Review Board. Among women who underwent chorionic villous sampling for fetal karyotyping as a result of clinical indications, 149 women consented to blood sampling for *βhCG* mRNA measurements. Maternal blood samples were collected into plain tubes immediately before chorionic villous sampling. The blood samples were centrifuged at 1600*g* for 10 min at 4 °C. The serum was carefully transferred into plain

polypropylene tubes, and 3.2 mL was immediately stored in 4 mL of Trizol and kept at −80 °C until RNA extraction. Serum RNA was extracted from 1.6 mL of serum with use of a modified RNeasy RNA Mini Kit (Qiagen) as described previously *(2)*. Total RNA was eluted with 30 μL of RNase-free water and stored at −80 °C until real-time quantitative RT-PCR analysis. DNase treatment was carried out to remove any contaminating DNA (RNase-Free DNase Set; Qiagen).

One-step real-time quantitative RT-PCR was used for *βhCG* mRNA quantification, as described previously, without knowledge of the karyotyping results *(2)*. The RT-PCR reactions were set up in a reaction volume of 25 μL. The primers and fluorescent probe were used at concentrations of 300 and 100 nM, respectively, and 6 μL of extracted serum RNA was used for amplification. The thermal profile used for the analysis was as follows: the reaction was initiated at 50 °C for 2 min for the included uracil *N*-glycosylase to act, followed by reverse transcription at 60 °C for 30 min. After a 5-min denaturation at 95 °C, 40 cycles of PCR was carried out with denaturation at 94 °C for 20 s and annealing/extension at 57 °C for 1 min. The sensitivity, linearity, and precision of the assay have been established as described previously *(2)*. We were able to detect down to 100 copies of the synthetic oligonucleotide in the reaction mixture. Concentrations of serum *βhCG* mRNA are expressed as copies/mL of serum. Because no recovery experiments had been done, the reported concentrations (copies/mL) are minimum estimates.

Among the 149 pregnant women recruited, trisomy 21 and trisomy 18 were confirmed by fetal karyotyping in 15 and 11 pregnancies, respectively. The remaining 123 cases had euploid fetuses and served as controls. The median gestational age of the controls was 12.5 (range, 11.2–14.3) weeks, and the median gestational ages of the trisomy 21 and trisomy 18 cases were 12.5 (12.1–14.2) weeks and 12.3 (11.4–14.1) weeks, respectively. No significant difference of the gestational age was observed among the three cohorts (Kruskal–Wallis, $P = 0.706$).

Maternal serum samples from the 149 studied cases were subjected to *βhCG* mRNA quantification. *βhCG* mRNA could be detected in the maternal serum of 140 of 149 pregnancies (94%). In the control cohort, the detection rate of *βhCG* mRNA was 97% (119 of 123). For the trisomy 21 and trisomy 18 cohorts, the detection rates were 93% (14 of 15) and 64% (7 of 11), respectively. The median serum *βhCG* mRNA concentrations of the three cohorts were 6108 (interquartile range, 2867–19 249) copies/mL for the control cohort, 13 165 (4403–25 265) copies/mL for the trisomy 21 cohort, and 652 (0–11 662) copies/mL for the trisomy 18 cohort (Fig. 1). The median *βhCG* mRNA concentrations differed significantly among the three cohorts (Kruskal–Wallis, $P = 0.024$). Pairwise multiple comparisons were performed and showed that differences were significant between the trisomy 18 and control cases (Dunn test, $P < 0.05$) and between the trisomy 18 and trisomy 21 cases (Dunn test, $P < 0.05$). No statistically significant difference was observed between the serum *βhCG* mRNA concentrations in trisomy 21 and control cases (Dunn test, $P > 0.05$).

In this study we confirmed that circulating *βhCG* mRNA is easily and robustly detectable in the serum of first-trimester pregnant women, with a detection rate of 94%. These data are largely concordant with our previous data on first-trimester pregnancies (median gestational age, 12.3 weeks) *(2)*. Our present data also demonstrated that the median concentration of serum *βhCG* mRNA in pregnancies with trisomy 18 was 9.4-fold lower than the median concentration in the control pregnancies and that the difference was statistically significant. On the other hand, although the median concentration of serum *βhCG* mRNA in pregnancies with trisomy 21 was 2.2-fold higher than the median concentration in the control pregnancies, the difference was not significantly different. Interestingly, similar relationships were demonstrated in several previous studies on placental tissue expression of *βhCG* mRNA. Although some inconsistent data exist in the literature *(7, 8)*, *βhCG* mRNA concentrations in placental tissues have been shown to be significantly lower in trisomy 18 than in control pregnancies *(9)*, whereas no difference has been reported for trisomy 21 pregnancies *(10)*. Thus, the *βhCG* mRNA concentration in maternal serum could potentially be a reflection of the placental tissue expression pattern as demonstrated in a study by Tsui et al. *(11)*.

The data presented here demonstrate for the first time that circulating *βhCG* mRNA concentrations in the first-trimester serum of trisomy 18 pregnancies is significantly lower than in non-trisomy 18 pregnancies. The mechanisms accounting for this difference require further investigation. Our findings indicate the potential diagnostic usefulness of circulating *βhCG* mRNA as a marker for predicting trisomy 18 pregnancies. However, our data also show that there is an overlap in the *βhCG* mRNA

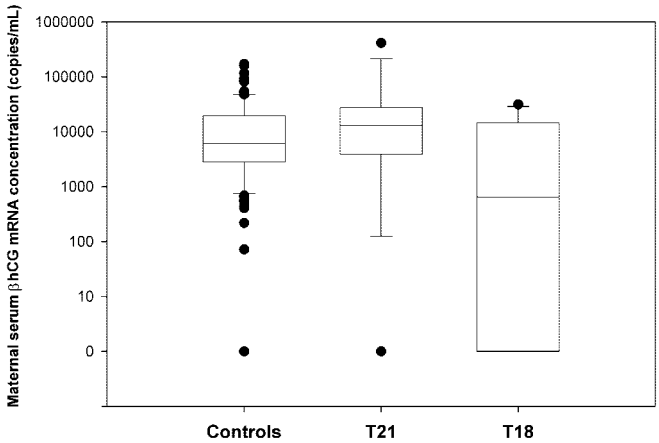

Fig. 1. Maternal serum *βhCG* mRNA concentrations in first-trimester aneuploid and control pregnancies.

Box-plots of *βhCG* mRNA concentrations (common logarithmic scale) in sera of control, trisomy 21 (*T21*), and trisomy 18 (*T18*) pregnancies. The *lines inside* the *boxes* denote the medians. The *boxes* denote the interval between the 25th and 75th percentiles. The *whiskers* denote the interval between the 10th and 90th percentiles. ● indicate data points outside the 10th and 90th percentiles.

concentrations between the trisomy 18 and control cases. This implies that a relatively low sensitivity and specificity would result if maternal serum *βhCG* mRNA measurement were used as the sole predictor for pregnancies with trisomy 18. In ROC curve analysis (using MedCalc 5.0 software), the mean (SE) area under the ROC curve was 0.734 (0.067) with a 95% confidence interval of 0.651–0.806. On the other hand, a larger scale study may be necessary to explore whether maternal serum *βhCG* mRNA is a useful marker in trisomy 21 screening.

In summary, our findings provide the first evidence for the value of circulating placental mRNA measurement in the noninvasive detection of a fetal chromosomal aneuploidy. The current study is designed primarily as a proof-of-concept investigation. The main technical advantage of the mRNA technology is the relative ease with which new mRNA markers can be developed, including genes coding for proteins for which no immunoassays are currently available. We believe that the availability of microarray technology could lead to development of panels of placenta-specific mRNA markers for future fetal aneuploidy screening.

This study was supported by the Innovation and Technology Fund (ITS/195/01).

References

1. Poon LLM, Leung TN, Lau TK, Lo YMD. Presence of fetal RNA in maternal plasma. Clin Chem 2000;46:1832–4.
2. Ng EKO, Tsui NBY, Lau TK, Leung TN, Chiu RWK, Panesar NS, et al. mRNA of placental origin is readily detectable in maternal plasma. Proc Natl Acad Sci U S A 2003;100:4748–53.
3. Ng EKO, Leung TN, Tsui NBY, Lau TK, Panesar NS, Chiu RWK, et al. The concentration of circulating corticotropin-releasing hormone mRNA in maternal plasma is increased in preeclampsia. Clin Chem 2003;49:727–31.
4. Oudejans CB, Go AT, Visser A, Mulders MA, Westerman BA, Blankenstein MA, et al. Detection of chromosome 21-encoded mRNA of placental origin in maternal plasma. Clin Chem 2003;49:1445–9.
5. Ng EKO, Tsui NBY, Lam NY, Chiu RWK, Yu SC, Wong SC, et al. Presence of filterable and nonfilterable mRNA in the plasma of cancer patients and healthy individuals. Clin Chem 2002;48:1212–7.
6. Tsui NBY, Ng EKO, Lo YMD. Stability of endogenous and added RNA in blood specimens, serum, and plasma. Clin Chem 2002;48:1647–53.
7. Eldar-Geva T, Hochberg A, deGroot N, Weinstein D. High maternal serum chorionic gonadotropin level in Downs' syndrome pregnancies is caused by elevation of both subunits messenger ribonucleic acid level in trophoblasts. J Clin Endocrinol Metab 1995;80:3528–31.
8. Massin N, Frendo JL, Guibourdenche J, Luton D, Giovangrandi Y, Muller F, et al. Defect of syncytiotrophoblast formation and human chorionic gonadotropin expression in Down's syndrome. Placenta 2001;22(Suppl A):S93–7.
9. Brizot ML, Jauniaux E, McKie AT, Farzaneh F, Nicolaides KH. Placental mRNA expression of α and β human chorionic gonadotrophin in early trisomy 18 pregnancies. Mol Hum Reprod 1996;2:463–5.
10. Brizot ML, Jauniaux E, McKie AT, Farzaneh F, Nicolaides KH. Placental expression of α and β subunits of human chorionic gonadotrophin in early pregnancies with Down's syndrome. Hum Reprod 1995;10:2506–9.
11. Tsui NBY, Chim SSC, Chiu RWK, Lau TK, Ng EKO, Leung TN, et al. Systematic microarray-based identification of placental mRNA in maternal plasma: towards non-invasive prenatal gene expression profiling. J Med Genet 2004;in press.

DOI: 10.1373/clinchem.2004.031260

Universal Sensing Strategy for the Detection of Nucleic Acid Targets by Optical Biosensor Based on Surface Plasmon Resonance, *Bi-feng Yuan, Yu-hua Hao, and Zheng Tan*[*] (Laboratory of Biochemistry and Biophysics, College of Life Sciences, Wuhan University, Wuhan 430072, People's Republic of China; * author for correspondence: fax 86-27-8788-2661, e-mail tanclswu@public.wh.hb.cn)

PCR is an important technique for identifying specific nucleic acid targets; for example, sequences associated with diseases and pathogens in clinical, environmental, and food samples. Many techniques currently used for sequence-specific detection of PCR products either require manual processing or are limited in the speed or scale of analysis. The development of biosensors in recent years has provided promising techniques for efficient sequence-specific DNA analysis *(1)*. Biosensors have been used to detect target sequences in PCR products. Most studies have been conducted with the commercially available biosensor BIAcore, which is based on surface plasmon resonance (SPR) technology. In those investigations, either sequence-specific oligonucleotide probe *(2–8)* or amplified products themselves *(8–11)* were immobilized on the sensor chip, limiting their application to one sequence or to one particular sample. Such a strategy suffers several drawbacks: (*a*) it compromises the automation and high-throughput capability of such instruments when different targets are analyzed; (*b*) chip-to-chip variation makes it difficult to compare different measurements; and (*c*) probe immobilization and chip consumption make running costs substantial.

To overcome these drawbacks, we describe here a "one-chip-for-all" strategy that is capable of, in principle, detecting different target sequences by use of the same sensor chip. Target sequences are amplified by asymmetric PCR using a primer pair in which the low-concentration primer carries a common tag sequence that is identical to that of the oligonucleotide capture probe immobilized on the sensor chip. The PCR product is then injected and captured on the sensor chip, and its sequence identity can be further verified by use of a target-specific probe (see Fig. 1 in the Data Supplement that accompanies the online version of this Technical Brief at http://www.clinchem.org/content/vol50/issue6/). We exemplify this application by analyzing three different genes: the cystic fibrosis transmembrane conductance regulator gene (*CFTR*), the mutation of which causes cystic fibrosis *(12)*; the *hTERT* gene, which encodes the catalytic component of the human telomerase complex *(13)*; and the human gene for the tumor suppressor p53 (Table 1).

Asymmetric PCRs were conducted with 100 ng of human genomic DNA from HeLa cells in a final volume of 50 μL, containing 50 mM KCl, 10 mM Tris-HCl (pH 8.8), 1 mM $MgCl_2$, 0.2 mM deoxynucleotide triphosphates, 1 μM high-concentration primer; 0.1 μM low-concentration primer, and 3 U/reaction of *Taq* polymerase (MBI). Thermal cycling was conducted on a Biometro thermal cycler with initial denaturation at 94 °C for 3 min, followed by 55 cycles of 94 °C for 30 s, 58 °C for 30 s, and

Table 1. Primers and probes used for *CFTR*, *hTERT*, and *p53* amplification and detection.

Target	Oligonucleotide	Sequence[a]
	Immobilized capture probe	5′-Biotin-C_{12}-TGCGTGGAGCCAGCGAGAGAA-3′
CFTR	High-concentration primer	5′-GCTAAGTCCTTTTGCTCACCTG-3′
	Low-concentration primer	5′-GGAGCCAGCGAGAGAATGAACACTGAAGGAGAAATCCAG-3′
	Probe, full match	5′-ATCGATGGTGTGTCTTGGGATTCAATAACTTTGCAACAGT-3′
	Probe, 1 mismatch	5′-ATCGATGGTGTGTtTTGGGATTCAATAACTTTGCAACAGT-3′
	Probe, 2 mismatches	5′-ATCGATGGTGTGTtTTGGGATTCAATcACTTTGCAACAGT-3′
	Probe, 3 mismatches	5′-ATCGATGGTtTGTCTTGGGgTTCAATAACaTTGCAACAGT-3′
hTERT	High-concentration primer	5′-CATCCTCTCAGGTTTCACGCA-3′
	Low-concentration primer	5′-GGAGCCAGCGAGAGAAATGACGCGCAGGAAAAATG-3′
	Probe, full match	5′-TGGGGTTCTTCCAAACTTGCTGATGAAATGGGAGCTGC-3′
p53	High-concentration primer	5′-CCTGTCATCTTCTGTCCCTTCC-3′
	Low-concentration primer	5′-GGAGCCAGCGAGAGAAACTTGGCTGTCCCAGAATGC-3′
	Probe, full match	5′-AAGAAGCCCAGACGGAAACCGTAGCTGCCCTGGTAGGTT-3′

[a] The underlined uppercase bases indicate the tag sequences. The underlined lowercase bases indicate mismatches.

72 °C for 30 s for *CFTR* and of 94 °C for 30 s, 60 °C for 30 s, and 72 °C for 30 s for *hTERT* and *p53*. Symmetric PCRs were conducted under the same conditions except that 0.1 μM each of both primers were used. PCR products were run in 12% polyacrylamide gels at 20 V/cm for 1 h in Tris-borate-EDTA buffer [90 mmol/L Tris-borate (pH 8.0), 2 mmol/L EDTA] and visualized by ethidium bromide staining.

Detection of PCR products by SPR was conducted at 30 °C on a BIAcore X biosensor with a streptavidin-coated SA5 sensor chip using HEPES-buffered saline containing, per liter, 10 mmol of HEPES (pH 7.4), 0.15 mol of NaCl, 3.4 mmol of EDTA, and 0.05 mL of the surfactant P20 as running buffer. The biotinylated probe was immobilized on the sensor chip surface by injection of 30 μL of probe at 6 ng/μL into one flow cell, giving a capture of ~300 response units (RU) of probe. The PCR sample was mixed with an equal volume of HEPES-buffered saline containing 1.6 mol/L NaCl, and a 20-μL aliquot of this mixture was injected at 2 μL/min followed by a flow of running buffer. In some experiments, 10 μL of 10 ng/μL sequence-specific or irrelevant oligonucleotide was subsequently injected at 2 μL/min, followed by a flow of running buffer. The sensorgram of a blank cell was simultaneously recorded as reference and subtracted from that of the sensing cell. The sensor chip was regenerated by a pulse of 5 μL of NaOH (20 mmol/L) in NaCl (1 mol/L).

Taking *CFTR* as an example, gel electrophoresis (Fig. 1A) showed that the tag sequence in the low-concentration primer was introduced into the symmetric and asymmetric PCR products based on their molecular sizes. The asymmetric PCR produced two weak bands with slower migration in addition to the double-stranded product. Evidence that these two bands were single-stranded DNA was that they were sensitive to mung-bean nuclease, which specifically digests single-stranded DNA. When the sample was incubated with the 40mer probe complementary to the *CFTR* gene before electrophoresis, these bands disappeared and a new band appeared, indicating that they were both the single-stranded form of the expected products. Similar results were obtained for *hTERT* and *p53*.

The BIAcore system monitors changes in mass of analyte at sensor chip surfaces by changes in refractive index *(14)*. The tag sequence introduced to the single-stranded PCR product is complementary to and can hybridize with the capture probe immobilized on the sensor chip. When PCR sample is injected, the hybridization between the PCR product and the probe is reflected by an increase in RU. The response is proportional to the quantity of PCR product captured *(15)*. As shown in Fig. 1B, the amplified product hybridized to the capture probe, as demonstrated by the increase in RU. Little hybridization was detected when the tag sequence was not present in the low-concentration primer or the gene was omitted or amplified by symmetric PCR (data not shown).

The sequence identity of the captured PCR product was further verified by an injection of target-specific probe complementary to the *CFTR* sequence, which led to an additional increase of 143 RU, indicating that the captured product was indeed what was expected. Because the target-specific probe had 40 and the expected PCR product had 127 bases, an increment of 143 RU corresponded to 454 (143 × 127/40) RU of expected PCR product. The captured PCR product had a response of 500 RU before injection of the target-specific probe. This means that >90% of the captured DNA was the expected PCR product of *CFTR*. Note that the captured PCR product underwent a slow dissociation from the immobilized probe. Taking this into account, we estimated that >95% of the captured DNA was the expected PCR product. When noncomplementary probes were injected, no hybridization was detected. These results indicate that the detection is specific. Similar results were obtained when we used this same sensor chip to detect the other two targets, i.e., the *hTERT* and *p53* genes (Fig. 2 in the online Data Supplement).

Because of mutations or single-nucleotide polymorphisms *(16)*, target genes may not fully match the sequence-specific probes. Probes with one to three mis-

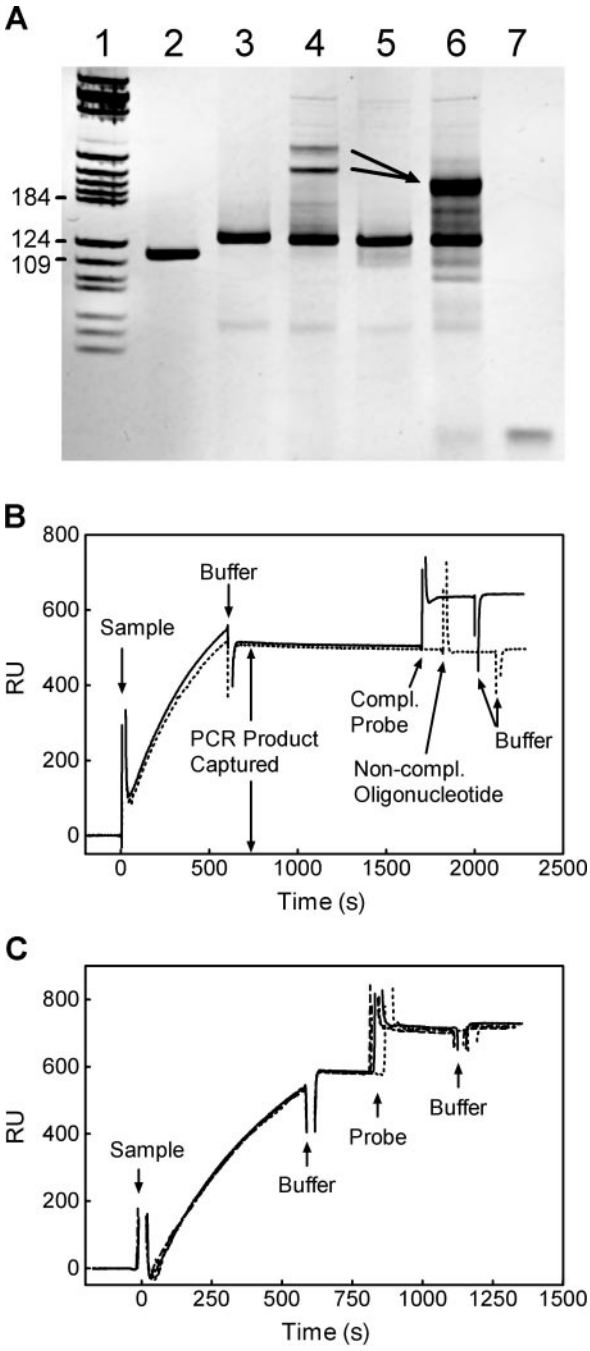

Fig. 1. Detection of PCR product of *CFTR* gene by gel electrophoresis and SPR.

(*A*), gel electrophoretic analysis of PCR product. *Lane 1*, marker (molecular weight in base pairs at *left*); *lane 2*, symmetric PCR product (111 bp) without tag sequence in primer; *lane 3*, symmetric PCR product (127 bp) with tag sequence in primer; *lane 4*, asymmetric PCR product with tag sequence in primer; *lane 5*, asymmetric PCR product with tag sequence in primer, treated with mung-bean nuclease; *lane 6*, asymmetric PCR product with tag sequence in primer, mixed with target-specific probe; *lane 7*, target-specific probe only. (*B*), detection of asymmetric PCR product by SPR using a "universal" sensing chip. Asymmetric PCR product of the *CFTR* gene was injected and captured by the immobilized probe as demonstrated by the increase in RU. After a period of running buffer flow, oligonucleotide probe complementary (*Compl.*) or noncomplementary (*Non-compl.*) to the target gene was injected followed by flow of running buffer. (*C*), effect of mismatch on the detection of PCR product. Asymmetric PCR product of *CFTR* gene was detected as in *B* except that the target-specific probe carried 0 (———), 1 (· · · ·), 2 (– – –), or 3 (· – ·) mismatched nucleotides.

matches were injected after PCR product was captured on chip surface. The results shown in Fig. 1C demonstrate that for a 40mer probe, mismatches of up to 3 bases had little effect on the hybridization. This indicates that target can be verified even when a few mismatches are present. On the other hand, this method should also be applicable to the detection of point mutations if a shorter probe (~ 10 bases) is used for the second hybridization *(11)*.

Optimization was conducted with respect to salt concentrations and temperatures (Fig. 3 in the online Data Supplement). Salt greatly enhanced the hybridization. This can be explained by the fact that both DNA and the carboxymethylated dextran coating at the sensor surface are negatively charged and salt will reduce the repulsion between them. Increasing the temperature also enhanced hybridization, although occasional increased noise signals might be produced at 35 °C. We therefore conducted our formal measurements at 30 °C in a high concentration (0.8 mol/L) of NaCl to obtain proper sensitivity and stability. For the BIAcore, background noise was within 1 RU (instrument specification). We obtained stable signals at ~600 RU for ≥50 ng and >500 RU for 10 ng of input genomic DNA (data not shown).

Flow-type biosensors such as the BIAcore biosensor are expected to be a valuable platform in diagnostics when automation and high-throughput capability are desired. Because there is no need to switch the chip for different targets or samples, the one-chip-for-all strategy described here should be especially suitable for automated, high-throughput analysis of large numbers of samples. The SPR technique avoids post-PCR processing, and the detection is highly specific, efficient, sensitive, and reproducible. The chip can be reused for hundreds of measurements in this particular case. After more than 260 measurements, the binding capacity of the chip we used decreased by <6%. Using one chip for different samples and targets should simplify operation, improve efficiency for routine analysis, and reduce the running costs associated with chip consumption and probe immobilization.

This work was supported by Grants 39925008 and 30270314 from the National Science Foundation of China and Grant G2000057001 from the Ministry of Science and Technology of China.

References

1. Rogers KR. Principles of affinity-based biosensors. Mol Biotechnol 2000; 14:109–29.
2. Sawata S, Kai E, Ikebukuro K, Iida T, Honda T, Karube I. Application of peptide nucleic acid to the direct detection of deoxyribonucleic acid amplified by polymerase chain reaction. Biosens Bioelectron 1999;14:401–8.
3. Feriotto G, Lucci M, Bianchi N, Mischiati C, Gambari R. Detection of the ΔF508 (F508del) mutation of the cystic fibrosis gene by surface plasmon resonance and biosensor technology. Hum Mutat 1999;13:390–400.
4. Kai E, Sawata S, Ikebukuro K, Iida T, Honda T, Karube I. Detection of PCR products in solution using surface plasmon resonance. Anal Chem 1999; 71:796–800.
5. Bianchi N, Rutigliano C, Tomassetti M, Feriotto G, Zorzato F, Gambari R. Biosensor technology and surface plasmon resonance for real-time detection of HIV-1 genomic sequences amplified by polymerase chain reaction. Clin Diagn Virol 1997;8:199–208.
6. Kai E, Ikebukuro K, Hoshina S, Watanabe H, Karube I. Detection of PCR

products of *Escherichia coli* O157:H7 in human stool samples using surface plasmon resonance (SPR). FEMS Immunol Med Microbiol 2000;29:283–8.
7. Asai R, Nakamura C, Ikebukuro K, Karube I, Miyake J. Detection technique of asymmetric RT-PCR-based amplified single-stranded DNA and its application to biosensor for detection of mRNA for cyanobacteria, *Anabaena variabilis*. Biotechnol Lett 2002;24:1677–82.
8. Feriotto G, Borgatti M, Mischiati C, Bianchi N, Gambari R. Biosensor technology and surface plasmon resonance for real-time detection of genetically modified Roundup Ready soybean gene sequences. J Agric Food Chem 2002;50:955–62.
9. Nilsson P, Persson B, Larsson A, Uhlen M, Nygren PA. Detection of mutations in PCR products from clinical samples by surface plasmon resonance. J Mol Recognit 1997;10:7–17.
10. Feriotto G, Corradini R, Sforza S, Bianchi N, Mischiati C, Marchelli R, et al. Peptide nucleic acids and biosensor technology for real-time detection of the cystic fibrosis W1282X mutation by surface plasmon resonance. Lab Invest 2001;81:1415–27.
11. Feriotto G, Ferlini A, Ravani A, Calzolari E, Mischiati C, Bianchi N, et al. Biosensor technology for real-time detection of the cystic fibrosis W1282X mutation in CFTR. Hum Mutat 2001;18:70–81.
12. Riordan JR, Rommens JM, Kerem B, Alon N, Rozmahel R, Grzelczak Z, et al. Identification of the cystic fibrosis gene: cloning and characterization of complementary DNA [Erratum in: Science 1989;245:1437]. Science 1989; 245:1066–73.
13. Poole JC, Andrews LG, Tollefsbol TO. Activity, function, and gene regulation of the catalytic subunit of telomerase (hTERT). Gene 2001;269:1–12.
14. Fivash M, Towler EM, Fisher RJ. BIAcore for macromolecular interaction. Curr Opin Biotechnol 1998;9:97–101.
15. Myszka DG. Kinetic analysis of macromolecular interactions using surface plasmon resonance biosensors. Curr Opin Biotechnol 1997;8:50–7.
16. Shastry BS. SNP alleles in human disease and evolution. J Hum Genet 2002;47:561–6.

DOI: 10.1373/clinchem.2003.030783

Molecular Beacons for Multiplex Detection of Four Bacterial Bioterrorism Agents, *Mandira Varma-Basil,[1†] Hiyam El-Hajj,[2] Salvatore A.E. Marras,[2] Manzour Hernando Hazbón,[1] Jessica M. Mann,[1] Nancy D. Connell,[1] Fred Russell Kramer,[2] and David Alland[1*]* ([1] Department of Medicine, Division of Infectious Disease, New Jersey Medical School, The University of Medicine and Dentistry of New Jersey, Newark, NJ; [2] Department of Molecular Genetics, The Public Health Research Institute, Newark, NJ; † current affiliation: Department of Microbiology, Vallabhbhai Patel Chest Institute, University of Delhi, Delhi, India; * address correspondence to this author at: Division of Infectious Disease, New Jersey Medical School, 185 South Orange Ave., MSB A920C, Newark, NJ 07103; fax 973-972-0713, e-mail allandda@umdnj.edu)

The advent of bioterrorism has highlighted the need for rapid, simple, and robust diagnostic assays to detect select agents. Mortality from select agents may be greatly reduced by prompt treatment *(1)*; however, treatment may be delayed if diagnostic assays are outsourced to reference laboratories. Most bacterial species that would likely be used as bioterrorism agents infect the blood stream during the course of life-threatening disease. Furthermore, even "nonseptic" syndromes may produce hematogenous bacterial DNA that could be detected by a sensitive assay *(2)*. This means that a rapid "molecular" version of a blood culture would fulfill many of the rapid diagnostic needs for biodefense.

Bacteria can be detected in blood and other sterile body sites by the identification of species-specific DNA sequences in their 16S rRNA genes. These species-specific sequences are flanked by conserved sequences, permitting most rRNA targets to be amplified by PCR using a limited set of "universal" primers *(3)*. Real-time PCR is well suited for sensitive and specific pathogen detection because it is performed in hermetically sealed wells, which greatly reduces the risk of cross-contamination, and it does not require post-PCR analysis *(4)*. Real-time PCR assays have been developed for some select agents, most of which use fluorogenic 5′-nuclease (TaqMan) probes *(5–7)*. However, TaqMan probes are difficult to use in multiplex PCR assays *(8, 9)*. In contrast, molecular beacons are real-time PCR probes that are particularly amenable to multiplexing *(10)*. They can be labeled with differently colored fluorophores *(11)*, use a common nonfluorescent quenching moiety *(9)*, and have thermodynamic properties that favor highly specific detection of nucleic acid sequences *(12)*.

Here we describe a real-time PCR assay that simultaneously detects four bacterial agents that could be used in bioterrorism. This assay is specifically designed to test sterile body fluids, where a rapid and simple assay would be beneficial. We developed a flexible assay format that can easily be adapted to the wide range of spectrofluorometric thermal cyclers that are in common use, including thermal cyclers that have only one- or two-color capabilities, and others that can detect four or more colors simultaneously.

Phenol–chloroform extraction of DNA from standard strains of *Bacillus anthracis* Vollum and Sterne, *Yersinia pestis* CO92, and *Burkholderia mallei* (ATCC 23344) was performed as described previously *(13)* in a biosafety level III laboratory certified to work with select agents (registration number 20011016-798; entity number C20031123-0125). A 180-bp amplicon for use as template in *Francisella tularensis* assays was also constructed in vitro from two overlapping oligonucleotides (Invitrogen). DNA was also extracted from clinical isolates of *Staphylococcus aureus*, *S. epidermidis*, *Streptococcus pneumoniae*, *Klebsiella pneumoniae*, *Escherichia coli*, *Enterobacter cloacae*, and *Serratia marcescens* to serve as controls.

The conservation of 16S rRNA gene sequences among bacteria enabled us to design primers FUHP (5′-GTGGACTTAGATACCCTGGTAGTCCAC-3′; underlined sequence indicates additional nucleotides added to create a hairpin structure) and RUP (5′-GCGTTGCATCGAATTAA-3′) to amplify short segments of the 16S rRNA genes of *Y. pestis*, *F. tularensis*, and *B. mallei* by PCR. The benefits of hairpin-shaped primers have been noted previously *(14–16)*. A second primer pair, FBa (5′-TGACGACAACCATGCACC-3′) and RBa (5′-ATGTGGTTTAATTCGAAGCAA-3′), was designed to amplify a segment of the 16S rRNA gene of *B. anthracis.*

We designed molecular beacons (Table 1) that bound to amplicons generated from *F. tularensis*, *B. mallei*, and *B. anthracis* and that could not bind to amplicons generated by other significant human pathogens. However, the *Y. pestis* molecular beacon also bound to amplicons gener-

Table 1. Molecular beacons used in the study.

Probe	Target	Molecular beacon sequence[a]
1	*Y. pestis*	FAM[b]-5′-CGCTGCCCCTTGAGGCGTGGCTGCAGCG-3′-D
2	*F. tularensis*	FAM/TET-5′-CGCTCGTGGAGTCGGTGTAAAGGCTCCGAGCG-3′-D
3	*B. mallei*	FAM/Texas red-5′-CGCTGCGTTGGGGATTCATTTCCTTAGTAAGCAGCG-3′-D
4	*B. anthracis*	FAM/Cy5-5′-CCGACGAGGGTTGTCAGAGGATGCGTCGG-3′-D/BHQ2

[a] Underlined sequences form the stem of each molecular beacon. If more than one fluorophore or quencher moiety is indicated, the second is used in multiplexed assays.

[b] FAM, 6-carboxyfluorescein; D, DABCYL; TET, tetrachlorofluorescein; BHQ2, Back Hole Quencher 2.

ated from *K. pneumoniae*, *E. coli*, *E. cloacae*, and *S. marcescens*, which share an identical 16S rRNA gene target sequence with *Y. pestis*. To standardize assay operating conditions, we also adjusted the probe and arm sequences of each molecular beacon so that all had similar melting temperatures in the presence of perfectly complementary targets.

We tested the ability of each molecular beacon to specifically identify its target in a single-color assay using multiple wells of a 384-well assay plate. The molecular beacons designed to detect *Y. pestis* (Table 1, probe 1), *F. tularensis* (probe 2), *B. mallei* (probe 3), and *B. anthracis* (probe 4) were labeled with the fluorophore fluorescein for these experiments. A 384-well assay plate was prepared containing a series of identical four-well assays with four different probes (200 nM) in each of the four wells. In addition, the wells contained 1× PCR buffer (Applied Biosystems); 4 mM $MgCl_2$; 250 μM each of dATP, dCTP, dGTP, and dTTP; 0.25 U of AmpliTaq Gold DNA polymerase (Applied Biosystems); 2.5 pmol each of both sets of primers; and 1 μL of template DNA in a final volume of 5 μL. Real-time PCR was performed with a 7900HT Prism spectrofluorometric thermal cycler (Applied Biosystems). The reaction mixtures were incubated

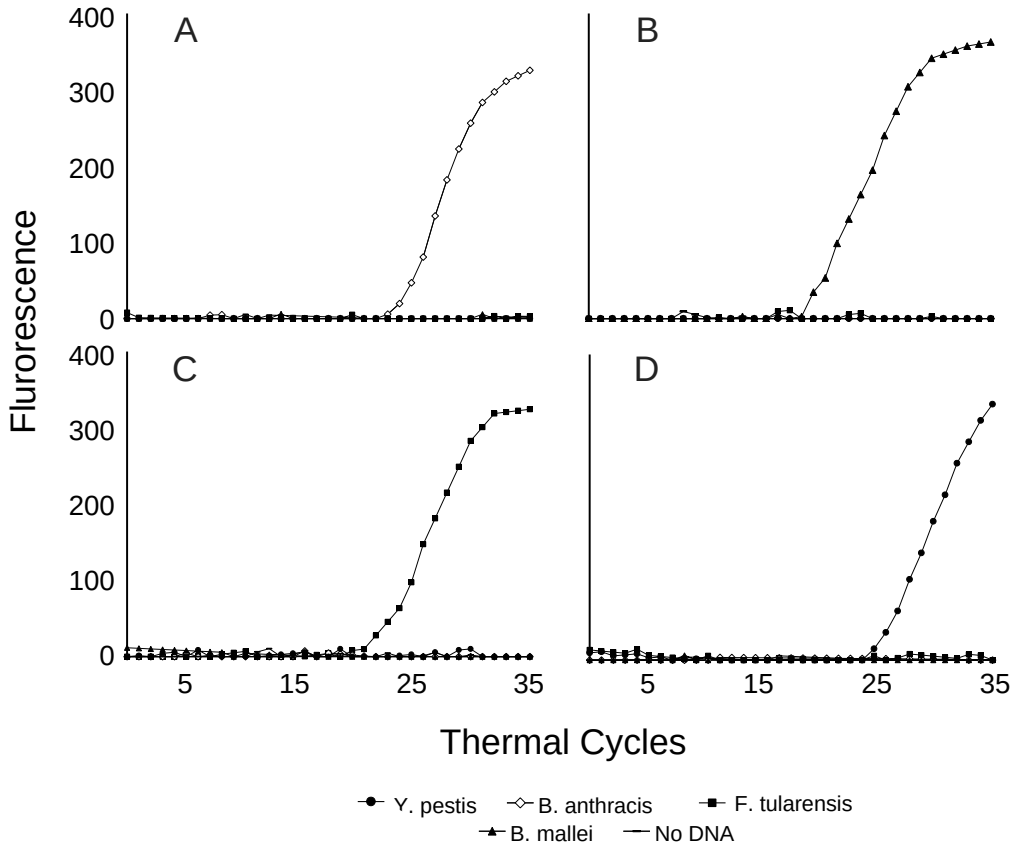

Fig. 1. Four-color multiplex assay.

Shown are the results of real-time PCRs containing DNA from different bacterial species, both primer pairs, and a mixture of four differently colored molecular beacons designed to detect all four select agents. Fluorescence signals are shown separately for the Cy5-labeled molecular beacon designed to detect *B. anthracis* (*A*), the Texas red-labeled molecular beacon designed to detect *B. mallei* (*B*), the tetrachlorofluorescein-labeled molecular beacon designed to detect *F. tularensis* (*C*), and the fluorescein-labeled molecular beacon designed to detect *Y. pestis* (*D*). These results show that in a mixture of the four molecular beacons, only the appropriate molecular beacon generates a fluorescence signal in the presence of its complementary DNA. Wells containing DNA from control organisms did not develop measurable fluorescence in any color.

for 10 min at 95 °C, followed by 40 cycles of 95 °C for 30 s, 55 °C for 60 s, and 72 °C for 30 s. Fluorescence was measured in every well or tube during each annealing step throughout the course of each reaction. The "threshold cycle" was automatically determined by the computer program controlling the spectrofluorometric thermal cycler. Significant fluorescence appeared only in the wells containing a molecular beacon complementary to the target sequence of the bacterial DNA added to that well.

We also studied whether the assay could be multiplexed into a single-color, single-well screening assay to identify the presence of a select agent in a simplified format but not to distinguish among them. All four fluorescein-labeled molecular beacons and both primer pairs were combined in a single reagent mixture. DNA from one of the select agents or control organisms was added to each well, and real-time PCR was performed. As expected, a detectable fluorescence signal developed in every well that contained DNA complementary to one of the four molecular beacons present in the well (data not shown). In both these assay formats, no fluorescence signals appeared in any well when DNA from *S. aureus*, *S. epidermidis*, *S. pneumoniae*, *B. cereus*, or a no-DNA control was added. Wells containing probe 1 fluoresced in the presence of *Y. pestis*, *K. pneumoniae*, *E. coli*, *E. cloacae*, and *S. marcescens* (all of which share the same molecular beacon target sequence).

We also estimated the lower limit of detection of the single-color multiplex assay. Triplicate DNA samples from each select agent were serially diluted in water and tested using the above protocol. We found positive PCR signals in all three replicates containing DNA extracted from the equivalent of ≥50 bacilli for *B. mallei* and ≥20 bacilli for the other bacteria.

The optimum biodefense assay should be able to both detect and distinguish among all select agents in a single assay well or tube. Each molecular beacon in the multiplex assay would have to be individually distinguishable to accomplish this goal. We met these design criteria by labeling each molecular beacon with a different fluorophore and performed the assay in a SmartCycler II (Cepheid) that could independently monitor the fluorescence generated by each fluorophore in an assay tube containing all four fluorophores. We selected each of the four fluorophores so that their emission maxima were well spaced from each other across the visible spectrum. All four molecular beacons and both primer pairs were multiplexed into a single reagent mixture to a final volume of 25 μL. DNA from one of the select agents or control organisms was added to each well, and real-time PCR was performed. A detectable fluorescence signal of the appropriate color developed in every well that contained DNA complementary to one of the four molecular beacons present in the well (Fig. 1). Each experiment was repeated at least three times to test its reproducibility.

The importance of bacterial diagnostics in sterile body fluids is supported by current medical practice in which blood cultures are performed on virtually all ill patients with fevers and a suspected bacterial source *(17)*. The ability of molecular beacons to be labeled with differently colored fluorophores, and the development of instruments that are able to detect them, raises the possibility that highly multiplexed PCR assays can be designed to serve as "molecular blood cultures", replacing current culture-based techniques. The availability of PCR screening assays would greatly advance our ability to rapidly detect a broad range of infections, including those introduced by bioterrorism. Although the *Y. pestis*-specific molecular beacon was also able to hybridize to other *Enterobacteriaceae,* we do not view this as a disadvantage. This feature expands the range of the assay, enabling the detection of other common agents that cause sepsis. Importantly, the assay did not detect pathogens from skin flora that can occasionally contaminate a blood draw (in contrast, the presence of *Enterobacteriaceae* in a sterile body site is almost always indicative of disease). Future assays can be designed to specifically detect *Y. pestis* by including a third primer pair and a molecular beacon that differentiates between *Y. pestis* and other *Enterobacteriaceae*.

This work was supported by Public Health Service Grant AI-056689 from the National Institutes of Health and by Department of Defense Grant DAMD 17-01-1-0787 from the United States Army Medical Research Materiel Command. Dr. Varma-Basil received support in the form of an overseas Associateship from the Indian Government, Department of Biotechnology. David Alland, Fred Kramer, and Salvatore Marras are among a group of co-inventors who hold patents in molecular beacons and receive income from licensing agreements.

References

1. Jernigan JA, Stephens DS, Ashford DA, Omenaca C, Topiel MS, Galbraith M, et al. Bioterrorism-related inhalational anthrax: the first 10 cases reported in the United States. Emerg Infect Dis 2001;7:933–44.
2. Kane TD, Alexander JW, Johannigman JA. The detection of microbial DNA in the blood: a sensitive method for diagnosing bacteremia and/or bacterial translocation in surgical patients. Ann Surg 1998;227:1–9.
3. Pace NR. A molecular view of microbial diversity and the biosphere. Science 1997;276:734–40.
4. El-Hajj HH, Marras SA, Tyagi S, Kramer FR, Alland D. Detection of rifampin resistance in *Mycobacterium tuberculosis* in a single tube with molecular beacons. J Clin Microbiol 2001;39:4131–7.
5. Drago L, Lombardi A, Vecchi ED, Gismondo MR. Real-time PCR assay for rapid detection of *Bacillus anthracis* spores in clinical samples. J Clin Microbiol 2002;40:4399.
6. Higgins JA, Ibrahim MS, Knauert FK, Ludwig GV, Kijek TM, Ezzell JW, et al. Sensitive and rapid identification of biological threat agents. Ann N Y Acad Sci 1999;894:130–48.
7. Oggioni MR, Meacci F, Carattoli A, Ciervo A, Orru G, Cassone A, et al. Protocol for real-time PCR identification of anthrax spores from nasal swabs after broth enrichment. J Clin Microbiol 2002;40:3956–63.
8. Marras SA, Kramer FR, Tyagi S. Efficiencies of fluorescence resonance energy transfer and contact-mediated quenching in oligonucleotide probes. Nucleic Acids Res 2002;30:e122.
9. Marras SA, Kramer FR, Tyagi S. Multiplex detection of single-nucleotide variations using molecular beacons. Genet Anal 1999;14:151–6.
10. Tyagi S, Kramer FR. Molecular beacons: probes that fluoresce upon hybridization. Nat Biotechnol 1996;14:303–8.
11. Tyagi S, Bratu DP, Kramer FR. Multicolor molecular beacons for allele discrimination. Nat Biotechnol 1998;16:49–53.
12. Bonnet G, Tyagi S, Libchaber A, Kramer FR. Thermodynamic basis of the enhanced specificity of structured DNA probes. Proc Natl Acad Sci U S A 1999;96:6171–6.
13. Maloy SR. Experimental techniques in bacterial genetics. Jones and Bartlett series in biology. Boston: Jones and Bartlett, 1990:180pp.

14. Hazbon M, Alland D. Hairpin primers for simplified single nucleotide polymorphism analysis of *Mycobacterium tuberculosis* and other organisms. J Clin Microbiol 2004;42:1236–42.
15. Nazarenko I, Lowe B, Darfler M, Ikonomi P, Schuster D, Rashtchian A. Multiplex quantitative PCR using self-quenched primers labeled with a single fluorophore. Nucleic Acids Res 2002;30:e37.
16. Fan XY, Hu ZY, Xu FH, Yan ZQ, Guo SQ, Li ZM. Rapid detection of rpoB gene mutations in rifampin-resistant *Mycobacterium tuberculosis* isolates in Shanghai by using the amplification refractory mutation system. J Clin Microbiol 2003;41:993–7.
17. Muller-Serieys C, Bergogne-Berezin E. [Blood culture update]. Presse Med 2002;31:27–32.

DOI: 10.1373/clinchem.2003.030767

Ischemia-Modified Albumin during Skeletal Muscle Ischemia, *Edgar Zapico-Muñiz,[1] Miquel Santaló-Bel,[2] Javier Mercé-Muntañola,[1] José A. Montiel,[2] Antonio Martínez-Rubio,[3] and Jordi Ordóñez-Llanos[1,4*]* ([1] Biochemistry, [2] Emergency, and [3] Cardiology Departments, Hospital de la Santa, Creu i Sant Pau, Barcelona, Spain; [4] Biochemistry and Molecular Biology Department, Universitat Autònoma, Barcelona, Spain; * address correspondence to this author at: Servei de Bioquímica, Hospital de la Santa Creu i Sant Pau, Avinguda Sant Antoni Maria Claret 167, 08025 Barcelona, Spain; fax 34-93-2919196, e-mail jordonez@hsp.santpau.es)

Ischemia-modified albumin (IMA) has been proposed as a biological marker of myocardial ischemia *(1, 2)*. Exposure to ischemic myocardium modifies circulating albumin at its NH_2 terminus by different mechanisms, and this modification is the basis of IMA measurement by the albumin cobalt binding (ACB) test *(3)*. The tissue-specific nature of the mechanism by which ischemia modifies albumin remains undetermined. Together with a nondiagnostic electrocardiogram and negative troponin values, IMA concentrations within the reference interval have high negative predictive value of myocardial ischemia in patients with suspected acute coronary syndromes *(1, 2)*. However, IMA cardiospecificity has not been validated and needs an evidence base before routine clinical use. A recent report showed significant IMA increases 24–48 h after a marathon race, with exercise-promoted gastrointestinal and/or delayed skeletal muscle ischemia being evoked as possible causes of such increases *(4)*. However, because IMA has shown rapid kinetics of increase (in minutes) and return to baseline no longer than 12 h after angioplastic procedures *(5)*, long-duration skeletal muscle ischemia (i.e., occurring during marathons) does not appear to be the most appropriate model to investigate the effect of such ischemia on IMA values or the kinetics of IMA occurring during acute coronary syndromes. The aim of this work was to analyze the possible contribution of skeletal muscle ischemia to IMA by investigating its short-term kinetics in an isolated skeletal-muscle ischemia model. Because lactate and ammonia concentrations increase sharply after a forearm ischemia test, their possible influence in the ACB assay was studied.

Ten healthy volunteers (4 men and 6 women) from our laboratory staff (age range, 48–61 years; median, 53 years) with no personal or family history of cardiovascular disease and no known cardiovascular risk factors after a medical examination underwent a forearm ischemia test *(6)*. Briefly, after an overnight fast (10–12 h) and 30 min of previous rest, a preexercise (0 min) blood sample was drawn, and blood systolic pressure was recorded twice within a 5-min interval. Thereafter, forearm ischemia was produced by inflating the blood pressure cuff up to 20–30 mmHg higher than the maximum systolic pressure registered. Under these ischemic conditions, a hand-grip exercise at maximum possible strength was performed for 1 min. Thereafter, the cuff was removed, and serial blood samples were drawn at 1, 3, 5, 10, 15, and 30 min. Serum for IMA, creatine kinase, and potassium; EDTA plasma for ammonia; and fluoride plasma for lactate and glucose were collected at each time point into Vacutainer® Tubes (Becton Dickinson). To establish reference values, IMA was tested in a group of 86 fasting (10–12 h), ambulatory (median age, 57 years; 38 women) sedentary individuals who underwent blood sampling after health examinations or before minor surgical procedures. Individuals with cardiovascular risk factors or past or present signs or symptoms of cardiovascular disease recorded during the medical examination were excluded. Volunteers and reference individuals gave written informed consent. All procedures were in accordance with our Institutional Review Board protocols.

Serum IMA was measured with the ACB test (Ischemia Technologies Inc.) adapted to a Roche Cobas Mira analyzer (ABX Diagnostics) according to the manufacturer's instructions for specimen and reagent handling. The principle of the test has been described previously *(3)*. In individuals undergoing the forearm ischemia test, ammonia, lactate, and glucose (all samples), and creatine kinase and potassium (basal and 5 min postexercise) were measured in a Vitros 250 analyzer (Ortho Diagnostics). Concentrations of L-(+)-lactic acid (lactic acid free acid; 300 g/L solution in water; Sigma, cat. no. L-1875; lot no. 052K1278; M_r 90.08) ranging from 50 to 900 mmol/L and ammonia (from ammonium chloride salt; Merck; cat. no. 1145; lot no. 7448183; M_r 53.49) ranging from 2 to 18 mmol/L were dissolved separately in 20 mmol/L MOPS buffer and added to a serum pool (IMA = 106 kilounits/L) at a constant ratio of 1/100 of the final sample volume. Lactate and ammonia concentrations of the enriched pool were measured by the above-described methods. All enriched samples were measured in quadruplicate. The Wilcoxon paired *t*-test and correlation equations were calculated with GraphPad Prism, Ver. 3.0 (GraphPad Software Inc.).

Between-batch imprecision (CV) of the ACB test was assessed at IMA concentrations of 69 and 114 kilounits/L and was <3% (n = 8) for both concentrations. The 95th percentile for IMA in the reference population was 101 kilounits/L (nonparametric). Results of the forearm ischemia test are shown in Table 1. Increases in lactate and ammonia were five- and sevenfold over basal values, respectively, during the first 5 min after exercise, demon-

Table 1. Mean (SD) lactate, ammonia, albumin, and IMA values and IMA:albumin ratios measured before (0 min) and after (1–30 min) the forearm ischemia test in 10 healthy volunteers.[a]

Time, min	Lactic acid, mmol/L	Ammonia, mmol/L	Albumin, g/L	IMA, kilounits/L	IMA:Albumin, kilounits/g
0	1.10 (0.30)	20 (10)	39.9 (2.3)	94.5 (9.1)	2.37 (0.27)
1	5.17 (1.14)[b]	116 (39)[b]	40.9 (2.8)	87.5 (8.9)[b]	2.14 (0.27)[b]
3	5.26 (1.14)[b]	136 (55[b]	40.3 (2.1)	87.1 (7.9)[b]	2.16 (0.25)[b]
5	4.35 (1.02)[b]	133 (60)[b]	39.8 (2.1)	89.1 (6.3)[b]	2.24 (0.22)[b]
10	2.77 (1.14)	90 (54)	39.4 (2.5)	90.7 (7.9)	2.30 (0.26)
15	2.07 (0.83)	62 (35)	39.2 (2.3)	91.8 (8.1)	2.34 (0.29)
30	1.22 (0.35)	32 (23)	39.2 (2.4)	93.8 (7.3)	2.29 (0.25)

[a] The test is described in detail in the text.
[b] $P < 0.05$ with respect to basal (0 min) values.

strative of ischemic-performed exercise (Table 1 and Fig. 1A). Creatine kinase, glucose, and potassium concentrations remained unchanged after exercise (data not shown). A significant, negative correlation between IMA values and albumin concentrations was found both in forearm ischemia and in reference samples [IMA (kilounits/L) = −2.366albumin (g/L) + 186.4; $r = -0.756$; $P < 0.001$; n = 152; Fig. 1B]. The ratio of IMA values to albumin (IMA:albumin) was also assessed, and the nonparametric 95th reference percentile was 2.59 kilounits/g. Mean IMA and IMA:albumin values obtained during the forearm ischemia test were below the respective 95th reference percentiles, although 6 of the 70 samples were above these limits. A significant ($P < 0.05$) decrease in both IMA and IMA:albumin at 1, 3, and 5 min was observed, with a return to baseline thereafter (Table 1 and Fig. 1A). Albumin concentrations did not change significantly. In the enriched serum pool, IMA concentrations decreased, whereas lactate increased, with negative mean differences of −9% at a lactic acid concentration of 5 mmol/L and −25% at the maximum concentration of 11 mmol/L (Fig. 1C). A significant correlation ($r = -0.98$; $P < 0.001$) was found between IMA and lactate values. After MOPS buffer addition in the proportion used for the assay, the pH range of the enriched pools varied only by 0.04 units. IMA values remained unaffected by ammonia

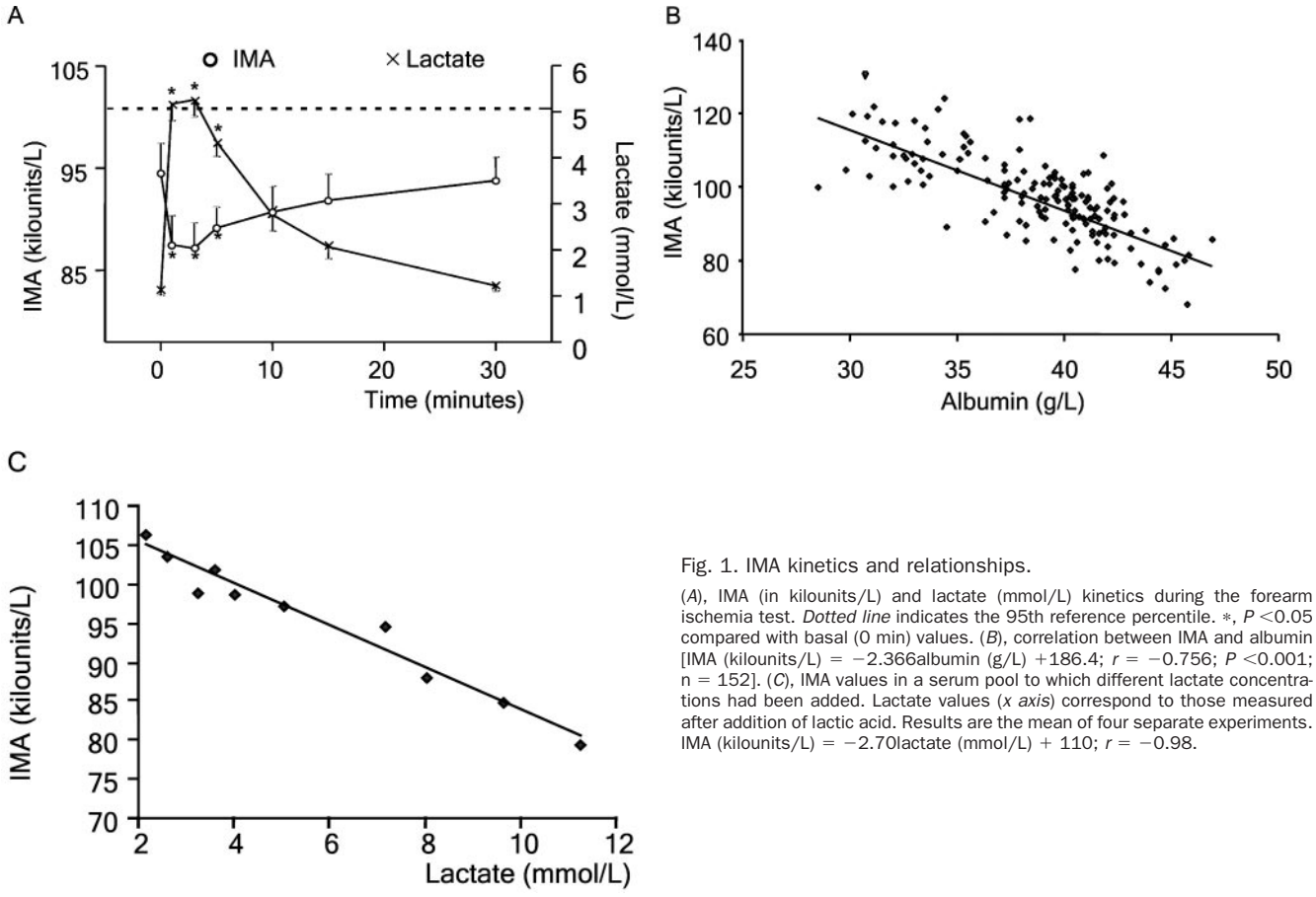

Fig. 1. IMA kinetics and relationships.

(*A*), IMA (in kilounits/L) and lactate (mmol/L) kinetics during the forearm ischemia test. *Dotted line* indicates the 95th reference percentile. ∗, $P < 0.05$ compared with basal (0 min) values. (*B*), correlation between IMA and albumin [IMA (kilounits/L) = −2.366albumin (g/L) +186.4; $r = -0.756$; $P < 0.001$; n = 152]. (*C*), IMA values in a serum pool to which different lactate concentrations had been added. Lactate values (*x axis*) correspond to those measured after addition of lactic acid. Results are the mean of four separate experiments. IMA (kilounits/L) = −2.70lactate (mmol/L) + 110; $r = -0.98$.

concentrations up to 250 μmol/L (mean difference ranging from −1% to 5%).

Biological evidence of myocardial ischemia remains a diagnostic challenge. Detection of IMA appears to be a promising tool for myocardial ischemia detection in patients with no increases in troponin *(1, 2)*. However, before IMA can be routinely used in clinical practice several questions, including its cardiospecificity, upper reference limit, and albumin relationship, must be answered. This work attempted to answer some of these questions. Release of biological markers from skeletal muscle is a major concern for specific myocardial damage detection. Thus, IMA tested under skeletal muscle ischemia conditions is an appropriate model. To date, only Apple et al. *(4)* have analyzed IMA in such conditions, showing increased basal IMA values in 31% of marathon runners, a drop to baseline values immediately after a marathon, and a return to increased values in 63% of cases 24–48 h thereafter. Skeletal muscle and gastrointestinal ischemia was implicated as a cause of such delayed increases in IMA values. However, this model of extensive, long-duration skeletal muscle ischemia likely does not reproduce the events occurring during myocardial ischemia.

The forearm ischemia test model, in which transient but complete blood flow occlusion is produced and skeletal muscle works under such conditions, produces skeletal muscle ischemia and is more analogous of myocardial ischemia. In the current study, during the forearm ischemia test, a significant decrease in IMA occurred 1–5 min after exercise, with recovery to basal values thereafter. Mean IMA values were always below our laboratory's 95th reference percentile, and only 9% of the analyzed samples were above this limit. However, our 95th reference limit of 101 kilounits/L was 20% higher than the 85 kilounits/L stated by the manufacturer. This is in accordance with the manufacturer's recommendation indicating the need for reference values derived from populations with the same characteristics as patients to be evaluated with the test. However, it should be noted that the small size of our reference population could also have influenced our 95th percentile.

Forearm exercise in ischemic conditions promoted sharp increases in lactate (fivefold) and ammonia (sevenfold). Because these increases occurred simultaneously with IMA decreases, possible interference of both metabolites on the ACB test was assessed. Addition experiments using a serum pool with both lactate and ammonia added produced different results. IMA values remained unchanged throughout increasing concentrations of ammonia. However, as lactate concentrations increased, IMA values decreased. Final lactate concentrations of 3–11 mmol/L reduced the initial IMA value by 7–25%, whereas concentrations of 4 and 5 mmol/L, which can be observed in clinical practice, decreased IMA values by 8% and 9%, respectively. Although an effect of lactate on the ACB test at plasma lactate concentrations within reference values could be negligible, our data suggest that lactate could interfere in the ACB test. In patients with increased lactate concentrations, decreasing true IMA values might decrease the diagnostic sensitivity. The potential of an interesting finding was the strong negative association between albumin and IMA values. Each 1 g/L change in albumin within the physiologic range of albumin (35–45 g/L) produced an opposite change of 2.6% in IMA values. This could partly explain IMA differences between populations, such as those observed between our reference value and that stated by the manufacturer. However, the contribution of interinstrument differences cannot be ruled out as a reason for such a difference. It could also suggest the need to evaluate IMA values together with those of albumin to avoid possible false-positive or -negative values in individuals with hypo- or hyperalbuminemia.

We are indebted to Ischemia Technologies for supplying part of the reagents used and to Christine O'Hara for editorial assistance. The work was supported by Grant C03/01 from Instituto de Salud Carlos III (Spain).

References

1. Christenson RH, Duh SH, Sanhai WR, Wu AHB, Holtman V, Painter P, et al. Characteristics of an albumin cobalt binding test for assessment of acute coronary syndrome patients: a multicenter study. Clin Chem 2001;47:464–70.
2. Bhagavan NV, Lai EM, Rios PA, Yang J, Ortega-López AM, Shinoda H, et al. Evaluation of human serum albumin cobalt binding assay for the assessment of myocardial ischemia and myocardial infarction. Clin Chem 2003;49: 581–5.
3. Bar-Or D, Lau E, Winkler JV. A novel assay for cobalt-albumin binding and its potential as a marker for myocardial ischemia—a preliminary report. J Emerg Med 2000;19:311–5.
4. Apple FS, Quist HE, Otto AP, Mathews WE, Murakami MM. Release characteristics of cardiac biomarkers and ischemia-modified albumin as measured by the albumin cobalt-binding test after a marathon race. Clin Chem 2002; 48:1097–100.
5. Sinha MK, Gaze DC, Tippins JR, Collinson PO, Kaski, JC. Ischemia modified albumin is a sensitive marker of myocardial ischemia after percutaneous coronary intervention. Circulation 2003;107:2403–5.
6. Zaman Z, De Raedt S. Ischemic exercise testing in suspected McArdle disease. Clin Chem 2000;46:198–9.

DOI: 10.1373/clinchem.2003.027789

DNA Methylation Changes in Sera of Women in Early Pregnancy Are Similar to Those in Advanced Breast Cancer Patients, *Hannes M. Müller,[1†] Lennart Ivarsson,[1†] Hans Schröcksnadel,[1] Heidi Fiegl,[1] Andreas Widschwendter,[1] Georg Goebel,[2] Susanne Kilga-Nogler,[3] Horst Philadelphy,[4] Wolfgang Gütter,[4] Christian Marth,[1] and Martin Widschwendter[1*]* (Departments of [1] Obstetrics and Gynecology, [2] Biostatistics and Documentation, and [3] Central Blood Transfusion and Immunology, Medical University Innsbruck, Innsbruck, Austria; [4] Institutes of Laboratory Medicine in Innsbruck and Wörgl, Tirol, Austria; † H.M. Müller and L. Ivarsson contributed equally to this work; * address correspondence to this author at: Department of Obstetrics and Gynecology, Medical University Innsbruck, Anichstrasse 35, A-6020 Innsbruck, Austria; fax 43-512-504-23112, e-mail martin.widschwendter@uibk.ac.at)

In normal human pregnancy, the uterus and its arterial system, including the decidua and the adjacent third of

the myometrium, are invaded by cytotrophoblasts *(1, 2)*, which initiate conversion of the decidual vascular system from a high-pressure/low-flow system to a low-pressure/high-flow system that meets the needs of the fetus and placenta *(3)*. The trophoblastic invasion in humans occurs between weeks 8 and 18 of pregnancy *(4)*. The invasion process into the uterus shows many similarities to the invasion of malignant cells during metastasis in that both types of cells have to pass through a basal membrane *(5)*. One of the most important diseases of pregnant women, preeclampsia, is known to be associated with a failure of complete trophoblastic invasion in the first third of the myometrium *(6)*.

Epigenetic alterations, including changes in DNA methylation status, are among the most common molecular alterations in human neoplasia *(7)*. DNA methylation changes are also involved in mammalian development, starting with a wave of demethylation during cleavage, followed by genome-wide de novo methylation after implantation *(8)*. Recently, Ohgane et al. *(9)* reported that the differentiation of a trophoblast lineage is associated with DNA methylation and demethylation. In many cases, aberrant methylation of the CpG island genes has been correlated with a loss of gene expression, and it has been proposed that DNA methylation provides an alternative to gene deletion or mutation for the loss of gene function *(7)*. Moreover, it is now widely known that methylated DNA can be detected in various body fluids, including serum and plasma, and that the methylation status of some genes can be used for early detection of, or even risk assessment for, various types of human neoplasia *(10)*.

Cell-free fetal and maternal DNA can be detected in the maternal bloodstream *(11)* and is reported to be robust and easy to obtain *(12)*. Cell-free fetal DNA in maternal plasma seems to be of importance in noninvasive prenatal diagnosis *(13)* and in the diagnosis of some pregnancy-associated diseases, such as preeclampsia *(14)*. Recently, Poon et al. *(15)* reported the first use of differential DNA methylation in maternal plasma to detect fetal DNA. The cellular origin of the increase in total plasma DNA is unclear at present, but Chan et al. *(16)* speculated that fetal DNA may be released into the plasma by trophoblasts, whereas maternal DNA may be released into the circulation by the decidua.

In this proof-of-principle study we addressed the question of whether the methylation pattern in the serum of pregnant women early in pregnancy of genes known to be involved in the invasion process shows similarities to the methylation pattern in patients with invasive cancers. We also asked whether such an invasion-specific methylation pattern in serum shows differences between women with normal pregnancies and women developing preeclampsia—a disease known to be accompanied by a disturbed invasion process in the first trimester *(6)*. We chose a panel of three genes (*CDH1*, *TIMP-3*, and *PTGS-2*) known to play key roles in the invasion process of tumor cells *(17–19)*, which are often regulated by promoter hypermethylation *(20–22)*, or in the invasion process of trophoblast cells *(2, 23–25)*. We also chose one gene (*BLT1*) involved in the regulation of immune response and regulated by promoter hypermethylation *(26)*. In addition, we selected two genes (*APC* and *RASSF1A*) known to be involved in pathways counteracting metastasis that are reported to be methylated in several human neoplasias *(27, 28)*. Recently, we were able to demonstrate that DNA sequences of these six genes are highly methylated in serum of patients with advanced breast cancer and show less methylation in primary breast cancer patients *(29)*.

We analyzed the methylation status of the above-mentioned six genes early in gestation in 32 serum samples from healthy pregnant women with normal pregnancy outcomes and in serum samples from 17 healthy pregnant women who were later diagnosed with either severe preeclampsia (diastolic blood pressure >110 mmHg and 3+ proteinuria), eclampsia, or HELLP syndrome [gestational age at time of sampling, 10–15 weeks (median, 12 weeks) and 6–17 weeks (median, 12 weeks), respectively]. The serum samples were obtained during normal blood drawing for screening during the early gestational weeks. The median patient ages were 32 years (range, 19.7–41.3 years) for pregnant women with normal pregnancy outcomes and 28.5 years (range, 8.6–42.4 years) for women who later developed severe preeclampsia, eclampsia, or HELLP syndrome. Clinical data for all included patients were analyzed anonymously, and persons performing methylation analyses were totally blinded to the clinical data.

Genomic DNA from serum samples was isolated by use of the High Pure Viral Nucleic Acid Kit (Roche Diagnostics) according to the manufacturer's protocol with some modifications for multiple loading of the DNA extraction columns to obtain a sufficient amount of DNA *(29)*. Sodium bisulfite conversion of genomic DNA and the MethyLight assay for methylation analysis were performed as described previously *(30, 31)*. Primers and probes for the analyzed genes were also as published previously *(29)*. Using the MethyLight assay, we obtained percentages of fully methylated reference values, and in this study we deemed a percentage of fully methylated reference value >0 as positive for methylation.

We detected various degrees of DNA methylation of the six loci in sera from pregnant women early in pregnancy who showed normal as well as pathologic pregnancy outcomes (Table 1). We found statistically significant differences between the methylation status of *APC* in sera of women who later developed severe preeclampsia, eclampsia, or HELLP syndrome (n = 17) vs healthy pregnant women (n = 32; $P = 0.041$) and an inverse trend ($P = 0.067$) for *RASSF1A* methylation in sera of these two groups of pregnant women (Table 1).

We also compared the methylation profiles of the pregnant women in early pregnancy who had normal as well as pathologic pregnancy outcomes with the methylation status of sera from 10 healthy controls, pretreatment

Table 1. Percentage of samples positive for methylation at a specific gene locus in sera of pregnant women, healthy controls, and breast cancer patients.

Group	Percentage of positive samples at each locus					
	TIMP-3	*CDH1*	*PTGS2*	*BLT1*	*APC*	*RASSF1A*
Healthy pregnant women (n = 32)	6	69	88	100	18	56
Pregnant women who later developed preeclampsia, eclampsia, or HELLP (n = 17)	18	59	100	100	47	29
Healthy controls (n = 10)	0	25	30	60	0	10
Patients with primary breast cancer (n = 26)	0	20	39	85	23	23
Patients with advanced breast cancer (n = 10)	20	90	100	100	80	80

sera from 26 patients with primary breast cancer, and sera from 10 patients with metastasized breast cancer. The sera of these patients had been analyzed previously for another reason in a recently published study *(29)*. All 10 control patients underwent core biopsies of the breast and were confirmed to have benign disease of the breast (age range, 20.5–71.5 years; median, 42.4 years). Within the group of primary breast cancer patients (age range, 36.1–83.9 years; median, 58 years), 2, 18, and 6 patients had pT1, pT2, and pT3 cancers, respectively, and 15, 10, and 1 patients had lymph node-negative, -positive, and unknown disease, respectively. The 10 patients with advanced breast cancer were diagnosed with metastases in the bone, lung, brain, or liver (age range, 49.3–68.7 years; median, 53.6 years).

We first addressed the question whether sera from the two groups of pregnant women had a methylation status different from that of healthy controls. We found strong statistically significant differences between the methylation status of *PTGS2* and *BLT1* in sera from pregnant women (n = 59) vs healthy controls (n = 10; $P < 0.001$ for both), a statistically significant difference for *RASSF1A* methylation ($P = 0.038$), a trend ($P = 0.051$) for *CDH1* methylation status, and no significant differences in the *TIMP-3* and *APC* methylation status (Table 1). Looking at the methylation status of these six gene loci in sera from healthy controls vs pretreatment sera from primary breast cancer patients we found no statistically significant differences (data not shown). Otherwise, looking at various methylation changes in healthy controls compared with those in patients with advanced breast cancer revealed statistically significant differences for *CDH1*, *PTGS2*, *APC*, and *RASSF1A* methylation ($P = 0.013$, 0.003, 0.001, and 0.005, respectively), a trend for *BLT1* methylation ($P = 0.087$), and no significant differences for *TIMP-3* methylation (Table 1).

With this proof-of-principle study we show for the first time that methylation changes in *TIMP-3*, *CDH1*, *PTGS2*, *BLT1*, *APC*, and *RASSF1A* can be detected in pregnant women. From our point of view, the most important finding is the similarity between pregnant women and metastasized breast cancer patients in the methylation changes in genes that are known to be involved in metastasis and tumor cell invasion *(17–19, 27, 28)* or even in the invasion process of trophoblast cells *(2, 23–25)* and in the regulation of the immune response *(26)*. As sera of those cancer patients without evidence of metastasis at the time of diagnosis lacked the methylation changes found in advanced breast cancer and pregnancy (Table 1), we speculate that the observed methylation pattern reflects DNA release from invasive cells, specifically trophoblast cells and tumor cells.

In summary, a statistically significant difference in methylation of *APC* was seen in sera of healthy pregnant women and women who later developed severe preeclampsia, eclampsia, or HELLP syndrome, perhaps offering a possible tool for early detection of this severe disease in pregnancy. We also describe for the first time in a phenomenologic way that methylation changes in sera of women in early pregnancy are similar to those in sera of patients with advanced breast cancer. Further studies are needed to clarify the importance of DNA methylation in regulating the invasion process of cells in general and of trophoblast cells in particular.

We thank Lisl Perkmann and Inge Gaugg for technical assistance. Research funding was received from the Austrian "Fonds zur Förderung der wissenschaftlichen Forschung" (Grants P15995-B05 and P16159-B05) and "Jubiläumsfonds der Österreichischen Nationalbank" (Grants 9856 and 7585). We also thank the laboratory of Dr. Richard Rohrer at Innsbruck for serum sample collection from women in early pregnancy.

References

1. Damsky CH, Fisher SJ. Trophoblast pseudo-vasculogenesis: faking it with endothelial adhesion receptors. Curr Opin Cell Biol 1998;10:660–6.
2. Fisher SJ, Cui TY, Zhang L, Hartman L, Grahl K, Zhang GY, et al. Adhesive and degradative properties of human placental cytotrophoblast cells in vitro. J Cell Biol 1989;109:891–902.
3. Roberts JM, Redman CW. Pre-eclampsia: more than pregnancy-induced hypertension. Lancet 1993;341:1447–51.
4. Pijnenborg R, Dixon G, Robertson WB, Brosens I. Trophoblastic invasion of human decidua from 8 to 18 weeks of pregnancy. Placenta 1980;1:3–19.
5. Mullen CA. Analogies between trophoblastic and malignant cells [Review]. Am J Reprod Immunol 1998;39:41–9.
6. Khong TY, De Wolf F, Robertson WB, Brosens I. Inadequate maternal vascular response to placentation in pregnancies complicated by pre-eclampsia and by small-for-gestational age infants. Br J Obstet Gynaecol 1986;93:1049–59.
7. Jones PA, Baylin SB. The fundamental role of epigenetic events in cancer. Nat Rev Genet 2002;3:415–28.
8. Jaenisch R, Bird A. Epigenetic regulation of gene expression: how the genome integrates intrinsic and environmental signals. Nat Genet 2003; 33(Suppl):245–54.
9. Ohgane J, Hattori N, Oda M, Tanaka S, Shiota K. Differentiation of

trophoblast lineage is associated with DNA methylation and demethylation. Biochem Biophys Res Commun 2002;290:701–6.

10. Müller HM, Widschwendter M. Methylated DNA as a possible screening marker for neoplastic disease in several body fluids. Expert Rev Mol Diagn 2003;3:443–58.
11. Lo YM. Fetal DNA in maternal plasma: biology and diagnostic applications. Clin Chem 2000;46:1903–6.
12. Angert RM, LeShane ES, Lo YM, Chan LY, Delli-Bovi LC, Bianchi DW. Fetal cell-free plasma DNA concentrations in maternal blood are stable 24 hours after collection: analysis of first- and third-trimester samples. Clin Chem 2003;49:195–8.
13. Chiu RW, Lo YM. Non-invasive prenatal diagnosis: on the horizon? Pharmacogenomics 2003;4:191–200.
14. Leung TN, Zhang J, Lau TK, Chan LY, Lo YM. Increased maternal plasma fetal DNA concentrations in women who eventually develop preeclampsia. Clin Chem 2001;47:137–9.
15. Poon LL, Leung TN, Lau TK, Chow KC, Lo YM. Differential DNA methylation between fetus and mother as a strategy for detecting fetal DNA in maternal plasma. Clin Chem 2002;48:35–41.
16. Chan LY, Leung TN, Chan KC, Tai HL, Lau TK, Wong EM, et al. Serial analysis of fetal DNA concentrations in maternal plasma in late pregnancy. Clin Chem 2003;49:678–80.
17. Christofori G. Changing neighbours, changing behaviour: cell adhesion molecule-mediated signalling during tumour progression. EMBO J 2003;22: 2318–23.
18. Kakiuchi Y, Tsuji S, Tsujii M, Murata H, Kawai N, Yasumaru M, et al. Cyclooxygenase-2 activity altered the cell-surface carbohydrate antigens on colon cancer cells and enhanced liver metastasis. Cancer Res 2002;62: 1567–72.
19. Tsujii M, Kawano S, DuBois RN. Cyclooxygenase-2 expression in human colon cancer cells increases metastatic potential. Proc Natl Acad Sci U S A 1997;94:3336–40.
20. Bachman KE, Herman JG, Corn PG, Merlo A, Costello JF, Cavenee WK, et al. Methylation-associated silencing of the tissue inhibitor of metalloproteinase-3 gene suggests a suppressor role in kidney, brain, and other human cancers. Cancer Res 1999;59:798–802.
21. Song SH, Jong HS, Choi HH, Inoue H, Tanabe T, Kim NK, et al. Transcriptional silencing of cyclooxygenase-2 by hyper-methylation of the 5′ CpG island in human gastric carcinoma cells. Cancer Res 2001;61:4628–35.
22. Chen CL, Liu SS, Ip SM, Wong LC, Ng TY, Ngan HY. E-Cadherin expression is silenced by DNA methylation in cervical cancer cell lines and tumours. Eur J Cancer 2003;39:517–23.
23. Zhou Y, Damsky CH, Fisher SJ. Preeclampsia is associated with failure of human cytotrophoblasts to mimic a vascular adhesion phenotype. One cause of defective endovascular invasion in this syndrome? J Clin Invest 1997;99:2152–64.
24. Bass KE, Li H, Hawkes SP, Howard E, Bullen E, Vu TK, et al. Tissue inhibitor of metalloproteinase-3 expression is upregulated during human cytotrophoblast invasion in vitro. Dev Genet 1997;21:61–7.
25. Xu P, Wang Y, Piao Y, Bai S, Xiao Z, Jia Y, et al. Effects of matrix proteins on the expression of matrix metalloproteinase-2, -9, and -14 and tissue inhibitors of metalloproteinases in human cytotrophoblast cells during the first trimester. Biol Reprod 2001;65:240–6.
26. Kato K, Yokomizo T, Izumi T, Shimizu T. Cell-specific transcriptional regulation of human leukotriene B(4) receptor gene. J Exp Med 2000;192:413–20.
27. Fearnhead NS, Britton MP, Bodmer WF. The ABC of APC. Hum Mol Genet 2001;10:721–33.
28. Dammann R, Schagdarsurengin U, Strunnikova M, Rastetter M, Seidel C, Liu L, et al. Epigenetic inactivation of the Ras-association domain family 1 (RASSF1A) gene and its function in human carcinogenesis. Histol Histopathol 2003;18:665–77.
29. Müller HM, Widschwendter A, Fiegl H, Ivarsson L, Goebel G, Perkmann E, et al. DNA methylation in serum of breast cancer patients: an independent prognostic marker. Cancer Res 2003;63:7641–5.
30. Eads CA, Danenberg KD, Kawakami K, Saltz LB, Blake C, Shibata D, et al. MethyLight: a high-throughput assay to measure DNA methylation. Nucleic Acids Res 2000;28:E32.
31. Eads CA, Lord RV, Wickramasinghe K, Long TI, Kurumboor SK, Bernstein L, et al. Epigenetic patterns in the progression of esophageal adenocarcinoma. Cancer Res 2001;61:3410–8.

DOI: 10.1373/clinchem.2003.030387

Standardized Evaluation of Instruments for Self-Monitoring of Blood Glucose by Patients and a Technologist,

Gunn B.B. Kristensen,[1] Kari Nerhus,[1] Geir Thue,[1] and Sverre Sandberg[1,2]* ([1] NOKLUS, Norwegian Center for Quality Improvement of Primary Care Laboratories, Division of General Practice, Department of Public Health and Primary Health Care, University of Bergen, Ulriksdal 8c, N-5009, Norway; [2] Laboratory of Clinical Biochemistry, Haukeland University Hospital, Bergen, Norway; * author for correspondence: fax 47-55586710, e-mail gunn.kristensen@isf.uib.no)

Self-monitoring of blood glucose (SMBG) is recommended to improve metabolic control for patients with diabetes because tight glycemic control can decrease microvascular complications in individuals with type 1 and type 2 diabetes *(1, 2)*. The worldwide market for SMBG is $2.7 billion per year, with annual growth estimated to be 10–12% *(3)*. The performance of these instruments is therefore an important issue.

In most studies evaluating instruments for SMBG, the patient is not involved, although user errors account for a large portion of the total error in SMBG *(4)*. In International Organization for Standardization document ISO/FDIS 15197, it is therefore recommended that a user performance evaluation should be performed in addition to testing by a medical laboratory technologist (MLT) *(5)*. We have developed a procedure based on these recommendations in which instruments are tested simultaneously by an experienced technologist and a group of patients under the same conditions, using blood from the same patients. The procedure was evaluated with two instruments: Glucometer Dex from Bayer (1999) and GlucoMen Glyco from Menarini (2002).

Norwegian patients with diabetes (type 1 and type 2) participated. For each meter, 100 patients were randomly divided into two groups, as shown in Supplement 1 of the Data Supplement that accompanies the online version of this Technical Brief at http://www.clinchem.org/content/vol50/issue6/. Before the evaluation, one group was given specific training by a MLT (1–2 h) on how to use the new meter, in addition to standard written instructions, whereas the other group received the meter by mail with the same standard instructions. Three lots of strips were used in the test. After receiving their new meter, the user manual, and 50 strips, the patients familiarized themselves with the meter for 2 weeks. In the period between 2 and 4 weeks, the patients performed five glucose measurements in duplicate on themselves on 5 different days. After 4 weeks, the patients met individually with the MLT for a consultation. During the consultation, the patients first performed two measurements on themselves with no instructions from the MLT. Within 5 min, the MLT took a sample from a different finger. With this blood sample, glucose measurements were performed twice on two different meters and twice with the reference method. Because the meters had no underfill detection, the MLT visually checked the strips and marked all

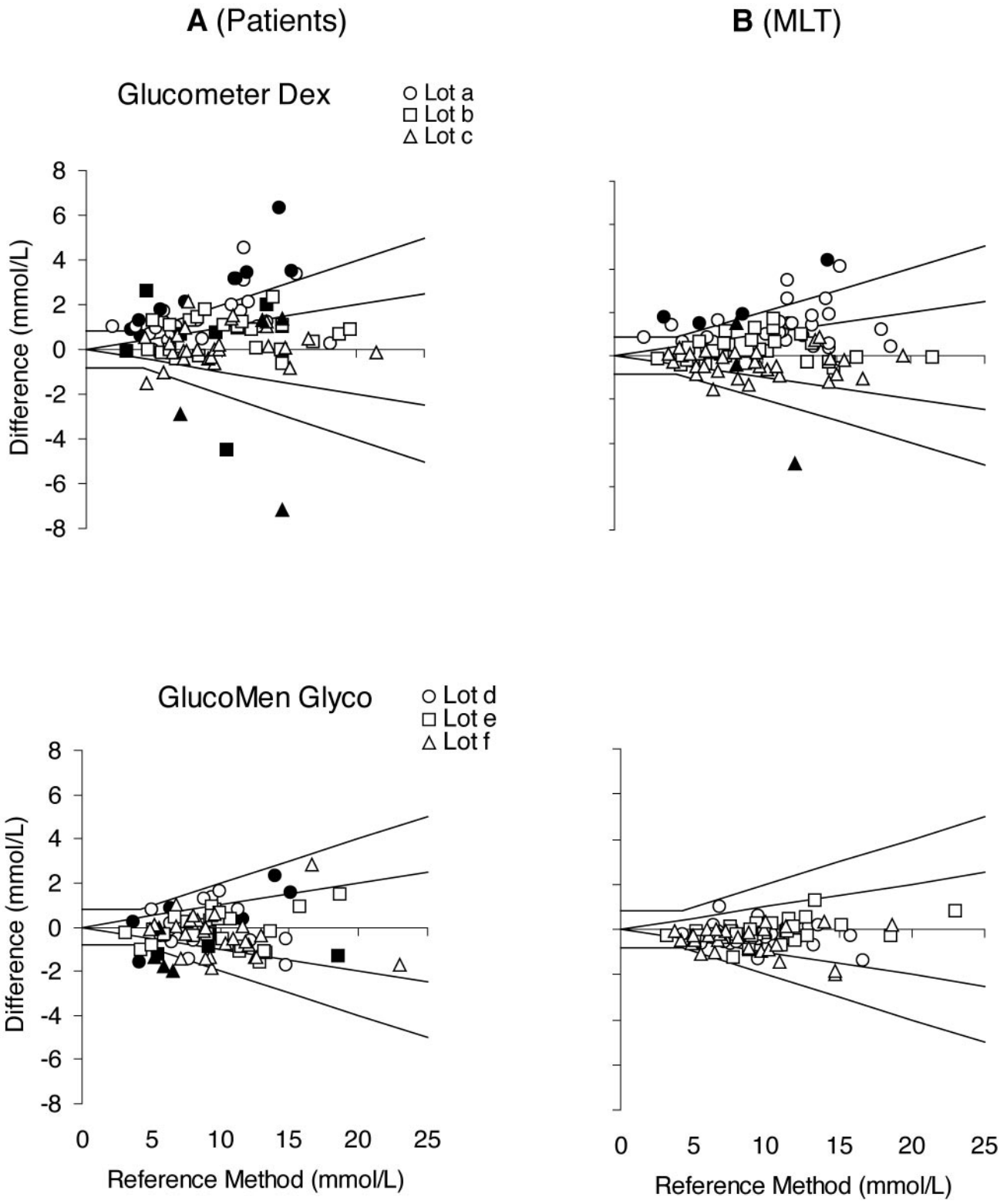

Fig. 1. Difference between Glucometer Dex or GlucoMen Glyco results (first measurement) and reference method results (mean of two measurements) plotted against the reference method results.

(*A*), patients (n = 93 and 90 for Glucometer Dex and GlucoMen Glyco respectively); (*B*), MLT (n = 95 and 92 for Glucometer Dex and GlucoMen Glyco, respectively). Measurements with strips filled incompletely with blood are indicated with *closed symbols*. *Open symbols* indicate measurements with different lots of test strips. *Lines* represent limits suggested from American Diabetes Association (*inner lines*) *(9)* and in ISO/FDIS 15197 (*outer lines*) *(5)*.

Table 1. Analytical quality.

		Accuracy[a]		Imprecision[b]			
Instrument	Examined by	n	Deviation >ISO standard,[c] %	n	Mean, mmol/L	Results excluded,[d] n	CV,[e] %
Glucometer Dex	MLT	95	11.6 (5.9–19.8)	187	10.5	2	5.6 (5.2–6.1)
	Patients at consultation	93	24.7 (16.3–34.8)	92	10.3	4	9.8 (8.8–11)
	Patients at home			396	9.0	9	8.6 (8.1–9.1)
GlucoMen Glyco	MLT	92	1.1 (0.1–6.1)	191	9.0	0	4.3 (4.0–4.7)
	Patients at consultation	90	6.7 (2.4–14.0)	94	9.2	2	6.8 (6.1–7.8)
	Patients at home			411	8.5	5	6.4 (6.1–6.9)
	Excluding results related to incorrect coding and incompletely filled strips				**Excluding results from incompletely filled strips**		
Glucometer Dex	MLT	88	6.8 (2.5–14.3)	140	10.5	1	4.2 (3.8–4.6)
	Patients at consultation	70	14.3 (7.4–25.2)	57	10.3	1	5.9 (5.1–7.0)
GlucoMen Glyco	MLT	92	1.1 (0.1–6.1)	191	9.0	0	4.3 (4.0–4.7)
	Patients at consultation	70	1.4 (0.1–8.8)	85	9.6	2	4.6 (4.1–5.3)

[a] Percentage of measurements (first of duplicate) that deviate from the reference method (mean of duplicate) by more than the difference allowed by the ISO standard *(5)*. When calculating the accuracy only measurements from the MLT's instrument for which all three lots were included are presented.

[b] Calculated from duplicate measurements from patients or from the MLT. When calculating the imprecision for instruments used by the MLT, measurements for both meters were included.

[c] Mean (95% confidence interval).

[d] Results were excluded based on the criterion promoted by Burnett *(16)*.

[e] 95% confidence interval in parentheses.

measurements with strips not completely filled with blood. The MLT also observed whether the instrument was coded correctly. Finally, the patients completed two questionnaires, one about the user manual and one about the user-friendliness of the device. The study protocol was approved by the Norwegian Regional Committee for Medical Research Ethics.

The comparison method for the Glucometer Dex was a glucose dehydrogenase method using hemolyzed blood with reagents from Roche Diagnostics (Unimate 7) run on a Cobas Fara centrifugal analyzer (Roche Diagnostics). The comparison method for GlucoMen Glyco was a method that measures glucose in plasma on an Advia 1650 with reagents from Bayer (Glucose Hexokinase Method II; prod. no. B01-597-01). Both methods were verified by SRM 965 from the NIST and by control solutions verified by the isotope dilution–gas chromatography/mass spectrometry reference method.

Imprecision (SD and CV) was calculated by use of paired measurements, based on the formula:

$$\mathrm{SD} = \sqrt{\frac{\sum d^2}{2n}}$$

where d is the difference between measurements, and n is the number of duplicate samples. The criterion promoted by Burnett *(6)* was used for detection of outliers.

According to ISO/FDIS 15197 *(5)* and the NCCLS *(7)*, the number of measurements deviating more than ±20% (results ≥4.2 mmol/L) and >0.83 mmol/L (results <4.2 mmol/L) should be <5%. None of the meters met these requirements when used by patients, but the GlucoMen Glyco met the requirements when used by the MLT (Fig. 1 and Table 1). However, several other, usually stricter quality specifications have been suggested *(8–11)*, e.g., the American Diabetes Association suggests a total error of ±10% *(9)*.

As can be seen in Table 1, the measurements performed by the patients had significantly poorer precision than measurements performed by the MLT ($P < 0.05$). On the basis of patient-derived quality specifications and simulation studies, it has been suggested that imprecision should be <5% *(9, 10)*. In a study where the analytical quality of five SMBG systems was investigated, the CV varied from 5% to 11% when patients used the instruments compared with 2.3–5.9% when a MLT used them *(12)*, which is in line with our results.

One important issue of incorporating a user test in the evaluation of SMBG devices is to discover user errors that will not be detected by the MLT. This was found for the GlucoMen Glyco, but not for the Glucometer Dex. For the GlucoMen Glyco, 6% of the measurements performed by the patients were done with too little blood, whereas the MLT had no such measurements. In addition, 16% of the patients had not coded the instrument correctly (Fig. 1 and Table 1). If measurements related to these errors were excluded from the calculations, the analytical quality of the meter would also be acceptable in the hands of the patients. Regarding the Glucometer Dex, there was a problem with the strip that led to poor uptake of blood. As many as 24% of the measurements performed by the patients with the Glucometer Dex at the consultation were done with too little blood. The MLT, as well as the patients who received training, had significantly fewer incompletely filled strips at the consultation than the group of untrained patients (15%, 18%, and 31%, respectively; Fig. 1 and Table 1). This problem thus would have

been detected by the MLT, but was more obvious when the patients used this meter.

To evaluate the lot-to-lot variation, we included only the measurements performed by the MLT. For the Glucometer Dex, the analytical quality of one lot was significantly poorer than the quality of the two others, even when we excluded the results for incompletely filled strips. For the GlucoMen Glyco there was no difference in analytical quality among the three lots, but all had a negative bias compared with the reference method, as shown in Supplement 2 in the online Data Supplement. Lot-to-lot variation may be a considerable problem with SMBG devices and could be a major factor in loss of analytical quality *(12)*. From 2004 onward, the quality of all lots on the Norwegian market will be examined.

Educational efforts might influence the performance of SMBG *(13–15)*. For the Glucometer Dex, the precision obtained both at the consultation and at home was better for the patient group trained on meter use by the MLT compared with the group that received only written instructions [CV, 12% and 28% for the trained patients and the untrained patients, respectively, at the consultation ($P < 0.05$) vs 5.6% for the trained patients and 8.8% for the untrained patients at home ($P < 0.05$)]. For the GlucoMen Glyco, the precision obtained at home was better for the trained group than for the nontrained group (CV, 5.2% vs 7.6%; $P < 0.05$). However, 12 patients in the nontrained group compared with 2 patients in the trained group had coded the GlucoMen Glyco incorrectly.

User errors that were assessed in the evaluations were highlighted in the questionnaires (Supplements 3 and 4 in the online Data Supplement). Regarding the Glucometer Dex, ~25% of the patients commented on the problem of poor uptake of blood. In the case of the GlucoMen Glyco, 13% answered that it was difficult to apply blood to the test strip, and 17% found it difficult to code the instrument. Manufacturing of SMBG instruments according to patients' wishes may lead to improvements in acceptability, compliance, and glucose control *(16)*.

Each evaluation lasted ~5 months. One month was used to prepare the work, 2.5 months were needed to complete the practical work, and 1 month was needed for result evaluation. The costs were estimated to be approximately NOK 150 000 (US $20 000) for each evaluation.

It is essential that important shortcomings of SMBG devices are disclosed before the instruments are made commercially available. A procedure for evaluating new instruments and strips should therefore be standardized, including both a user part and a part that deals with analytical quality in the hands of experienced technologists. The evaluation should not be too costly to perform. We believe that our procedure fulfills these demands, and the Norwegian Health Authorities have decided that all SMBG instruments marketed in Norway should be examined by a procedure similar to the one described in this study. In addition, all lots of strips on the market will be tested in a special survey because they cannot be included in the procedure for practical reasons.

The Glucometer Dex and GlucoMen Glyco instruments and strips used and tested by the MLT and the patients in the study were kindly supplied by Bayer Diagnostics (Tarrytown, NY) and Menarini (Firenzi, Italy), respectively. The National Office for Social Insurance in Norway provided financial support for the study. The study is part of the Global Campaign of Diabetes Mellitus launched by the IFCC.

References

1. DCCT Research Group. The effect of intensive treatment of diabetes on the development and progression of long-term complications in insulin-dependent diabetes mellitus. N Engl J Med 1993;329:977–86.
2. UKPDS Group. Intensive blood-glucose control with sulphonylureas or insulin compared with conventional treatment and risk of complications in patients with type 2 diabetes. Lancet 1998;352:837–53.
3. Thayer A. Deciphering diseases. Chem Eng News 1999;30:19–28.
4. Center for Devices and Radiological Health (CDRH). Human factors in self-monitoring of blood glucose: Task IV report, Vol. 1. Rockville, MD: US Food and Drug Administration, April 1990.
5. International Organization for Standardization. In vitro diagnostic test systems—requirements for blood glucose monitoring systems for self-testing in managing diabetes mellitus. ISO/TC 212/SC. Final Draft International Standard ISO/FDIS 15197. Geneva, Switzerland: ISO, 2003.
6. Burnett RW. Accurate estimation of standard deviations for quantitative methods used in clinical chemistry. Clin Chem 1975;21:1935–8.
7. National Committee for Clinical Laboratory Standards. Point-of-care blood-glucose testing in acute and chronic care facilities; approved guideline, 2nd ed. NCCLS document C30–A2. Wayne, PA: NCCLS, 2002.
8. American Diabetes Association. Consensus statement on self-monitoring of blood glucose. Diabetes Care 1987;10:95–9.
9. American Diabetes Association. Consensus statement on self-monitoring of blood glucose. Diabetes Care 1996;19:S62–6.
10. Boyd JC, Bruns DE. Quality specifications for glucose meters: assessment by simulation modeling of errors in insulin dose. Clin Chem 2001;47:209–14.
11. Skeie S, Thue G, Sandberg S. Patient-derived quality specifications for instruments used in self-monitoring of blood glucose. Clin Chem 2001;47:67–73.
12. Skeie S, Thue G, Nerhus K, Sandberg S. Instruments for self-monitoring of blood glucose: comparisons of testing quality achieved by patients and a technician. Clin Chem 2002;48:994–1003.
13. Proposed strategies for reducing user error in capillary blood glucose monitoring. The National Steering Committee for Quality Assurance in Capillary Blood Glucose Monitoring. Diabetes Care 1993;16:493–8.
14. One J. Standardization and recommendations for the appropriate use of automated devices for self-monitoring blood glucose. Rinsho Byori 2001;49:1190–8.
15. Barcelo A, Robles S, White F, Jadue L, Vega J. [An intervention to improve diabetes control in Chile]. Rev Panam Salud Publica 2001;10:328–33.
16. Halimi S, Charpentier G, Grimaldi A, Grenier JL, Baut F, Germain B, et al. Effect on compliance, acceptability of blood glucose self-monitoring and HbA(1c) of a self-monitoring system developed according to patient's wishes. The ACCORD study. Diabetes Metab 2001;27:681–7.

DOI: 10.1373/clinchem.2004.031575

Elimination of the Cardiac Natriuretic Peptides B-Type Natriuretic Peptide (BNP) and N-Terminal proBNP by Hemodialysis, *Hans Günther Wahl,[1*] Stephanie Graf,[2] Harald Renz,[1] and Winfried Fassbinder[2]* ([1] Klinikum der Philipps-Universität Marburg, Department of Clinical Chemistry and Molecular Diagnostics, 35033 Marburg, Germany; [2] Klinikum Fulda, Department of Internal Medicine III, Fulda, Germany; * author for correspondence: fax 49-6421-2865594, e-mail hg.wahl@med.uni-marburg.de)

The measurement of natriuretic peptides for the diagnosis of heart failure has been a major breakthrough in cardi-

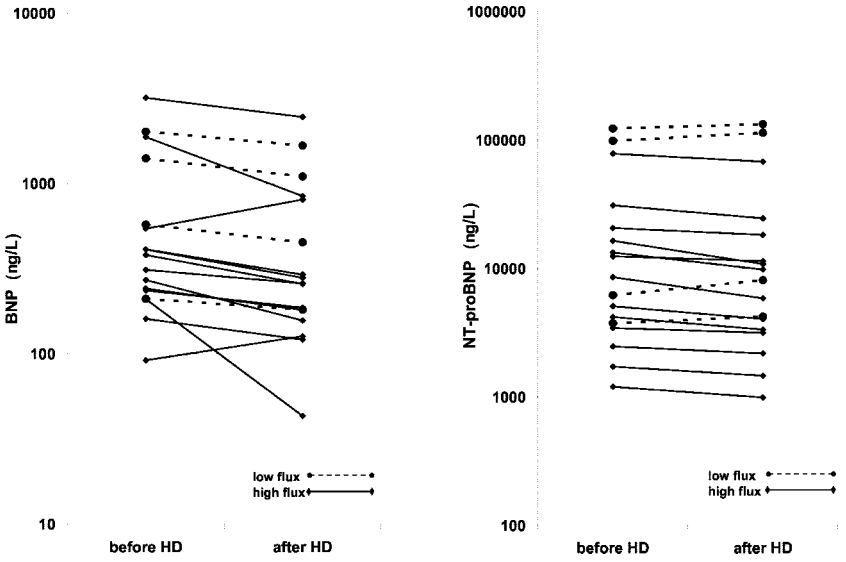

Fig. 1. BNP and NT-proBNP plasma concentrations in individual patients (n = 17) before and after hemodialysis (*HD*).

High-flux membrane (*solid lines*), n = 13; low-flux membrane (*dashed lines*), n = 4.

ology *(1, 2)*. B-Type natriuretic peptide (BNP) is synthesized as preproBNP mainly in the ventricular myocardium. On ventricular myocyte stretch, preproBNP is enzymatically cleaved to proBNP and released in the form of the hormonally active BNP and the inactive N-terminal proBNP (NT-proBNP). Both BNP and NT-proBNP have been shown to reflect heart failure severity *(1)*, but studies on their sensitivity and specificity for different degrees of heart failure produced conflicting results *(3–6)*. Both BNP and NT-proBNP can be used for the diagnosis of heart failure, but there are important differences between the two tests, particularly regarding influence of age and renal function *(1)*. In addition to glomerular filtration, BNP is eliminated from plasma mainly through natriuretic peptide receptors and degraded by neutral endopeptidases *(7–9)*. In contrast, NT-proBNP possibly is largely eliminated by glomerular filtration only *(4)*. This explains the strong influence of renal function on NT-proBNP concentrations. Because of the normal decrease in glomerular filtration rate with increasing age, the diagnostic cutoff for NT-proBNP depends on age *(1)*. This is also true for BNP *(10)*, but to a much lesser extent. Importantly, both BNP and NT-proBNP concentrations can be increased in the setting of hemodialysis *(11–14)*. The prevalence of chronic heart failure is significantly increased in dialysis patients and is associated with left ventricular hypertrophy, which may be secondary to volume overload and hypertension *(15–17)*. Reports on the effect of hemodialysis on plasma concentrations of BNP and NT-proBNP showed significant decreases in BNP *(11, 14, 18)* and significant increases in NT-proBNP *(11)*. This different behavior was explained *(11)* by both the different sizes of BNP (3.5 kDa) and NT-proBNP (8.5 kDa) and their different half-lives [~20 min *(19)* and 60–120 min *(20, 21)*, respectively]. The decrease in BNP plasma concentrations could be attributable to reduced production/secretion of BNP caused by a reduction in plasma volume, elimination by dialysis, or both of these factors *(1, 11)*.

In this study we investigated the effect of the dialysis procedure on BNP concentrations by hemodialysis, measuring BNP (ADVIA BNP assay; Bayer) and NT-proBNP (Elecsys proBNP; Roche Diagnostics). To address the unanswered question of elimination, we measured the concentrations in both plasma and, for the first time reported, in the corresponding dialysis fluid. Although these assays have not been validated for dialysis fluid, the results can be used to compare the relative effects of different membranes. Pre- and postdialysis samples (EDTA plasma) were drawn from 17 chronic hemodialysis patients [11 men and 6 women; mean (SD) age, 72.3 (6.2) years; mean (SD) duration of hemodialysis treatment, 5.6 (2.9) years]. Patients were treated with the Genius Therapy System (Fresenius Medical Care) and assigned to either low-flux (Polyflux 14 L; Gambro) or high-flux membranes (F 60 S; Fresenius Medical Care). The term high-flux membrane refers to a membrane with a high ultrafiltration rate. Because high-flux membranes tend to have larger pores, clearance of mid-molecular-weight molecules is usually higher than with low-flux membranes. Aliquots of the dialysis fluid were collected in EDTA-containing tubes for plasma preparation. The mean (SD) duration of dialysis was 4.4 (0.5) h, and the mean volume of the ultrafiltration was 2.6 (0.9) L. All samples were centrifuged immediately and stored at −20 °C, and all were analyzed at the same time. Postdialysis samples were adjusted for volume changes by use of the hematocrit.

All patients (n = 17) showed increased mean (SE) concentrations for BNP [738 (120) ng/L] and NT-proBNP [25 366 (9062) ng/L] in predialysis specimens. Even the postdialysis concentrations of both BNP [555 (159) ng/L] and NT-proBNP [24 933 (9828) ng/L] were increased. The approved cutoffs for the diagnosis of heart failure in non-renal-decreased populations *(1)* are 100 ng/L for BNP, and 125 ng/L (age <75 years) and 450 ng/L (age ≥75 years) for NT-proBNP. Hemodialysis caused mean (SE) decreases of 21.6 (7.1)% for BNP and 10.1 (4.3)% for

NT-proBNP (n = 17). The mean BNP decrease in the group of patients treated with the low-flux membrane (n = 4) was 18.5 (1.9)% compared with 22.5 (9.4)% in the group treated with the high-flux membrane (n = 13). Whereas treatment with the high-flux membrane also caused a decrease in NT-proBNP of 18.4 (2.3)%, treatment with the low-flux membrane led to an increase in NT-proBNP of 16.8 (4.9)%. Moreover, each patient treated with the low-flux membrane showed this increase in NT-proBNP plasma concentration after hemodialysis (Fig. 1), but none of the patients treated with the high-flux membrane showed this postdialysis increase. With the exception of two patients (both treated with the high-flux membrane), all patients had decreased BNP concentrations after hemodialysis (Fig. 1). One of the two patients mentioned above had the lowest predialysis BNP value (92 ng/L). The other patient was the only one with no change in blood volume, as estimated by a hematocrit of 0.35 before and after dialysis. The length of hemodialysis treatment (4 h) for these two patients was within the range for all other patients, as was the ultrafiltrate volume (2.2 L). Without these two cases, the mean decrease of 21.6 (7.1)% for BNP becomes 30.2 (5.8)% for all patients, and for the patients treated with the high-flux membrane (n = 11), it changes from 22.5 (8.1)% to 34.5 (5.5)%.

Natriuretic peptide concentrations in the combined dialysis and ultrafiltrate fluid were 13–183 ng/L (median, 25 g/L) for BNP and 75–846 ng/L (median, 223 ng/L) for NT-proBNP. Mass balances were calculated as the product of these concentrations and the total volume (dialysis fluid and ultrafiltrate). The mean (SE) mass balance for BNP was 3282 (871) ng with higher values for the group treated with the high-flux membrane [3603 (1106) ng] compared with the group treated with the low-flux membrane [2238 (900) ng]. The total amount of NT-proBNP eliminated showed a mean mass balance of 40 382 (14 809) ng with higher values for the group treated with the high-flux membrane [49 910 (18 674) ng] compared with the group treated with the low-flux membrane [9416 (4416) ng].

Recently, Clerico and Emdin *(22)* published a review on the diagnostic accuracy and prognostic relevance of the measurement of cardiac natriuretic peptides. They pointed out the conflicting results of the few studies published for the clinical relevance of these assays in patients with renal failure. In our study, we therefore investigated the effect of the dialysis procedure on concentrations of BNP and NT-proBNP in hemodialysis patients. Both BNP and NT-proBNP are clearly increased in plasma from hemodialysis patients, with much higher concentrations for NT-proBNP, causing a mean (SE) NT-proBNP:BNP ratio of 28.0 (4.4). After hemodialysis, this ratio increased to a mean value of 36.0 (6.8). The mean NT-proBNP:BNP ratio in ambulatory patients with heart failure was reported to be 8.53 (0.33) *(23)*, but we must emphasize that in the case of dialysis with low-flux membranes, where we observed an increase in plasma NT-proBNP, there is still elimination of NT-proBNP by hemodialysis, as was demonstrated by the results obtained for the dialysis fluid.

Both BNP and NT-proBNP are eliminated during hemodialysis, but they show different behaviors depending on the chosen dialysis membrane. BNP is cleared by both high- and low-flux membranes, with high-flux membranes giving higher clearance (mass balance) and reduction rates. NT-proBNP has clearance and reduction rates similar to BNP when high-flux membranes are used but very low clearance with low-flux membranes, leading to an increase in postdialysis plasma concentrations. This may be explained in part by the different molecular masses of BNP (3.5 kDa) and NT-proBNP (8.5 kDa). Both BNP and NT-proBNP seem to be released into the circulation during the hemodialysis session as shown by increasing postdialysis plasma concentrations in spite of demonstrated clearance. In contrast to NT-proBNP, circulating plasma BNP concentrations seem to be affected by acute intradialytic events. Additional studies are needed to test the influence of dialysis treatment on plasma concentrations of BNP and NT-proBNP and to elucidate the interdependence of the production, release, and elimination of these peptides in dialysis treatment.

We thank B. Scheckel, A. Honig, S. Geis, and B. Metzler for excellent technical assistance.

References

1. McCullough PA, Sandberg KR. Sorting out the evidence on natriuretic peptides. Rev Cardiovasc Med 2003;4(Suppl 4):S13–9.
2. Clerico A, Del Ry S, Giannessi D. Measurement of cardiac natriuretic hormones (atrial natriuretic peptide, brain natriuretic peptide, and related peptides) in clinical practice: the need for a new generation of immunoassay methods. Clin Chem 2000;46:1529–34.
3. Pfister R, Scholz M, Wielckens K, Erdmann E, Schneider CA. The value of natriuretic peptides NT-pro-BNP and BNP for the assessment of left-ventricular volume and function. A prospective study of 150 patients. Dtsch Med Wochenschr 2002;127:2605–9.
4. Alehagen U, Lindstedt G, Eriksson H, Dahlstrom U. Utility of the amino-terminal fragment of pro-brain natriuretic peptide in plasma for the evaluation of cardiac dysfunction in elderly patients in primary health care. Clin Chem 2003;49:1337–46.
5. Hammerer-Lercher A, Neubauer E, Muller S, Pachinger O, Puschendorf B, Mair J. Head-to-head comparison of N-terminal pro-brain natriuretic peptide, brain natriuretic peptide and N-terminal pro-atrial natriuretic peptide in diagnosing left ventricular dysfunction. Clin Chim Acta 2001;310:193–7.
6. Cataliotti A, Malatino LS, Jougasaki M, Zoccali C, Castellino P, Giacone G, et al. Circulating natriuretic peptide concentrations in patients with end-stage renal disease: role of brain natriuretic peptide as a biomarker for ventricular remodeling. Mayo Clin Proc 2001;76:1111–9.
7. Smith MW, Espiner EA, Yandle TG, Charles CJ, Richards AM. Delayed metabolism of human brain natriuretic peptide reflects resistance to neutral endopeptidase. J Endocrinol 2000;167:239–46.
8. Espiner EA, Richards AM, Yandle TG, Nicholls MG. Natriuretic hormones. Endocrinol Metab Clin North Am 1995;24:481–509.
9. Kenny AJ, Bourne A, Ingram J. Hydrolysis of human and pig brain natriuretic peptides, urodilatin, C-type natriuretic peptide and some C-receptor ligands by endopeptidase-24.11. Biochem J 1993;291:83–8.
10. McCullough PA, Duc P, Omland T, McCord J, Nowak RM, Hollander JE, et al. B-type natriuretic peptide and renal function in the diagnosis of heart failure: an analysis from the Breathing Not Properly Multinational Study. Am J Kidney Dis 2003;41:571–9.
11. Clerico A, Caprioli R, Del Ry S, Giannessi D. Clinical relevance of cardiac natriuretic peptides measured by means of competitive and non-competitive immunoassay methods in patients with renal failure on chronic hemodialysis. J Endocrinol Invest 2001;24:24–30.
12. Nitta K, Kawashima A, Yumura W, Naruse M, Oba T, Kabaya T, et al. Plasma concentration of brain natriuretic peptide as an indicator of cardiac ventricular function in patients on hemodialysis. Am J Nephrol 1998;18:411–5.

13. Goto T, Takase H, Toriyama T, Sugiura T, Kurita Y, Tsuru N, et al. Increased circulating levels of natriuretic peptides predict future cardiac event in patients with chronic hemodialysis. Nephron 2002;92:610–5.
14. Naganuma T, Sugimura K, Wada S, Yasumoto R, Sugimura T, Masuda C, et al. The prognostic role of brain natriuretic peptides in hemodialysis patients. Am J Nephrol 2002;22:437–44.
15. Parfrey PS. Cardiac disease in dialysis patients: diagnosis, burden of disease, prognosis, risk factors and management. Nephrol Dial Transplant 2000;15(Suppl 5):58–68.
16. Locatelli F, Pozzoni P, Tentori F, del Vecchio L. Epidemiology of cardiovascular risk in patients with chronic kidney disease. Nephrol Dial Transplant 2003;18(Suppl 7):vii2–vii9.
17. Parfrey PS, Foley RN, Harnett JD, Kent GM, Murray DC, Barre PE. Outcome and risk factors for left ventricular disorders in chronic uraemia. Nephrol Dial Transplant 1996;11:1277–85.
18. Nishikimi T, Futoo Y, Tamano K, Takahashi M, Suzuki T, Minami J, et al. Plasma brain natriuretic peptide levels in chronic hemodialysis patients: influence of coronary artery disease. Am J Kidney Dis 2001;37:1201–8.
19. Holmes SJ, Espiner EA, Richards AM, Yandle TG, Frampton C. Renal, endocrine, and hemodynamic effects of human brain natriuretic peptide in normal man. J Clin Endocrinol Metab 1993;76:91–6.
20. Hammerer-Lercher A, Puschendorf B, Mair J. Cardiac natriuretic peptides: new laboratory parameters in heart failure patients. Clin Lab 2001;47:265–77.
21. Gegenhuber A, Mueller T, Firlinger F, Lenz K, Poelz W, Haltmayer M. Time course of B-type natriuretic peptide (BNP) and N-terminal proBNP changes in patients with decompensated heart failure. Clin Chem 2004;50:454–6.
22. Clerico A, Emdin M. Diagnostic accuracy and prognostic relevance of the measurement of cardiac natriuretic peptides: a review. Clin Chem 2004;50:33–50.
23. Masson S, Vago T, Baldi G, Salio M, De Angelis N, Nicolis E, et al. Comparative measurement of N-terminal pro-brain natriuretic peptide and brain natriuretic peptide in ambulatory patients with heart failure. Clin Chem Lab Med 2002;40:761–3.

DOI: 10.1373/clinchem.2003.030692

Use of PCR-Based Amplification Analysis as a Substitute for the Southern Blot Method for *CYP21* Deletion Detection in Congenital Adrenal Hyperplasia, *Hsien-Hsiung Lee,[1*] Yann-Jinn Lee,[2] Peter Chan,[1] and Ching-Yu Lin[1]* ([1] King Car Food Industrial Co., Yuan-Shan Research Institute, Taiwan, Republic of China; [2] Department of Pediatrics, Mackay Memorial Hospital, and College of Medicine, Taipei Medical University, Taiwan, Republic of China; * address correspondence to this author at: King Car Food Industrial Co., Ltd., Yuan-Shan Research Institute, No. 326 Yuan Shan Rd., Sec. 2, Yuan Shan, Ilan 264, Taiwan, ROC; fax 886-3-9228030, e-mail hhlee@ms2.kingcar.com.tw)

Congenital adrenal hyperplasia (CAH) is a common autosomal recessive disorder caused mainly by defects in the steroid 21-hydroxylase gene (*CYP21*). The defective *CYP21* genes in CAH fall into one of three categories: (*a*) small-scale conversions from *CYP21P*; (*b*) spontaneous mutations; and (*c*) chimeric RCCX modules that include the chimeric *CYP21P/CYP21* gene *(1)* and the chimeric *TNXA/TNXB* gene *(2–4)*. The RCCX module in chromosome 6p21.3 of the human MHC class III region is composed of a part of the *RP* gene (serine/threonine nuclear protein kinase) *(5)*, a full-complement *C4* gene, a full *CYP21*(*P*) gene, and a portion of the *TNX* gene *(6, 7)*. The C4 protein is coded by two genes, *C4A* and *C4B*. The occurrence of a long (20.4 kb) or short (14.1 kb) *C4* gene is attributable to the presence of an endogenous retroviral sequence (6.7 kb), namely HERV-K (C4), in intron 9 *(8)*. The *TNX* gene contains *XA* (*TNXA*) and *TNXB*. *TNXB*, in the downstream *CYP21* gene, is partially duplicated in the downstream *CYP21P* gene, where a truncated gene is termed *TNXA*. Both *TNXA* and *TNXB* are transcribed on the opposite strand. There are two *RP* genes, *RP1* and *RP2*. The *RP2* gene is truncated and corresponds to *RP1* adjacent to *TNXA*. These genes are arranged in the *RP1-C4A-CYP21P-XA-RP2-C4B-CYP21-TNXB* gene sequence and are designated as the bimodule of RCCX (Fig. 1A).

The bimodule is composed of a long module including part of *RP1*, *C4A* (long), *CYP21P*, and *TNXA*, and a short module containing *RP2*, *C4B* (short), *CYP21*, and part of the *TNXB* gene *(2)* (Fig. 1A). In Caucasians, the RCCX module has three possible forms: monomodule, bimodule, and trimodule; the bimodular form is the most frequently occurring form *(9)*. To date, 75 different *CYP21* mutations have been reported *(10)*. Approximately 70% of cases of *CYP21* mutations, including 15 mutations *(10, 11)*, have been attributed to the intergenic recombination of DNA sequences from the highly homologous *CYP21P* pseudogene. The other 60 mutations (in ~10% of cases) are spontaneous. On the other hand, gross gene deletions of the ~30-kb genome, which leave behind the *C4A* and a single *CYP21A*-like gene, have been reported to occur in 20% of alleles in patients with CAH involving a 21-hydroxylase deficiency *(12)*. Obviously, this kind of deletion (and/or conversion) is caused by loss of the *-XA-RP2-C4B-* gene array between these two RCCX modules. However, from recent studies, the consequence of such a gene deletion produces at least two different features of gene arrangement. One of them presents a *-C4A-CYP21P/CYP21-TNXB* gene array, which produces four kinds of chimeric *CYP21P/CYP21* genes *(1, 13)*, whereas the other presents a *-C4A-CYP21P-TNXA/TNXB* array, which contains two kinds of chimeric *TNXA/TNXB* genes *(2, 4)*.

Identification of such a 30-kb gross gene deletion (and/or conversion) in the RCCX region has traditionally required the Southern blot method with multiple isotope-labeled probes and separate restriction endonuclease digestion *(14)*; *Taq*I generates 3.7- (functional) and 3.2-kb (pseudogene) fragments, whereas 2.5- (functional) and 2.0-kb (pseudogene) fragments are produced by double digestion with *Bgl*II/*Eco*RI. Although a nonisotopic Southern method has been used *(15)*, the blocking procedure is still laborious. Furthermore, a heterozygous allele for the deleted *CYP21* gene cannot be detected in the presence of a wild-type allele, and the results may be hard to interpret without a family study. It is possible that an allele with the trimodule *CYP21P-XA-RP2-C4B-CYP21P-XA-RP2-C4B-CYP21-TNXB* may interfere with identification of a bimodule with the *XA-RP2-C4B-* deletion. In such cases, densitometric screening of fragments is prone to errors and may produce a discordant diagnosis.

To circumvent these problems, we developed a long PCR product with allele-specific primers covering the 5′

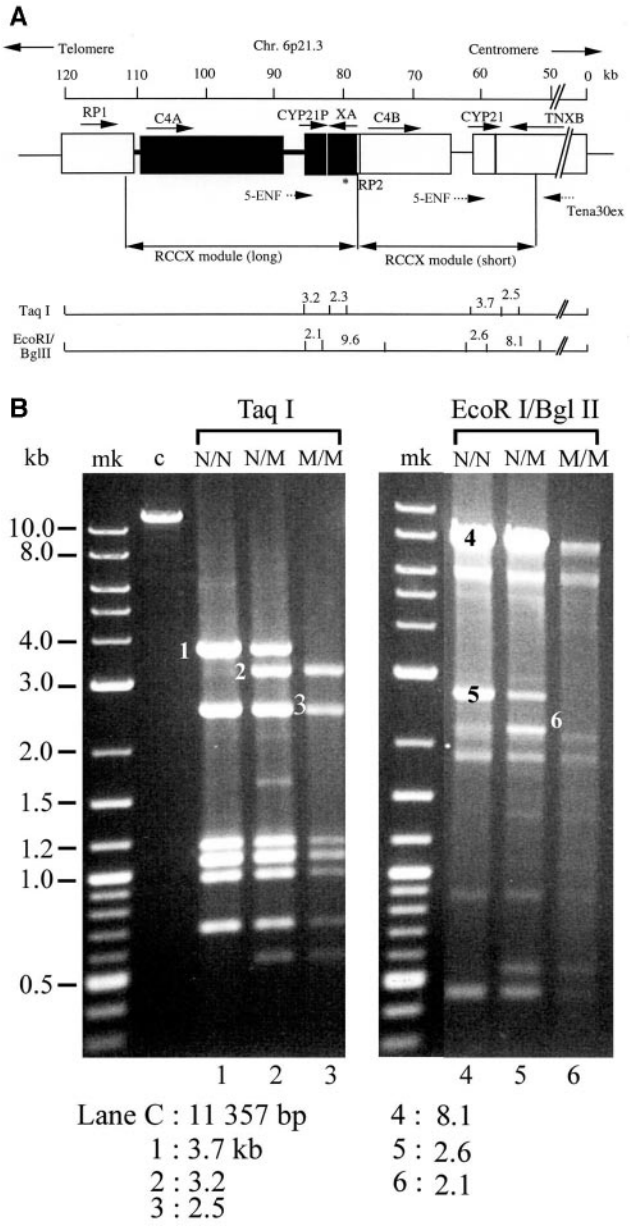

Fig. 1. Bimodular form (*RP1-C4A-CYP21P-XA-RP2-C4B-CYP21-TNXB*) of the RCCX region of chromosome (*Chr.*) 6p21.3 (*A*), and analysis of the 11 357-bp PCR product digested with different restriction enzymes on a 0.8% agarose gel (*B*).

(*A*), □ represents the structure of the wild-type gene, whereas ■ represents a nonfunctional gene (*CYP21P*, *XA*, and *RP2* genes) or a different functional gene (*C4A*). The sizes of the genes (ATG>TGA), including *RP1*, *C4A*, *CYP21P*, *XA*, *RP2*, *C4B*, *CYP21*, and *TNXB*, in the RCCX module are based on the sequence of GenBank accession nos. AL049547 and AF019413. The presence of *C4A* [long gene (20.4 kb)] or *C4B* [short gene (14.1 kb)] depends on the presence of the endogenous 6.7-kb retroviral sequence HERV-K (C4) in intron 9. The bimodular form in the *C4-CYP21* area, consisting of long and short RCCX modules, is also shown. *Solid arrows* indicate the orientation of the transcription, and *dashed arrows* indicate the locations of the primers for PCR amplification. A 120-bp deletion in exon 36 of the *TNXA* gene is marked with an ∗. (*Top*), scale in kb, with the *TNXB* gene starting at 0. (*Bottom*), Southern blot analysis of *Taq*I and *Eco*RI/*Bgl*II restriction fragments in the *C4-CYP21* area. (*B*), *lane c*, 11 357-bp PCR product from a wild-type individual amplified with the paired primers 5-ENF/Tena30exF; *lanes 1–3*, after *Taq*I digestion; *lanes 4–6*, after double digestion with *Bgl*II/*Eco*RI; *lane mk*, 2-log DNA ladder marker (New England BioLabs). *N*, wild-type allele; *M*, allele with a 30-kb deletion of *-XA-RP2-C4B-* in the bimodule of the RCCX region.

end of the *CYP21P* and/or the *CYP21* and *TNXB* genes (Fig. 1A). The PCR product was subjected to *Taq*I and *Bgl*II/*Eco*RI digestions and analyzed by electrophoresis on an agarose gel. The samples used in development of the protocol were from two known CAH families. Both families provided informed consent.

For PCR amplification, genomic DNA, 2.0 U of *Taq*/*Pow* DNA polymerase (Expand Long Template PCR System; Roche Diagnostics), primers (10 pmol each), deoxynucleotide triphosphates (250 μM each), and 10× PCR buffer (commercially supplied) were used for PCR amplification in an 80-μL reaction. The primers Tena30exF (5′-TGACAGATGCGACCCCTGACT-3′; nucleotides 77113~77133l; GenBank accession no. AL049547) and 5-ENF (5′-CTCCATGCACCTCACTGTCTT-3′; nucleotides 88470~88450; GenBank accession no. AL049547; Fig. 1A) were used for amplification of the 11 357-bp PCR product (Fig. 1B, lane c) covering the 5′ end of nucleotide −1810 of the *CYP21* gene and/or *CYP21P* and the *TNXB* gene of exon 31. According to GenBank (accession nos. AL0495470 and AF019413) and past studies *(16, 17)*, these two primers are specific for these two loci, and no polymorphic site exists.

From analysis of the 11.3-kb PCR product of *Taq*I digestion (Fig. 1B, lane c), we found a 3.7-kb fragment possessing the functional *CYP21* gene and a 2.5-kb fragment containing a product of exon 45 to intron 36 of the *TNXA* and *TNXB* genes *(1)* in an apparently healthy individual (Fig. 1B, lane 1). A sample from carrier with a 30-kb deletion in one allele gave 3.7-, 2.5-, and 3.2-kb fragments (*CYP21P*; Fig. 1B, lane 2), whereas a sample from a CAH patient with two alleles containing a 30-kb deletion gave only 3.2- and 2.5-kb fragments (Fig. 1B, lane 3). After *Bgl*II/*Eco*RI double digestion, the sample from the healthy individual (Fig. 1B, lane 4) gave 8.1- (*TNXB*) and 2.6-kb fragments (the *CYP21* gene, more commonly shown in the literature as being 2.5 kb long), whereas the sample from the carrier (Fig. 1B, lane 5) gave 8.1-, 2.6-, and 2.1-kb fragments (*CYP21P*, more commonly shown in the literature as being 2.0 kb long), and the sample from the patient (Fig. 1B, lane 6) gave the 8.1- and 2.1-kb fragments, but not the 2.6-kb fragment. Production of a 3.2-kb fragment by *Taq*I digestion (Fig. 1B, lane 2) and a 2.1-kb fragment by *Bgl*II/*Eco*RI double digestion (Fig. 1B, lane 5) resulted from the 5′-end sequence of *CYP21* being replaced by a *CYP21P*-like sequence, which was caused by a 30-kb deletion of the *-XA-RP2-C4B* gene locus (Fig. 1A). In addition, the absence of the 3.7-kb fragment after *Taq*I digestion (Fig. 1B, lane 3) and of the 2.6-kb fragment after *Bgl*II/*Eco*RI double digestion (Fig. 1B, lane 6) indicated that neither allele in the CAH patient carried the functional *CYP21* gene, whereas they both carried the *CYP21P*-like gene. Obviously, most fragments produced by digestion with these restriction enzymes in the PCR product analysis (Fig. 1B) were also revealed by the conventional Southern blot analysis (Fig. 1A, bottom).

The allele with the heterozygous carrier defect in the single case (Fig. 1B, lane 2) could be directly verified by

Table 1. Frequency of the *CYP21* gene with the 3.2-kb *Taq*I fragment in ethnic Chinese CAH patients.

	Chromosomes	
***CYP21* with the 3.2-kb *Taq* I-produced fragment**	**n**	**%**
IVS2 −12A/C>G combined with 707–714delGAGACTAC mutation	24	77
Chimeric *CYP21P/CYP21*	6[a]	19
CYP21 deletion	1	3
Total	31	

[a] These six chromosomes include one with *CH-1*, two with *CH-2*, and three with *CH-3*. The designations *CH-1*, *CH-2*, and *CH-3* are based on the studies of Lee et al. *(1)*.

the restriction fragments. It is sufficient that the 3.2-kb fragment produced by *Taq*I analysis (Fig. 1B, lane 2) was used to verify deletion of the *-XA-RP2-C4B* gene locus in the RCCX region. It should be noted that the 2.5-kb fragment produced by *Taq*I may be replaced by a 2.4-kb fragment the case of the chimeric *TNXA/TNXB (2)*, in which *TNXB* is replaced by *TNXA*, which extends to exon 36 beyond the 120-bp boundary. We therefore suggest that the use of *Taq*I for restriction enzyme digestion may produce a satisfactory result for diagnosing a 30-kb gross gene deletion (and/or gene conversion) in CAH. The use of *Eco*RI/*Bgl*II double digestion does not seem to be absolutely necessary.

We also used PCR amplification products and amplification-created restriction site analysis *(18)* to analyze samples from 31 ethnic Chinese (i.e., Taiwanese; Table 1) CAH families with one chromosome carrying the 3.2-kb fragment produced by *Taq* I digestion. Members of 6 of these 31 (19%) CAH families carried the chimeric *CYP21P/CYP21* gene *(19)*, and members of 24 families (77%) carried the mutations IVS2 −12A/C>G and 707–714delGAGACTAC *(20)*, whereas only 1 CAH family (3%) carried a *CYP21* deletion *(4)*. Hence, we concluded that the 30-kb gene deletion producing the 3.2-kb fragment by *Taq*I digestion shows diversity and that mutations of IVS2 −12A/C>G combined with 707–714delGAGACTAC among the three *CYP21* haplotypes are abundant and may be the most prevalent ones in ethnic Chinese CAH patients.

Our results indicate that PCR product analysis can reveal the continuity and entirety of fragments of analyzed gene loci and that these do not require densitometry for identification of the gene copy number or the use of family studies for interpreting the heterozygous defective allele. This procedure is saves time and is convenient and practical for the routine laboratory diagnosis of CAH patients.

The two CAH families that provided samples for demonstration of the PCR protocol were referred by Dr. Y.J. Lee from the Department of Pediatrics, Mackay Memorial Hospital, Taipei. This work was supported by the King Car Research Foundation from the King Car Food Industrial Co., Taiwan, Republic of China.

References

1. Lee HH, Chang SF, Lee YJ, Raskin S, Lin SJ, Chao MC, et al. Deletion of the C4-CYP21 repeat module leading to the formation of a chimeric *CYP21P/CYP21* gene in a 9.3-kb fragment as a cause of steroid 21-hydroxylase deficiency. Clin Chem 2003;49:319–22.
2. Koppens PFJ, Hoogenboezem T, Degenhart HJ. Carriership of a defective tenascin-X gene in steroid 21-hydroxylase deficiency patients: *TNXB-TNXA* hybrids in apparent large-scale gene conversions. Hum Mol Genet 2002;11:2581–90.
3. Koppens PFJ, Degenhart HJ. PCR-based detection of *CYP21* deletions. Clin Chem 2003;49:1555–7.
4. Lee HH, Lee YJ, Lin CY, Lee HH, Lee YJ, Lin CY. PCR-based detection of the *CYP21* deletion and *TNXA/TNXB* hybrid in the RCCX module. Genomics 2004;83:944–50.
5. Shen L, Wu LC, Sanlioglu S, Chen R, Mendoza AR, Dangel AW, et al. Structure and genetics of the partially duplicated gene RP located immediately upstream of the complement C4A and the C4B genes in the HLA class III region. Molecular cloning, exon-intron structure, composition retroposon, and breakpoint of gene duplication. J Biol Chem 1994;269:8466–76.
6. Gitelman SE, Bristow J, Miller WL. Mechanism and consequences of the duplication of the human C4/P450c21/gene X locus. Mol Cell Biol 1992;12:2124–34.
7. Bristow J, Tee MK, Gitelman SE, Mellon SH, Miller WL. Tenascin-X: a novel extracellular matrix protein encoded by the human XB gene overlapping P450c21B. J Cell Biol 1993;122:265–78.
8. Yu CY. The complete exon-intron structure of a human complement component C4A gene. DNA sequences, polymorphism, and linkage to the 21-hydroxylase genes. J Immunol 1991;146:1057–66.
9. Blanchong CA, Zhou B, Rupert KL, Chung EK, Jones KN, Sotos JF, et al. Deficiencies of human complement component C4A and C4B and heterozygosity in length variants of RP-C4-CYP21-TNX (RCCX) modules in Caucasians: the load of RCCX genetic diversity on major histocompatibility complex-associated disease. J Exp Med 2000;191:2183–96.
10. Human Gene Mutation Database. Cytochrome P450, subfamily XXIA (steroid 21-hydroxylase, congenital adrenal hyperplasia), polypeptide 2. http://uwcmml1s.uwcm.ac.uk/uwcm/mg/search/120605.html (accessed October 2003).
11. Lee HH. CYP21 mutations and congenital adrenal hyperplasia. Clin Genet 2001;59:293–301.
12. White PC, Speiser PW. Congenital adrenal hyperplasia due to 21-hydroxylase deficiency. Endocr Rev 2000;21:245–91.
13. L'Allemand D, Tardy V, Gruters A, Schnabel D, Krude H, Morel Y. How a patient homozygous for a 30-kb deletion of the *C4-CYP21* genomic region can have a nonclassic form of 21-hydroxylase deficiency. J Clin Endocrinol Metab 2000;85:4562–7.
14. White PC, Vitek A, Dupont B, New MI. Characterization of frequent deletions causing steroid 21-hydroxylase deficiency. Proc Natl Acad Sci U S A 1988;85:4436–40.
15. Krone N, Roscher AA, Schwarz HP, Braun A. Comprehensive analytical strategy for mutation screening in 21-hydroxylase deficiency. Clin Chem 1998;44:2075–82.
16. Higashi Y, Yoshioka H, Yamane M, Gotoh O, Fujii-Kuriyama Y. Complete nucleotide sequence of two steroid 21-hydroxylase genes tandemly arranged in human chromosome: a pseudogene and a genuine gene. Proc Natl Acad Sci U S A 1986;83:2841–5.
17. Rodrigues NR, Dunham I, Yu CY, Carroll MC, Porter RR, Campbell RD. Molecular characterization of the HLA-linked steroid 21-hydroxylase B gene from an individual with congenital adrenal hyperplasia. EMBO J 1987;6:1653–61.
18. Lee HH, Chao HT, Ng HT, Choo KB. Direct molecular diagnosis of *CYP21* mutations in congenital adrenal hyperplasia. J Med Genet 1996;33:371–5.
19. Lee HH. The chimeric CYP21P/CYP21 gene and 21-hydroxylase deficiency. J Hum Genet 2004;49:65–72.
20. Lee HH, Chang SF, Tsai FJ, Tsai LP, Lin CY. Mutation of IVS2-12 A/C > G in combination with 707-714delGAGACTAC in the *CYP21* gene is caused by deletion of the C4-CYP21 repeat module with steroid 21-hydroxylase deficiency. J Clin Endocrinol Metab 2003;88:2726–9.

DOI: 10.1373/clinchem.2003.028597

Optimum Collection and Storage Conditions for Ghrelin Measurements: Octanoyl Modification of Ghrelin Is Rapidly Hydrolyzed to Desacyl Ghrelin in Blood Samples, *Hiroshi Hosoda,[1,3] Kentaro Doi,[1] Noritoshi Nagaya,[2] Hiroyuki Okumura,[2] Eiichiro Nakagawa,[2] Mitsunobu Enomoto,[2] Fumiaki Ono,[2] and Kenji Kangawa[1,3*]* ([1] Department of Biochemistry, National Cardiovascular Center Research Institute, and [2] Department of Internal Medicine, National Cardiovascular Center, Osaka 565-8565, Japan; [3] Translational Research Center, Kyoto University Hospital, Kyoto 606-8507, Japan; * address correspondence to this author at: Department of Biochemistry, National Cardiovascular Center Research Institute, National Cardiovascular Center, Osaka 565-8565, Japan; fax 81-6-6835-5402, e-mail kangawa@ri.ncvc.go.jp)

Ghrelin is an acylated peptide with growth-hormone-releasing activity *(1)*. It was first isolated from rat and human stomach during the search for an endogenous ligand to the "orphan" G-protein-coupled receptor, growth hormone secretagogue receptor *(2)*. The peptide contains 28 amino acids, and n-octanoylation of the Ser-3 hydroxyl group is necessary for biological activity. Most studies have focused on the somatotropic and orexigenic roles of ghrelin; therefore, little is known about the kinetics of this peptide. Because the ester bond is both chemically and enzymatically unstable, elimination of the octanoyl modification of ghrelin can occur during storage, handling, and/or dissolution in culture medium *(3)*. Because of increased interest in ghrelin measurements, a standardized method of sample collection is required.

In the present study, which focused on the active form of ghrelin, we investigated the effects of anticoagulants and storage conditions on ghrelin stability. To distinguish the active form of ghrelin, we established two ghrelin-specific RIAs; N-RIA recognizes the N-terminal, octanoyl-modified portion of the peptide, whereas C-RIA recognizes the C-terminal portion. Thus, the value determined by N-RIA specifically measures active ghrelin, whereas the value determined by C-RIA gives the total ghrelin immunoreactivity, including both active and desacyl ghrelin *(4–6)*. The minimum detectable quantities in the N- and C-RIAs were 5.0 and 50 pmol/L, respectively. The respective intra- and interassay CV were 3% and 6% for the N-RIA and 6% and 9% for the C-RIA (n = 8 assays). Data are reported as the mean (SD). Comparisons of the time course of ghrelin concentrations between subgroups were made by two-way ANOVA for repeated measures, followed by the Scheffé test. $P < 0.05$ was considered statistically significant.

All blood samples were taken from three healthy male volunteers who gave written informed consent. Blood was taken from the forearm vein and immediately divided into tubes for serum and plasma preparation using (*a*) disodium EDTA (1 g/L) with aprotinin (500 000 kIU/L), (*b*) disodium EDTA alone, (*c*) heparin sodium, or (*d*) no anticoagulant. Synthetic human ghrelin was added to each blood sample at a final concentration of 40 μg/L; each sample was then sequentially divided into two aliquots for incubation at either 4 or 37 °C. After incubation for 0, 30, and 60 min, blood samples were centrifuged, diluted 1:200 in RIA buffer, and subjected to ghrelin-specific RIAs. A comparison of the effects of different anticoagulants on the detected ghrelin concentrations is shown in Table 1A. Although the serum and three different plasma samples tested gave comparable results for total ghrelin by C-RIA, the N-RIA gave ghrelin concentrations that were significantly decreased at 37 °C. When the ghrelin was measured by N-RIA, serum samples were highly affected by such treatment; samples stored for 60 min at 37 °C lost ~35% of the ghrelin compared with the basal values at 0 min ($P < 0.05$). The ghrelin concentrations in samples containing heparin as an anticoagulant were also significantly decreased ($P < 0.05$). When EDTA–aprotinin was used as the anticoagulant for plasma treatment, the decreases in ghrelin stability were smaller than for other procedures. Storage at 4 °C also improved ghrelin stability.

To explore optimum storage conditions, we examined the effect of plasma pH on ghrelin stability. The EDTA–aprotinin-treated plasma (n = 3) was divided into five samples; the pH was then adjusted to 3, 4, 5, 6, or 7.4 with 1 mol/L HCl. Synthetic human ghrelin was then added to each sample aliquot at a final concentration of 75 μg/L. Each of the five plasma aliquots was then subdivided into two, with one stored at 4 °C and the other stored at 37 °C. The effects of acidification on ghrelin stability in plasma are summarized in Table 1B. When stored at 37 °C, ghrelin concentrations measured by N-RIA gradually decreased at all pH values tested. However, ghrelin was most stable in highly acidified plasma samples (pH 3–4). At pH 3–5 and a storage temperature of 4 °C, the stability of ghrelin in plasma did not change significantly over a 6-h period. By C-RIA, ghrelin concentrations remained stable across the different pH and storage temperature conditions.

We then evaluated the effects of repeated freezing and thawing on the stability of ghrelin. EDTA–aprotinin-treated plasma samples were divided into two pH groups; one was acidified to pH 4, whereas the other was not acidified (pH 7.4). After the addition of synthetic human ghrelin (75 μg/L), we subjected the samples to four freeze–thaw cycles. Repeated freezing and thawing also influenced ghrelin stability (Table 1C). As in the N-RIA, ghrelin concentrations in untreated plasma samples decreased significantly with each successive freeze–thaw cycle, whereas the ghrelin remained relatively stable after acidification. Ghrelin concentrations by C-RIA were unchanged despite repeated freeze–thaw treatments in both acidified and untreated plasma samples.

As well as differences in assay methodologies, differences in sample handling, such as the method of storage, effects of anticoagulants, or previous freezing and thawing of the samples, could influence the reported values *(7–10)*. Instability of peptides and proteins can be divided into two forms: chemical and physical instability *(11, 12)*.

Table 1. Effect of anticoagulants and storage conditions on ghrelin stability.[a]

A. Ghrelin measurements in serum and different plasma samples

		Mean (SD) percentage of baseline					
		C-RIA			N-RIA		
		0 min	30 min	60 min	0 min	30 min	60 min
EDTA–aprotinin	37°C	100.0 (6.2)	101.0 (4.4)	102.9 (10.4)	100.0 (9.1)	102.6 (5.1)	89.6 (1.8)
	4°C		100.4 (4.0)	101.1 (4.5)		97.4 (1.3)	99.9 (12.3)
EDTA	37°C	100.0 (7.4)	98.5 (5.4)	98.4 (3.8)	100.0 (3.7)	83.6 (9.9)	85.3 (3.3)
	4°C		98.2 (2.6)	98.6 (7.6)		96.5 (1.8)	88.3 (6.5)
Heparin	37°C	100.0 (10.0)	104.3 (6.6)	91.1 (13.1)	100.0 (5.0)	88.1 (2.3)	77.4 (2.2)[b]
	4°C		104.4 (6.2)	102.1 (12.2)		92.5 (0.8)	86.9 (4.3)
Serum	37°C	100.0 (9.9)	100.4 (10.3)	98.2 (11.8)	100.0 (10.9)	87.5 (1.3)	65.1 (6.9)[b]
	4°C		96.2 (7.1)	98.4 (8.7)		96.5 (0.8)	94.6 (7.4)

B. Effects of storage pH, duration, and temperature on ghrelin stability

			Mean (SD) percentage of baseline					
		pH	0 h	1 h	2 h	3 h	4 h	6 h
C-RIA	RT	7.5	100.0 (6.6)	95.7 (5.0)	95.5 (6.3)		98.5 (5.4)	102.1 (6.5)
		6	100.0 (5.2)	96.0 (5.3)	91.3 (8.2)		96.6 (6.1)	97.9 (4.6)
		5	100.0 (6.1)	101.9 (8.2)	99.0 (6.0)		100.3 (8.4)	104.1 (5.2)
		4	100.0 (9.2)	96.0 (6.4)	98.0 (3.5)		100.2 (2.9)	97.1 (3.4)
		3	100.0 (2.2)	96.1 (4.9)	95.6 (4.7)		95.2 (2.7)	89.8 (3.9)
	4°C	7.5	100.0 (2.0)			100.9 (8.3)		99.3 (3.3)
		6	100.0 (3.6)			95.1 (4.1)		98.1 (1.8)
		5	100.0 (4.0)			101.2 (7.8)		105.9 (5.1)
		4	100.0 (7.1)			99.1 (3.3)		99.1 (4.1)
		3	100.0 (4.2)			99.4 (1.7)		101.3 (5.0)
N-RIA	RT	7.5	100.0 (5.0)	81.8 (1.0)[c]	72.0 (3.1)[d]		50.6 (2.9)[d]	37.5 (2.6)[d]
		6	100.0 (8.8)	93.3 (5.7)	78.8 (2.7)[c]		54.7 (1.2)[d]	38.8 (2.9)[d]
		5	100.0 (12.8)	92.8 (4.1)	86.4 (2.2)		74.1 (3.8)[b]	59.2 (7.6)[c]
		4	100.0 (12.5)	94.5 (7.4)	90.8 (5.2)		78.8 (3.1)[b]	74.0 (9.8)[c]
		3	100.0 (6.0)	98.4 (1.9)	96.9 (0.9)		82.2 (2.4)[b]	76.4 (6.1)[c]
	4°C	7.5	100.0 (6.9)			66.5 (4.4)		40.4 (3.5)[b]
		6	100.0 (6.1)			96.3 (0.2)		83.0 (1.2)[b]
		5	100.0 (5.5)			103.2 (2.0)		87.7 (11.7)
		4	100.0 (0.8)			102.2 (0.4)		99.6 (5.7)
		3	100.0 (12.8)			105.8 (0.3)		103.5 (1.6)

C. Effects of repeated freeze–thaw cycles on plasma ghrelin stability

		Cycles				
		1	2	3	4	5
C-RIA	HCl (−)	100.0 (8.8)	94.7 (7.2)	92.8 (6.6)	95.5 (5.1)	91.2 (7.3)
	HCl (+)	100.0 (5.2)	96.0 (5.3)	91.3 (8.2)	96.6 (6.1)	97.9 (4.6)
N-RIA	HCl (−)	100.0 (4.0)	89.8 (2.7)[b]	59.9 (6.3)[d]	28.1 (5.2)[d]	14.5 (3.3)[d]
	HCl (+)	100.0 (4.3)	94.1 (4.2)	94.4 (5.7)	95.4 (4.2)	93.8 (7.0)

[a] Results are for triplicate measurements. Values measured at 0 min, 0 h, or zero cycles are the baseline values.
[b–d] Compared with baseline: [b] $P < 0.05$; [c] $P < 0.01$; [d] $P < 0.001$.

The chemical degradation of peptides is influenced by the pH of the aqueous solution; human parathyroid hormone and luteinizing-hormone-releasing hormone derivatives are examples *(13–15)*. We demonstrated that in whole blood and plasma, ghrelin is unstable. The degradation of octanoylated ghrelin was shown to be attributable to hydrolysis to desacyl ghrelin (see Fig. 1 in the Data Supplement that accompanies the online version of this Technical Brief at http://www.clinchem.org/content/vol50/issue6/). Acidification is a simple, reliable procedure that protected against degradation of the acylated modification and dramatically improved stability at pH 4. On the other hand, the stability of the octanoyl modification of ghrelin was markedly decreased in strongly acidic (below pH 2), neutral, and alkaline solutions (data not shown).

We evaluated the effectiveness of measuring active ghrelin compared with total ghrelin in response to oral glucose tolerance tests (OGTTs). Four healthy male volunteers (age range, 28–35 years; body mass index, 21.5–23.7 kg/m^2) were examined on 2 separate days (100 g of glucose administered on 1 day, and 50 g of glucose administered on the other day) at least 2 weeks apart in a randomized, crossover study. After the volunteers fasted overnight, 50 or 100 g of glucose was administered orally between 0930–1000. Blood samples were obtained at 0, 1, 2, 3, and 4 h after glucose ingestion. To each plasma sample was added 1 mol/L HCl (10% of plasma volume), which acidified the sample to pH ~4; samples were then treated with Sep-Pak C_{18} cartridges for ghrelin RIAs. After glucose ingestion, the mean plasma ghrelin concentrations as determined by N-RIA and C-RIA decreased to a nadir at 1 h (Fig. 1). At this point, 60.3% and 73.0% of the basal concentration was detected by the N-RIA and C-RIA, respectively, after the 100-g OGTT, and 64.2% and 78.7% of the basal concentration was detected after the 50-g OGTT. Plasma ghrelin values increased thereafter, although plasma ghrelin concentrations measured by the C-RIA were significantly lower for up to 2 h after the 100-g glucose load. The N-RIA for ghrelin could detect differences in the changes in ghrelin concentrations between the 50-g and 100-g OGTTs at 3 h. The ghrelin values observed with the C-RIA exhibited changes similar those in the N-RIA, but the changes were small and delayed. These effects may be attributable to the differential rates of metabolic turnover for octanoylated and desacylated ghrelin in circulating blood (see Fig. 2 in the online Date Supplement).

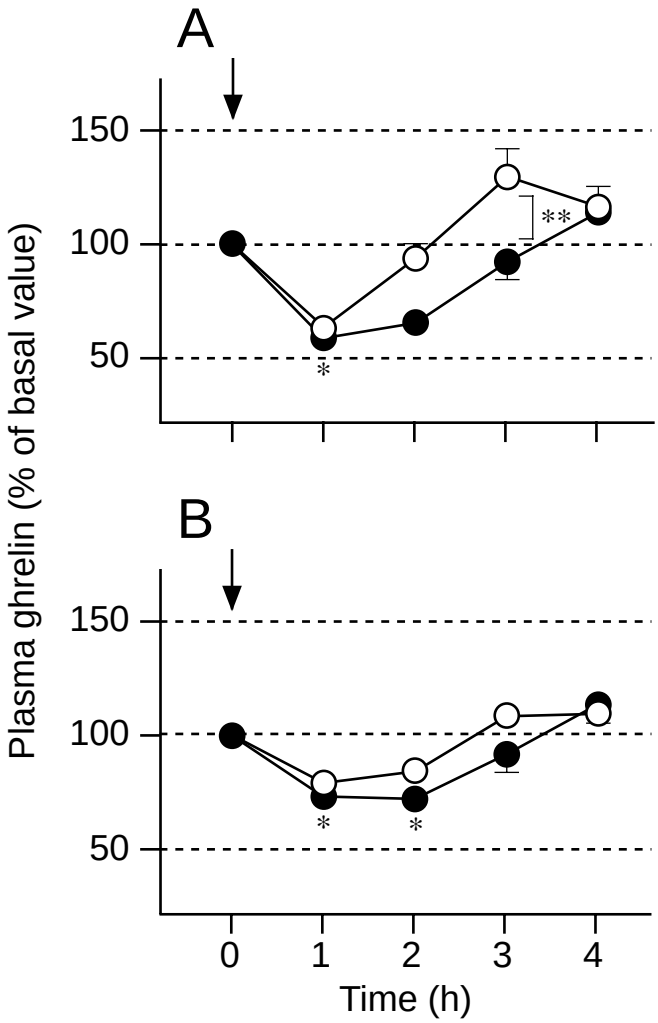

Fig. 1. Plasma ghrelin response to 50-g (○) and 100-g (●) OGTTs in four healthy individuals.

Plasma ghrelin concentrations assayed by N-RIA (*A*) and C-RIA (*B*) are given as the mean (SD; *error bars*) percentage change from basal values. *, $P < 0.05$ compared with basal values; **, $P < 0.05$ for difference in plasma ghrelin between 50-g and 100-g glucose loads.

The results for the plasma ghrelin response to the OGTTs show that measuring the concentration of active ghrelin is useful for studying plasma ghrelin changes over short time periods. Plasma concentrations of active ghrelin changed more rapidly and dynamically than those of total ghrelin immunoreactivity. Fasting led to markedly increased plasma ghrelin values as measured by N-RIA, and the values decreased in a clearer dose-dependent manner in rats after glucose injection compared with those measured by C-RIA *(16)*. The proportion of active ghrelin in plasma was 2–5% of total ghrelin in rodents. In this study, the quantity of active ghrelin was ~10% of the total ghrelin in human plasma (data not shown). These findings imply that inactive desacyl ghrelin circulates in the bloodstream at much higher concentrations than active ghrelin. Similar to previous studies in which ghrelin concentrations were measured by C-RIA *(17)*, desacyl ghrelin is relatively stable, and its stability is not altered by different storage conditions. An analogous situation has been reported for the activity of pancreatic beta cells, which secrete insulin and C-peptide in a 1:1 molar ratio. However, the half-life of C-peptide is much longer than that of insulin, leaving more C-peptide available in the circulation for quantification *(18, 19)*. Measurement of C-peptide provides an assessment of β-cell secretory activity. Similarly, desacyl ghrelin concentrations may serve as an indicator of ghrelin secretory function *(20)*.

To acquire accurate data on ghrelin concentrations, this study recommends a standard procedure for the collection of blood samples: (*a*) the collection of blood samples with EDTA–aprotinin is preferred; (*b*) blood samples should be chilled and centrifuged as soon as possible, at least within 30 min after collection; and (*c*) because acidification is the best method for the preservation of plasma ghrelin, 1 mol/L HCl (10% of sample volume) can be added to the plasma sample for adjustment to pH 4.

We thank H. Mondo and M. Miyazaki for technical assistance. This work was supported by grants from the Ministry of Education, Science, Sports and Culture of Japan; the Ministry of Health, Labor and Welfare of Japan; the Promotion of Fundamental Studies in Health Science

from the Organization for Pharmaceutical Safety and Research of Japan; and the Takeda Science Foundation.

References

1. Kojima M, Hosoda H, Date Y, Nakazato M, Matsuo H, Kangawa K. Ghrelin is a growth-hormone-releasing acylated peptide from stomach. Nature 1999; 402:656–60.
2. Howard AD, Feighner SD, Cully DF, Arena JP, Liberator PA, Rosenblum CI, et al. A receptor in pituitary and hypothalamus that functions in growth hormone release. Science 1996;273:974–7.
3. Kanamoto N, Akamizu T, Hosoda H, Hataya Y, Ariyasu H, Takaya K, et al. Substantial production of ghrelin by a human medullary thyroid carcinoma cell line. J Clin Endocrinol Metab 2001;86:4984–90.
4. Hosoda H, Kojima M, Matsuo H, Kangawa K. Ghrelin and des-acyl ghrelin: two major forms of rat ghrelin peptide in gastrointestinal tissue. Biochem Biophys Res Commun 2000;279:909–13.
5. Date Y, Kojima M, Hosoda H, Sawaguchi A, Mondal MS, Suganuma T, et al. Ghrelin, a novel growth hormone-releasing acylated peptide, is synthesized in a distinct endocrine cell type in the gastrointestinal tracts of rats and humans. Endocrinology 2000;141:4255–61.
6. Hosoda H, Kojima M, Mizushima T, Shimizu S, Kangawa K. Structural divergence of human ghrelin. Identification of multiple ghrelin-derived molecules produced by post-translational processing. J Biol Chem 2003;278: 64–70.
7. Nelesen RA, Dimsdale JE, Ziegler MG. Plasma atrial natriuretic peptide is unstable under most storage conditions. Circulation 1992;86:463–6.
8. Flower L, Ahuja RH, Humphries SE, Mohamed-Ali V. Effects of sample handling on the stability of interleukin 6, tumour necrosis factor-α and leptin. Cytokine 2000;12:1712–6.
9. Miki K, Sudo A. Effect of urine pH, storage time, and temperature on stability of catecholamines, cortisol, and creatinine. Clin Chem 1998;44(8 Pt 1):1759–62.
10. Evans MJ, Livesey JH, Ellis MJ, Yandle TG. Effect of anticoagulants and storage temperatures on stability of plasma and serum hormones. Clin Biochem 2001;34:107–12.
11. Reubsaet JL, Beijnen JH, Bult A, van Maanen RJ, Marchal JA, Underberg WJ. Analytical techniques used to study the degradation of proteins and peptides: chemical instability. J Pharm Biomed Anal 1998;17:955–78.
12. Reubsaet JL, Beijnen JH, Bult A, van Maanen RJ, Marchal JA, Underberg WJ. Analytical techniques used to study the degradation of proteins and peptides: physical instability. J Pharm Biomed Anal 1998;17:979–84.
13. Nabuchi Y, Fujiwara E, Kuboniwa H, Asoh Y, Ushio H. The stability and degradation pathway of recombinant human parathyroid hormone: deamidation of asparaginyl residue and peptide bond cleavage at aspartyl and asparaginyl residues. Pharm Res 1997;14:1685–90.
14. Strickley RG, Brandl M, Chan KW, Straub K, Gu L. High-performance liquid chromatographic (HPLC) and HPLC-mass spectrometric (MS) analysis of the degradation of the luteinizing hormone-releasing hormone (LH-RH) antagonist RS-26306 in aqueous solution. Pharm Res 1990;7:530–6.
15. Hoitink MA, Beijnen JH, Boschma MU, Bult A, van der Houwen OA, Wiese G, et al. Degradation kinetics of three gonadorelin analogues: developing a method for calculating epimerization parameters. Pharm Res 1998;15: 1449–55.
16. Ariyasu H, Takaya K, Hosoda H, Iwakura H, Ebihara K, Mori K, et al. Delayed short-term secretory regulation of ghrelin in obese animals: evidenced by a specific RIA for the active form of ghrelin. Endocrinology 2002;143:3341–50.
17. Groschl M, Wagner R, Dotsch J, Rascher W, Rauh M. Preanalytical influences on the measurement of ghrelin. Clin Chem 2002;48:1114–6.
18. Myrick JE, Gunter EW, Maggio VL, Miller DT, Hannon WH. An improved radioimmunoassay of C-peptide and its application in a multiyear study. Clin Chem 1989;35:37–42.
19. Horwitz DL, Starr JI, Mako ME, Blackard WG, Rubenstein AH. Proinsulin, insulin, and C-peptide concentrations in human portal and peripheral blood. J Clin Invest 1975;55:1278–83.
20. Cummings DE, Purnell JQ, Frayo RS, Schmidova K, Wisse BE, Weigle DS. A preprandial rise in plasma ghrelin levels suggests a role in meal initiation in humans. Diabetes 2001;50:1714–9.

DOI: 10.1373/clinchem.2003.025841

Substitution of 3′-Phosphate Cap with a Carbon-Based Blocker Reduces the Possibility of Fluorescence Resonance Energy Transfer Probe Failure in Real-Time PCR Assays, *Kendall W. Cradic,[1] Jason E. Wells,[2] Lindsay Allen,[2] Kent E. Kruckeberg,[1] Ravinder J. Singh,[1] and Stefan K.G. Grebe[1,3*]* (Departments of [1] Laboratory Medicine and Pathology and [3] Medicine, Mayo Clinic, Rochester, MN; [2] Idaho Technology Inc., Salt Lake City, UT; * address correspondence to this author at: Endocrine Laboratory, Hilton 730C, Mayo Clinic, 200 1st St. SW, Rochester, MN 55905; fax 507-284-9758, e-mail grebs@mayo.edu)

During the last decade, research and clinical use of real-time PCR applications has continued to grow in importance *(1)*. Many laboratories that use real-time PCR with fluorescent probes experience an unexplained loss of probe fluorescence at some stage, in particular with pairs of fluorescence resonance energy transfer (FRET) probes. Photobleaching is often assumed to be the cause. Structural integrity of the oligonucleotides is also a major factor, and its loss has been shown to correlate with repeated freeze–thaw cycles *(2)*. Laboratories guard against these two problems by aliquoting probes and protecting them from light. Despite these precautions, inexplicable FRET probe failures are still observed. In one recent such case, we were able to determine an additional mechanism for FRET probe failure: loss of the phosphate cap from the 3′ end of a probe. To our knowledge, this has not been described previously. Our studies revealed that this may be a common and important problem, intrinsic to 3′-phosphate-blocking chemistry. We also found that alternative terminating groups may be a preferable option to 3′-phosphate blocking.

A 3-nmol/L synthesis-scale LightCycler™ hybridization probe set was purchased from Idaho Technology Inc. Biochem in April 2003. As is common practice, the manufacturer produced a large-scale synthesis and, after shipping our order, archived the remainder for a possible future reorder. The first half of the batch (α-probe set) was sent immediately, whereas the second half (β-probe set) was stored lyophilized for 6 months at −20 °C and then shipped with our next order.

Oligonucleotides from the first shipment were used in PCR reactions in a LightCycler with satisfactory results. PCR conditions were as follows: 1× LightCycler FastStart DNA Master Hybridization Probe Mix (Roche Diagnostics), $MgCl_2$ (final concentration, 3.5 mM), 0.5 μM each of the forward (5′-GGCCTTTCTGAAGCAAG-3′) and reverse (5′-GACGATTTCTTATTTCACAGCTCC-3′) primers, 0.2 μM each of the donor (5′-GGACGCAGAGGGGATGG-FITC-3′, where FITC is fluorescein isothiocyanate) and acceptor (LCRed640-GTGTATGGGACCCGCCAG-phosphate) probes, and 2 μL of cDNA template mixture. The final reaction volume was 10 μL. The reaction started with an initial melting step at 95 °C for 10 min followed by 45 cycles of 95 °C for 2 s, 57 °C for 10 s, and 72 °C for 5 s.

Loss of fluorescence activity was first observed when we received the β-probe set. PCR reactions were carried out under the same conditions, but the amplification

curves displayed extremely low signal intensities relative to the α-probe set that was being replaced (Fig. 1A). We excluded photobleaching by measuring raw probe fluorescence. We then set up two additional PCR reactions, pairing each α-set of oligonucleotides with the corresponding β-set FRET partners. The loss of fluorescent activity corresponded with the β-set LCRed640 probe, whereas the α-set LCRed640 probe and the fluorescein donor probes from both the α- and β-sets were fully functional (Fig. 1A).

Agarose gel electrophoresis demonstrated a diminished target band at 389 bp as well as a strong additional band between the 50- and 150-bp size markers in the reaction that contained the suspect β-set LCRed640 probe. The extra band in the β-probe reaction corresponded to the size of a PCR product that would have been formed if the β-probe had acted as a primer. Additional PCR reactions were run to explore this possibility, including the use of an unlabeled primer identical in sequence to the LCRed640 probe, which confirmed our hypothesis (Fig. 1B). Finally, we excised the low-molecular-weight band in the β-probe reaction from the gel and sequenced it, using the reverse PCR primer as a sequencing primer. The DNA fragment had the sequence predicted if the β-set LCRed640 probe had acted as a PCR primer, including the full acceptor probe sequence, and terminated at its 5′ end (data not shown).

In a typical FRET probe arrangement, it is critical that neither the donor nor the acceptor probe can be elongated during PCR. For the donor probe, the fluorescent dye at the 3′ end blocks PCR extension, whereas for the acceptor probe, a nonfluorescent blocking agent, typically a phosphate group, is linked to the 3′ hydroxyl of the terminal base. If a blocking group is lost, then a probe can act as a PCR primer. Because of the shorter length of the PCR product formed by this aberrant priming and the higher melting temperature (T_m) of the probes compared with the PCR primers, formation of these aberrant products will be greatly favored over the intended full-length target. If the blocking group is lost from the 3′ FRET probe, very few targets will be produced that contain sequences complementary to both the 5′ and the 3′ FRET probes; hence, little or no detection signal will be observed. Our results demonstrate that this has indeed happened and that extension has occurred from our acceptor probe, implying loss of its 3′-phosphate cap.

We suspect that this is the cause of a significant proportion of FRET probe failures. When we evaluated an unrelated probe set that had suddenly and inexplicably failed and was also purchased in two batches (from Genset Oligos), we found a low-molecular-weight PCR product that was consistent with phosphate-cap loss from the 3′ probe (data not shown). We therefore decided to explore whether alternative 3′ capping moieties might be less susceptible to degradation. After exploring the available chemistries and their costs, we selected a C3 carbon spacer (cat. no. 20-2913; Glen Research) as a blocker of potentially enhanced stability. A 72-base single-stranded template was designed and synthesized as a complement

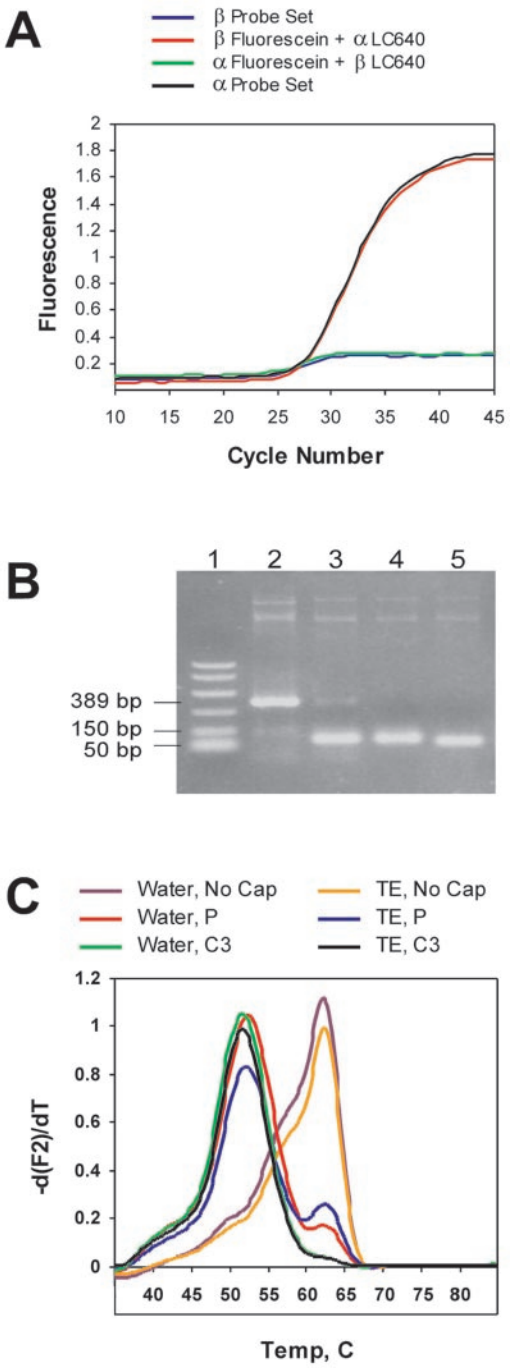

Fig. 1. Amplification curves showing a loss of signal intensity in reactions containing the β-LCRed640 probe (*A*); electrophoresis of LightCycler PCR products (*B*); and negative derivative melting curve profiles of probe extension reactions of probe sets with differently 3′-capped LCRed640 3′ probes (*C*).

(*B*), *lane 1*, size markers; *lane 2*, α-probe set reaction; *lane 3*, β-probe set reaction; *lane 4*, PCR reaction run with β-LCRed640 probe and reverse primer only (the forward primer and the fluorescein probe were omitted); *lane 5*, PCR reaction run with reverse primer together with a forward primer matching the β-LCRed640 probe sequence and omitting the original forward primer and all probes. The LCRed640 probe appears to act as a primer, implying loss of 3′-capping phosphate. The slightly faster migration of the PCR product in *lane 5* reflects the absence of the LCRed640 dye. (*C*), profiles were generated after week 8 of probe storage in water or Tris-EDTA (*TE*) at 4 °C. *P*, phosphate; *C3*, C3 carbon spacer.

for probe hybridization (5′-GTCCCTTAAGTAACTAGA-ATAATGGAATTGGGCTCCTTATAATCAAGCACTCAT-AACAACATAATCATTGC-3′). Probes were then designed such that the donor fluorescein probe (5′-AATGATTATGTTGTTATGAGTGCTTG-FITC-3′) acted as the anchor with a T_m of 62 °C. Three LCRed640 probes were synthesized with identical sequences (5′ LCRed640-TATAAGGAGCCCAATT-3′) and different 3′ terminations. The first had no cap and served as a positive control, the second had a standard phosphate cap, and the third was synthesized with a 3′ C3 carbon spacer. Each probe was stored in both water and Tris-EDTA (738 mmol/L Tris-HCl, 0.5 mol/L EDTA, pH 8.3) at 4 and −20 °C. On a weekly basis, the probes were tested in a LightCycler in separate primer extension reactions followed by melting curve analysis, The 10-μL reactions contained (final concentrations) 1× PCR buffer (Idaho Technology Inc.), 4 mM $MgCl_2$, 0.2 mM each of the deoxynucleotide triphosphates, 0.1 MU/L KlenTaq1™ (Ab Peptides, Inc.), and 0.2 μM each of the complementary strand, LCRed640 probe, and fluorescein probe. The melting curve analysis conditions were 3–15 cycles of 94 °C for denaturing and 50 °C for annealing, followed by melting from 35 to 85 °C. In this experiment, any loss of 3′ capping of the acceptor FRET probe will lead to probe extension. As the acceptor probe becomes extended, its T_m increases from 51 °C to ~70 °C, making it the anchor for formation of a secondary peak at 62 °C in the negative-derivative melting profiles (Fig. 1C). This secondary peak corresponds to the dissociation of the fluorescein donor probe. For every secondary peak found, we calculated the peak area and determined the percentage of signal in the secondary peak compared with the total signal. This percentage was used to estimate the amount of extended probe per reaction.

At 4 °C, the 3′-phosphate terminus was unstable in both Tris-EDTA and water. By contrast, the three-carbon cap remained stable throughout all storage conditions tested. Even when stored at 4 °C for 8 weeks, the C3 probe showed no indication of probe extension (Fig. 1C and Table 1). None of the oligonucleotides stored at −20 °C showed evidence of degradation during 8 weeks. However, in circumstances in which different buffer systems are used and freeze–thaw cycles are more common, one might see a higher amount of phosphate cap degradation even at lower temperatures.

Table 1. Percentage of 3′ LCRed640 probe extended for different 3′ caps, storage conditions, and storage intervals.

3′ Cap	Storage solution (at 4 °C)	Probe extension, %		
		Week 1	Week 4	Week 8
None	Water	100	100	100
	1× Tris-EDTA	100	100	100
Phosphate	Water	0	5	17
	1× Tris-EDTA	0	18	18
C3	Water	0	0	0
	1× Tris-EDTA	0	0	0

Many factors can induce cleavage of the 3′-phosphate ester bond, which is an intrinsically unstable bond, but most are likely to involve hydrolysis. Therefore, high salt concentrations and acidic or basic pH will probably play a major role *(3)*. Oligonucleotide synthesis involves many chemicals, in particular ammonia compounds, that would fit this profile *(4)*. Various postsynthesis purification methods are aimed at removing these substances, but on occasion, hydrolytic attack on reconstitution of the probe may occur as a result of even minor variations in lyophilization efficiency or pH of the chromatography eluent or as a result of residual salts trapped in the lyophilysate, e.g., as a consequence of an exhausted chromatography column. The fact that the loss of the phosphate cap seems to be slightly accelerated in Tris-EDTA might suggest that microbial contamination could also play a role. The organic matrix and the buffering conditions of Tris-EDTA may allow microorganisms to proliferate and produce catabolic enzymes.

Because of the greater stability of a phosphodiester linkage, as used in the C3 linker, relative to a single phosphoester bond, it appears that all of these concerns can be alleviated by replacing the phosphate cap with an alkyl group via common phosphoramidite chemistries. In our case, we have demonstrated that the C3 linker is indeed an excellent choice for such a blocking agent, but alternatives may include other carbon spacers and 3′-terminal dideoxynucleotides, although the latter would add substantially to synthesis costs. Users interested in such alternatives should discuss availability with their oligonucleotide manufacturers. For probes with conventional 3′-phosphate caps, we would recommend frozen storage, ideally lyophilized, and minimization of any storage time at 4 °C or above, as well as any handling that might allow bacterial contamination.

References

1. Wilhelm J, Pingoud A. Real-time polymerase chain reaction [Review]. Chembiochem 2003;4:1120–8.
2. Davis DL, O'Brien EP, Bentzley CM. Analysis of the degradation of oligonucleotide strands during the freezing/thawing processes using MALDI-MS. Anal Chem 2000;72:5092–6.
3. Voet D, Voet JG. Thermodynamics of phosphate compounds. In: Biochemistry, 2nd ed. New York: John Wiley & Sons, 1995:428–34.
4. Brown T, Dorcas JS. Modern machine-aided methods of oligonucleotide synthesis. In: Eckstein F, ed. Oligonucleotides and analogues a practical approach. Oxford: IRL Press, 1995:1–24.

DOI: 10.1373/clinchem.2004.033183

Microsatellite Instability in Colorectal Cancer: Considerations for Molecular Diagnosis and High-Throughput Screening of Archival Tissues, *Manuel Salto-Tellez,[1,2] Soo Chin Lee,[3] Lily L. Chiu,[2] Chi Kuen Lee,[1] May Chin Yong,[3] and Evelyn S.C. Koay[1,2*]* ([1] Department of Pathology, National University of Singapore; [2] Molecular Diagnosis Centre, Department of Laboratory Medicine, and [3] Department of Hemato-Oncology, National University Hospital, Singapore; * address correspondence to this author at: Department of Pathology, National University of Singapore, 5

Lower Kent Ridge Road, Singapore 119074; fax 65-67751757, e-mail patkoaye@nus.edu.sg)

Microsatellite instability (MSI) *(1)* is the consequence of a failure in the DNA replication proofreading mechanism. In two-thirds of colorectal cancer (CRC) patients with high-frequency MSI (H-MSI), the cause is an epigenetic hypermethylation of one of the mismatch repair (MMR) genes; in the remaining 30% [the hereditary non-polyposis colorectal cancer (HNPCC) subgroup], the cause is inherited mutations in these genes. Distinction between H-MSI and microsatellite-stable (MSS) CRC may also have prognostic and therapeutic implications *(2, 3)*.

The MSI test should be complemented with morphologic *(4)* and clinicopathologic evaluation, immunohistochemical (IHC) staining *(5)* (as manifested by absence of hMLH1 and/or hMSH2 antibody reactivity), and when indicated, screening and confirmation of MMR gene mutations. Direct sequencing, another viable diagnostic approach, is limited by the complex nature of the genes, the broad mutational spectrum, and the cost *(6)*.

In the present study, we reviewed the MSI testing performed in our routine molecular diagnostic laboratory and correlated the findings with mutation analysis and IHC studies; we also propose the most cost-effective manner of diagnosing CRC and report the fidelity of tissue microarrays (TMAs) for high-throughput analysis of large tissue archives.

Approximately 20% (29 tumors from 27 patients) of the 131 MSI cases we analyzed underwent surgery in our hospital; thus, samples for IHC studies and sequencing were available. CRC tissue and noncancerous colonic mucosa were manually microdissected, and DNA was extracted with the DNeasy™ Tissue Kit (Qiagen GmbH). The microsatellite repeat sequences analyzed were Bat-25 (4q12/*c*-kit), Bat-26 (2p16.3/*hMSH2*), D2S123 (2p16/*hMSH2*), D5S346 (5q21/*APC*), and D17S250 (17q11.2/*BRCA1*). The method *(7)* was modified from that of Berg et al. *(8)* and based on international recommendations *(9, 10)*. Individual PCR tubes were set up for each of the five markers, each tube containing ~50 ng (5 μL) of DNA extract from the healthy or tumor tissue; a PCR control [with β-globin primers *(8)*] and a water blank control were included. PCR was performed on an ABI PE9600 thermocycler, and the amplified products were detected by use of the ABI PRISM® 310 Genetic Analyzer and GeneScan™ software [Applied Biosystems Incorporation (ABI)] *(7)*.

TMAs were constructed with double punches 1 mm in diameter from formalin-fixed, paraffin-embedded surgical resection specimens (CRC and healthy colon tissue) of the 25 patients, as described previously *(11)*. For IHC analysis, monoclonal antibodies against h-MLH1 and h-MLH2 (Ab-1 and Ab-2; Oncogene Research Products) at antibody dilutions of 1:10 and 1:50, respectively, were applied to 4-μm-thick TMA sections, according to the manufacturer's instructions. Cases with unequivocal nuclear staining were considered positive. If no staining was noted in the internal control cells (the normal fibro-

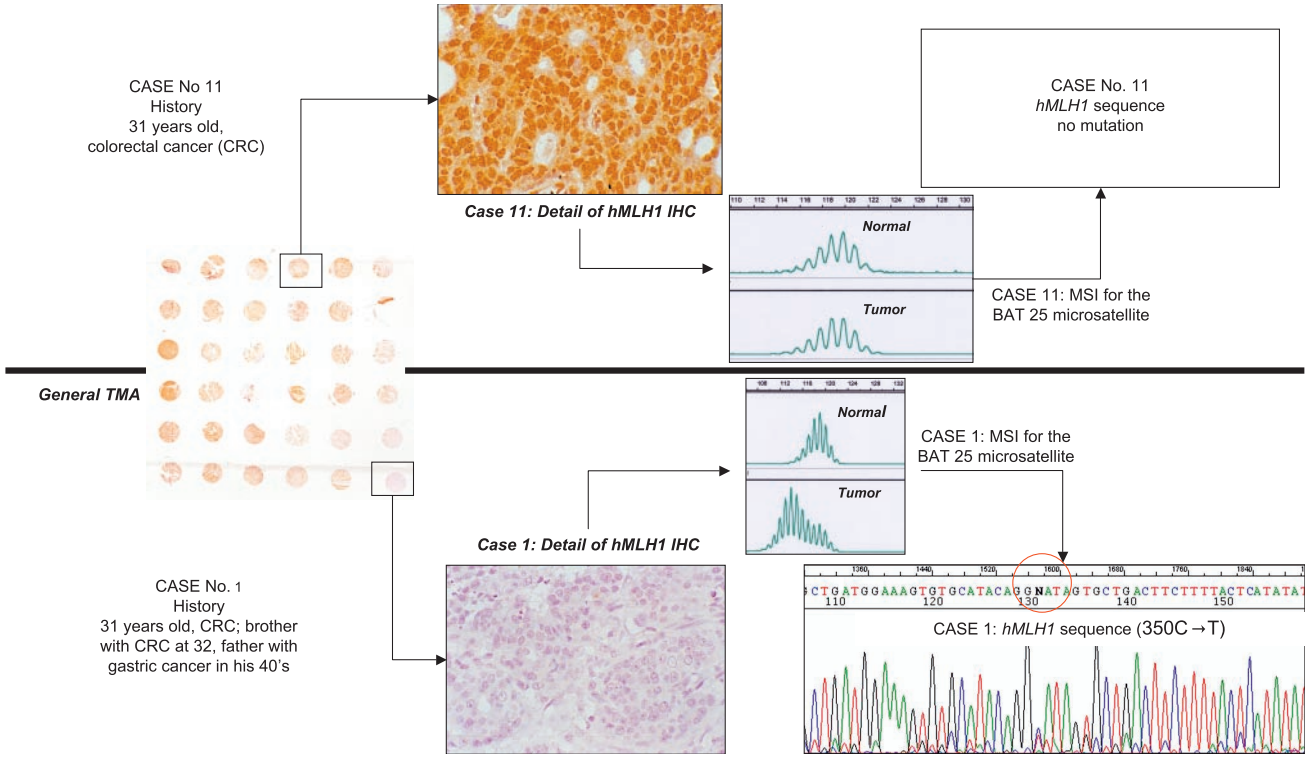

Fig. 1. Illustration of two cases of the study, including clinical history, immunophenotype as identified in the tissue microarray study, microsatellite analysis for the BAT25 mononucleotide repeat, and genetic sequence segment with a *hMLH1* mutation for case 1.

Table 1. Summary of results.

		Unstable microsatellite markers					IHC[a]		Sequencing	
Case	MSI status	BAT25	BAT26	D2S123	D5S346	D17S250	hMSH2	hMLH1	*hMSH2*	*hMLH1*
1	H-MSI	+	+	+	+	−	P	N	Negative	Mutation
2	L-MSI[b]	−	−	+	−	−	P	P	Negative	Negative
3	MSS	−	−	−	−	−	P	P	Negative	Negative
4	H-MSI	+	+	+	+	+	P	P	Negative	Negative
5	MSS	−	−	−	−	−	P	P	Negative	Negative
6	H-MSI	+	+	+	+	+	P	P	Negative	Negative
7	H-MSI	+	+	+	−	−	P	P	Negative	Negative
8	MSS	−	−	−	−	−	P	P	Negative	Negative
9	H-MSI	−	−	+	−	+	??	P	Negative	Negative
10	H-MSI	−	−	−	+	+	P	P	Negative	Negative
11	MSS	−	−	−	−	−	P	P	Negative	Negative
12 and 13	H-MSI (both)	−	−	−	+	+	P	P	Negative	Negative
14	MSS	−	−	−	−	−	P	P	Negative	Negative
15	H-MSI	+	+	+	+	−	N	P	Mutation	Negative
16	MSS	−	−	−	−	−	P	P	Negative	Negative
17	MSS	−	−	−	−	−	P	P	Negative	Negative
18	MSS	−	−	−	−	−	P	P	Negative	Negative
19	MSS	−	−	−	−	−	P	P	Negative	Negative
20	MSS	−	−	−	−	−	P	P	Negative	Negative
21 and 22	MSS (21); H-MSI (22)	−	−	+	−	+	P	P	Negative	Negative
23	MSS	−	−	−	−	−	P	P	Negative	Negative
24	H-MSI	+	+	−	+	+	P	P	Negative	Mutation
25	L-MSI	−	−	NA	−	+	P	P	Negative	Negative
26	MSS	−	−	−	−	−	P	P	Negative	Negative
27	MSS	−	−	−	−	−	P	P	Negative	Negative
28	NA	NA	NA	NA	NA	NA	P	P	Negative	Negative
29	MSS	−	−	−	−	−	P	P	Negative	Negative

[a] P, antibody positive; N, antibody negative; ??, indeterminate case.

[b] L-MSI, low-frequency MSI; NA, no amplification [in case 25, one of the markers (D2S123) failed to show satisfactory amplification for diagnostic assessment, whereas in case 28 the DNA preservation was suboptimal].

inflammatory and vascular component), the result was labeled indeterminate.

For the *hMLH1* and *hMSH2* sequencing, genomic DNA was extracted from peripheral mononuclear cells by use of the Puregene™ DNA Isolation Kit (Gentra Systems). Each of the 19 exons of *hMLH1* and 16 exons of *hMSH2* was amplified by PCR, with 50–200 ng of genomic DNA used as template. PCR products were visualized on 1% agarose gels and purified with the QIAquick PCR Purification Kit (Qiagen). Purified PCR products were sequenced on the ABI PRISM 3100 Genetic Analyzer with the Big Dye Terminator, Ver. 3.0, reagent set (ABI), either with the forward or reverse PCR primer or with an internal primer, when appropriate, and analyzed with Sequencing Analysis, Ver. 3.0, software. See Fig. 1 for representative sample results.

The mean age of the patients involved (17 males and 10 females) was 43 years [mean overall age of CRC patients in Singapore is ~60 years *(12)*]. There were 22 (81%) of Chinese, 4 (15%) of Malay, and 1 (4%) of Indian descent, compared with 89%, 7%, and 4% for CRC patients in Singapore in general *(12)*. The tumors were right-sided in almost 50% of our cases, whereas the right-to-left ratio in Singapore is 1:10 *(12)*. Clinically, the patients were grouped as follows: satisfying all Amsterdam criteria (n = 2); three or more family members with CRC or HNPCC-like cancer (n = 5); two family members with CRC or HNPCC-like cancer (n = 11); index patient in the pedigree with multiple primary CRC or HNPCC-like cancer (n = 3); and young CRC diagnosed before age 40 without family history (n = 6). The most common features identified in the series were poor differentiation (n = 12), pushing infiltrative margin (n = 11), Crohn-like reaction (n = 10), and cribiform architecture (n = 8). These features were also prominent among the H-MSI cases. The cases that we found who had more of these features were not necessarily those with H-MSI status.

Selective results are shown in Table 1 (for the full results, see Table 1 in the Data Supplement that accompanies the online version of this Technical Brief at http://www.clinchem.org/content/vol50/issue6/). Eleven tumors (38%) were H-MSI, 2 tumors (7%) showed one unstable microsatellite (the low-frequency MSI group), and 16 tumors (55%) were MSS CRC. The most frequent microsatellite markers exhibiting instability were D2S123 and D17S250 (in eight cases each), followed by D5S346 (in

seven cases) and the mononucleotide repeats (in six cases each).

IHC analysis of full sections from all H-MSI cases produced full concordance with the TMA IHC results. Full concordance was also achieved with the duplicate punches for every case. Analysis of the IHC staining on TMA sections (done "blinded" by the histopathologist) showed 1 case (case 15) with loss of hMSH2 reactivity and 1 case (case 1) with loss of hMLH1 reactivity (7.4% of all patients and 18% of those with H-MSI status). One case (case 9) was indeterminate. Interestingly, lack of antibody reactivity was not 100% accurate when used as a surrogate test to predict the presence of MMR gene mutations. The sequencing analysis showed *hMLH1* gene mutations in two cases: a 887T>G mutation in case 24, which changed a leucine-encoding codon to a termination codon; and a 350C>T (splice-site) mutation in case 1. However, concurrent loss of hMLH1 reactivity was found only in case 1; case 24 had seemingly paradoxical conserved reactivity for the hMLH1 antibody and showed no HNPCC-related histologic features. A single *hMSH2* mutation (2446C>T; glutamine > termination) was identified in case 15, which was H-MSI and showed no hMSH2 antibody reactivity. Case 9, with an indeterminate result for hMSH2 IHC staining, showed no *hMSH2* mutation.

The clinicopathologic profiles of our patients were in keeping with the known profiles of H-MSI patients. This was also reflected in the high percentage of H-MSI in our series (37.9%), which is more than double that described in the general population *(1)* and in the ethnic group distribution *(12)*. Our results raise several issues of clinical relevance. For example, they confirm the difficulty in predicting H-MSI status on histologic grounds *(4, 13)* alone (even one of the cases with *hMLH1* mutations was a left-sided carcinoma with no characteristic histologic features). In addition, both cases with a known mutation in our series were in the H-MSI subgroup. Moreover, in our series, the dinucleotide markers D2S123 and D17S250 were the more frequent and relevant ones for instability. Had we not performed tests for these markers routinely, four cases in our series (cases 9, 10, 12, and 22) would not have been classified as H-MSI, whereas not testing for the mononucleotide repeats [postulated as the microsatellite marker with a higher informativity *(8)*] would not have changed the overall H-MSI status of our cases. The reason is difficult to ascertain in a relatively small sample group, but it indeed has a clear molecular diagnostic implication.

We observed that antibody reactivity may not be a reliable indicator of MMR gene abnormality. Case 24 is a cogent reminder that mutations may be present with at least partial antibody reactivity *(14)*. This is also relevant for TMA-based screening to detect MMR gene mutations. This study shows how a duplicate tissue array of 1-mm-diameter punches offers full correlation with the same analysis in full sections, as we have described for other neoplasms *(11)*.

We propose a diagnostic flowchart for cost-efficient analysis of samples from HNPCC-like patients. Because the chances of having a MSS tumor with *hMLH1* or *hMSH2* mutations are uncertain *(15)*, MSI testing should be the first-line laboratory investigation. We propose that the MSI-documented cases be followed by IHC analysis, which would allow the targeting of specific genes for follow-up mutation analysis, minimizing costs and eliminating unwarranted testing. Although the cost of first-line direct sequencing of the three most common genes for all cases in our series would have been ~US $81 000, which would be followed in the negative cases with full MSI/IHC analysis (another US $12 150), a protocol that started with the MSI test as a first-line investigation with subsequent IHC staining, to be followed by sequencing only in those cases that require it [three-gene (*hMLH1*, *hMSH2*, and *hMSH6*) or one-gene sequencing depending on the IHC result], would substantially reduce the cost of diagnostic investigations, to US $43 850, or by ~50–60%.

In summary, our study highlights the importance of the microsatellite dinucleotide repeats D2S123 and D17S250 in MSI testing; the necessity of using MSI testing as the first-line investigation, followed by selective IHC analysis to recommend MMR gene sequencing in the appropriate patients; and the general cost-effectiveness of this approach. Furthermore, our study establishes the adequacy of TMAs for high-throughput screening of paraffin-embedded tissue collections of known genes.

This work was funded by grants from the Health Services Development Program, Ministry of Health, Singapore (HSDP01N02) and the National Health Group of Singapore (NHG-RP01121). The study was carried out with the ethics approval of our Institutional Review Board (IRB Reference Code 03.104).

References

1. de la Chapelle A. Microsatellite instability. N Engl J Med 2003;349:209–10.
2. Hemminki A, Mecklin JP, Jarvinen H, Aaltonen LA, Joensuu H. Microsatellite instability is a favorable prognostic indicator in patients with colorectal cancer receiving chemotherapy. Gastroenterology 2000;119:921–8.
3. Ribic CM, Sargent DJ, Moore MJ, Thibodeau SN, French AJ, Goldberg RM, et al. Tumor microsatellite-instability status as a predictor of benefit from fluorouracil-based adjuvant chemotherapy for colon cancer. N Engl J Med 2003;349:247–57.
4. Alexander J, Watanabe T, Wu TT, Rashid A, Li S, Hamilton SR. Histopathological identification of colon cancer with microsatellite instability. Am J Pathol 2001;158:527–35.
5. Marcus VA, Madlensky L, Gryfe R, Kim H, So K, Millar A, et al. Immunohistochemistry for hMLH1 and hMSH2: a practical test for DNA mismatch repair-deficient tumors. Am J Surg Pathol 1999;23:1248–55.
6. Boland CR. Hereditary nonpolyposis colorectal cancer. In: Vogelstein B, Kinzler KW, eds. The genetic basis of human cancer, 2nd ed. New York: McGraw-Hill, 2002:315.
7. Salto-Tellez M, Zhang D, Chiu LL, Wang SC, Nilsson B, Koay ES. Immunocytochemistry versus molecular fingerprinting of metastases. Cytopathology 2003;14:186–90.
8. Berg KD, Glaser CL, Thompson RE, Hamilton SR, Griffin CA, Eshleman JR. Detection of microsatellite instability by fluorescence multiplex polymerase chain reaction. J Mol Diagn 2000;2:20–8.
9. Bocker T, Diermann J, Friedl W, Gebert J, Holinski-Feder E, Karner-Hanusch J, et al. Microsatellite instability analysis: a multicenter study for reliability and quality control. Cancer Res 1997;57:4739–43.
10. Boland CR, Thibodeau SN, Hamilton SR, Sidransky D, Eshleman JR, Burt RW, et al. A National Cancer Institute workshop on microsatellite instability for cancer detection and familial predisposition: development of international criteria for the determination of microsatellite instability in colorectal cancer. Cancer Res 1998;58:5248–57.
11. Zhang D, Salto-Tellez M, Putti TC, Do E, Koay ES. Reliability of tissue

microarrays in detecting protein expression and gene amplification in breast cancer. Mod Pathol 2003;16:79–84.

12. Chia KS, Seow A, Lee HP. Cancer incidence in Singapore 1993–1997. Singapore Cancer Registry Report No. 5. Singapore: Singapore Cancer Registry, 2000.
13. Jass JR. Diagnosis of hereditary non-polyposis colorectal cancer. Histopathology 1998;32:491–7.
14. Raevaara TE, Vaccaro C, Abdel-Rahman WM, Mocetti E, Bala S, Lonnqvist KE, et al. Pathogenicity of the hereditary colorectal cancer mutation hMLH1 del616 linked to shortage of the functional protein. Gastroenterology 2003;125:501–9.
15. Farrington SM, Lin-Goerke J, Ling J, Wang Y, Burczak JD, Robbins DJ, et al. Systematic analysis of hMSH2 and hMLH1 in young colon cancer patients and controls. Am J Hum Genet 1998;63:749–59.

DOI: 10.1373/clinchem.2003.030700

Rapid, Simple Laser-Light-Scattering Method for HDL Particle Sizing in Whole Plasma, *Emersom S. Lima[1] and Raul C. Maranhão[1,2*]* [[1] Lipid Metabolism Laboratory, Heart Institute (InCor) of the Medical School Hospital, and [2] Faculty of Pharmaceutical Sciences, University of São Paulo, São Paulo 05403-000, Brazil; * author for correspondence: fax 55-11-3069-5574, e-mail ramarans@usp.br]

HDL particles are composed of an outer layer of phospholipids and free cholesterol surrounding a hydrophobic core that consists primarily of cholesterol esters and small amounts of triglycerides *(1)*. Apolipoprotein A-I (apo A-I) accounts for ~60% of the protein content of HDL. Other apolipoprotein species found in HDL particles include apo A-II, apo A-IV, apo CI, apo CIII, and apo E. Several subfractions of HDL have been identified on the basis of density, electrophoretic mobility, particle size, and apolipoprotein composition *(2)*. Differences in particle size are ascribed mainly to the number of apolipoprotein molecules on the particle surface and the amounts of cholesterol esters in the core *(1, 2)*. Furthermore, there is growing evidence suggesting that most of the cardioprotective properties of HDL are associated with the HDL_2 fraction (larger particles) rather than the HDL_3 fraction (smaller particles) in patients with coronary artery disease *(3, 4)*, in postmenopause women *(5)*, in diabetes *(6)*, and in patients with familial hypercholesterolemia *(9)*.

Several methods, such as sequential ultracentrifugation, chemical precipitation, immunoaffinity chromatography, and nondenaturing polyacrylamide gradient gel electrophoresis, have been used to separate HDL subfractions *(8)*. The sizes of the subfractions have been estimated by nondenaturing polyacrylamide gradient gel electrophoresis *(9)* and, more recently, by nuclear magnetic resonance spectroscopy *(10)*. In general, these procedures are either laborious or expensive.

Laser-light scattering (LLS) has been used in the measurement of LDL particle sizes after isolation of this fraction by ultracentrifugation *(11)*. There is great similarity between the data obtained with this approach and those obtained with the nondenaturing polyacrylamide gradient gel electrophoresis method ($P < 0.0001$; $r = 0.78$). To date, however, LLS has not been used to perform HDL sizing. HDL sizing by LLS can be performed after chemical precipitation of the apo B-containing lipoprotein *(8)*. This approach is more practical than ultracentrifugation or gel electrophoresis. Here we describe the separation of HDL by chemical precipitation and determine the particles size in the supernatant by the LLS method.

Twenty-nine healthy individuals, 4–66 years of age, participated in the experiments. The plasma concentrations of total cholesterol, HDL-cholesterol, and triglycerides were measured by automated enzymatic methods, and LDL-cholesterol was calculated by the Friedewald formula. Blood samples (15 mL) were collected from an antecubital vein of each participant into three 5-mL glass tubes, one containing EDTA (1.5 g/L), one containing heparin (5 IU/mL), and one containing no anticoagulant. EDTA plasma, heparin plasma, and serum were then obtained by centrifugation at 4 °C for 15 min at 1250*g*. Some samples were kept at 4 °C and some at −70 °C to examine the effect of storage temperature on the assay. For the isolation of HDL for subsequent sizing by LLS, several combinations of polyanions and divalent cations were tested to precipitate apo B-containing lipoproteins *(8)*. The following precipitants were tested: phosphotungstate-Ca^{2+} (3 g/L and 15 mmol/L, respectively), dextran sulfate-Mg^{2+} (15 g/L and 40 mmol/L, respectively), heparin-Mg^{2+} (40 IU/mL and 30 mmol/L, respectively), and polyethylene glycol (PEG) 8000 (400 g/L) in 0.2 mol/L glycine buffer adjusted to pH 10 with sodium hydroxide. To assess the reliability of the HDL particle size data obtained with the different precipitation techniques used here, we also obtained the HDL fraction for comparison with a standard sequential flotation ultracentrifugation procedure *(8)* that uses a 90ti rotor in an Optima XL-100K ultracentrifuge (Beckman Instruments Inc.).

Compared with the other tested precipitants, use of PEG gave HDL particle diameter measurements by LLS that were the most reproducible and that most closely resembled those obtained by ultracentrifugation. When LLS analysis was made using samples processed by PEG precipitation, the mean (SD) HDL particle size was 9.1 (0.6) nm, which is consistent with those obtained by the ultracentrifugation procedure [9.3 (0.7) nm; n = 8]. The phosphotungstate-Ca^{2+}- and Mg^{2+}-based methods yielded HDL diameter results that were not reproducible and with means >14 nm, i.e., inconsistent with the mean values expected for HDL. These results suggest that cations at high concentrations, as required for precipitation of apo B-containing lipoproteins by phosphotungstate-Ca^{2+}- or Mg^{2+}-based methods, may interfere with LLS measurements of HDL particle size. In this respect, Dias et al. *(12)* also reported that PEG was the most suitable for HDL isolation by precipitation. Thus, HDL isolation for further LLS analysis was standardized as follows: 0.5 mL of PEG (Merk-Schuchardt) was added to each EDTA-plasma sample (0.5 mL) and stirred in a vortex-mixer for 30 s. Samples were then centrifuged at 1800*g* for 10 min at 25 °C in a microcentrifuge (Model 5415 C; Eppendorf). A 0.5-mL portion of the supernatant was added to 1.5 mL of 10 mmol/L NaCl, passed through a

Table 1. Age, body mass index, plasma glucose and lipid concentrations, and sizes of the HDL particles for the study participants according to gender.

	Mean (SD)	
	Men (n = 14)	**Women (n = 13)**
Age, years	24 (15)	24 (14)
BMI,[a] kg/m^2	26.4 (7)	24 (5)
Glucose, mg/L	930 (260)	800 (130)
Cholesterol, mg/L	1890 (930)	1660 (800)
LDL-cholesterol, mg/L	1600 (670)	1100 (780)
HDL-cholesterol, mg/L	480 (210)	510 (80)
Triglycerides, mg/L	1330 (350)	1090 (290)
HDL particle diameter, nm	8.4 (1.1)	9.1 (1.0)[b]

[a] BMI, body mass index.

[b] Significant difference between men and women (Mann–Whitney test, $P < 0.05$).

0.22 μm filter (Millipore Products Division) to exclude dust particles, and poured into a disposable 10 × 10 × 48 mm cuvette (Sarstedt).

The diameters of HDL particles were determined by use of a ZetaPALS Zeta Potential Analyzer (Brookhaven Instruments Corporation). This instrument uses a 29 mW helium-neon laser at 658 nm to excite the samples. Scattered light is collected at an angle of 90° by a photon-counting photomultiplier tube and is then directed to a correlator. The software (BIC particle sizing) derives particle sizes from the correlator function. Results of each sample were expressed as the mean, which is the harmonic intensity-averaged particle diameter. For this study, all LLS measurements were performed at 25 °C, and the results are means (SD) of five runs of 2 min each. To verify the accuracy of the instrument, before conducting the study, we subjected commercially available nanosphere size standards (Duke Scientific) of known diameters [92 (3.7) nm] to size determination under the operating conditions described above. The intraassay CV for the HDL particle diameter measurement (n = 10) obtained with this procedure was 2.1%.

The physical characteristics and laboratory data for the study participants, as grouped by gender, are shown in Table 1. There were no differences between genders with respect to age and body mass index, plasma lipids, and glucose. The HDL particle size measurements are also shown in Table 1, and it is clear that the HDL particles are larger in females than in males. The correlation plots for HDL particle size vs total cholesterol and LDL-cholesterol are shown in Fig. 1. We found negative correlations (Pearson correlation test) between HDL particle size and plasma total cholesterol ($r = -0.484$; $P < 0.05$) and between HDL particle size and LDL-cholesterol ($r = -0.464$; $P < 0.05$). The correlations between HDL particle size and HDL-cholesterol and triglyceride concentrations were not significant ($P = 0.560$ and 0.168, respectively). We observed no significant changes in particle diameter size in the frozen EDTA plasma over the first 7 days at −70 °C; thereafter, however, the particle size steadily increased (no data shown). Regarding the EDTA-plasma samples maintained at 4 °C, increases in particle size began to occur as early as after 24 h of storage. Use of serum or heparinized plasma was inadequate for LLS HDL sizing because the diameter values were increased ~12% compared with those obtained from EDTA plasma. The larger diameter values could be attributable to formation of

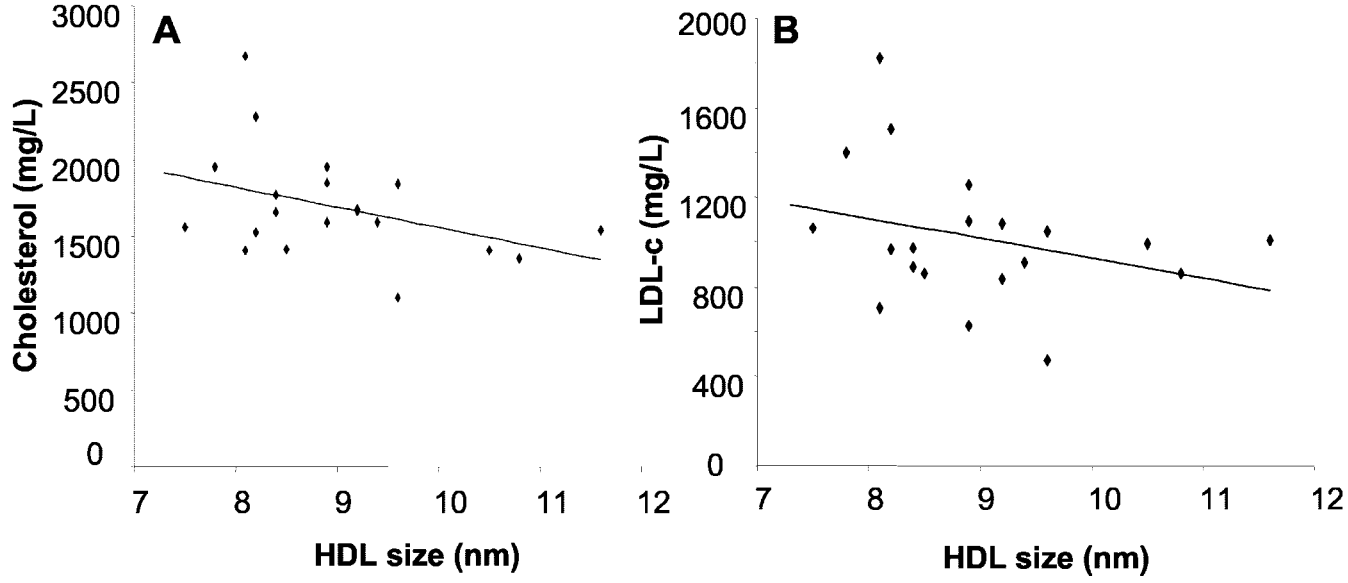

Fig. 1. Plots of HDL particle diameter vs plasma total cholesterol (*A*) and LDL-cholesterol (*B*) concentrations.

(*A*), correlation (Pearson correlation test, $r = -0.484$; $P = 0.0193$) between plasma total cholesterol (mg/L) and HDL particle diameter (nm) determined in whole plasma by LLS after chemical precipitation of apo B-containing lipoproteins. (*B*), correlation (Pearson correlation test, $r = -0.461$; $P = 0.0468$) between plasma LDL-cholesterol concentration (mg/L) and HDL particle diameter (nm) determined in whole plasma by LLS after chemical precipitation of apo B-containing lipoproteins.

HDL particle aggregates after precipitation of apo B-containing lipoproteins.

The data on HDL particle size obtained in this study (mean diameter, 8.8 nm) are in agreement with the values described in the literature for other techniques. In healthy normolipidemic individuals, HDL sizing by nuclear magnetic resonance spectroscopy yielded diameters of ~9.2 nm *(10)*, whereas the values obtained from gradient gel electrophoresis ranged from 8.4 to 9.6 nm *(9, 13)*. In this study, similar to other published results obtained by gradient gel electrophoresis *(13)*, the HDL particle diameter (nm) was greater in premenopausal women than in men (9.1 vs 8.4 nm; Mann–Whitney test, $P = 0.013$). Negative correlations between HDL particle size and total cholesterol and LDL-cholesterol were also reported by Pascot et al. *(13)*, thus strengthening the link between HDL particle size and coronary artery disease. In the present study, the correlations between HDL particle size and HDL-cholesterol and triglyceride concentrations were not statistically significant, probably because of the small number of samples. Pascot et al. *(13)* may have found significant correlations for these relationships because they studied >400 individuals. Therefore, LLS analysis after chemical precipitation of apo B-containing lipoproteins gave results for HDL diameter in the same range as those obtained by established techniques for lipoprotein sizing *(9, 10, 13)*. Furthermore, the differences between genders and the correlations reported here are in agreement with those described in the literature *(13)*.

Because LLS analysis after chemical precipitation is a practical and less time-consuming approach for HDL sizing, it could be used in large trials and in routine clinical laboratory analysis.

This study was supported by Fundação de Amparo à Pesquisa do Estado de São Paulo (FAPESP) Grant 99.01229-2 (to R.C.M.).

References

1. Barter P, Kastelein J, Nunn A, Hobbs R. High density lipoproteins (HDLs) and atherosclerosis; the unanswered questions. Atherosclerosis 2003;168: 195–211.
2. Skinner ER. High-density lipoprotein subclasses. Curr Opin Lipidol 1994;5: 241–7.
3. Lamarche B, Moorjani S, Cantin B, Dagenais GR, Lupien PJ, Després JP. Associations of HDL_2 and HDL_3 subfractions with ischemic heart disease in men. Prospective results from the Quebec Cardiovascular Study. Arterioscler Thromb Vasc Biol 1997;17:1098–105.
4. Johansson J, Carlson LA, Landou C, Hamsten A. High density lipoproteins and coronary atherosclerosis. A strong inverse relation with the largest particles in confined to normotriglyceridemic patients. Arterioscler Thromb 1991;11:174–82.
5. Tangney CC, Mosca LJ, Otvos JD, Rosenson RS. Oral 17b-estradiol and medroxyprogesterone acetate therapy in postmenopausal women increases HDL particle size. Atherosclerosis 2001;155:425–30.
6. Syvanne M, Ahola M, Lahdenperii S, Kahri J, Kuusi T, Virtanen KS, Taskinen MR. High density lipoprotein subfractions in non-insulin-dependent diabetes mellitus and coronary artery disease. J Lipid Res 1995;36:573–82.
7. Moriguchi EH, Tamachi H, Goto Y. Hepatic lipase activity and high-density lipoprotein in hypercholesterolemia familial: adaptational mechanisms for LDL-receptor deficient state. Tokai Exp Clin Med 1990;15:401–6.
8. Warnick RG, Nauck M, Rifai N. Evolution of methods for measurement of HDL-cholesterol: from ultracentrifugation to homogeneous assays. Clin Chem 2001;47:1579–96.
9. Pérusse M, Pascot A, Deprés JP, Couillard C, Lamarche B. A new method for HDL particle sizing by polyacrylamide gradient gel electrophoresis using whole plasma. J Lipid Res 2001;42:1331–4.
10. Soedamah-Muthu SS, Chang YF, Otvos J, Evans RW, Orchard TJ. Lipoprotein subclass measurements by nuclear magnetic resonance spectroscopy improve the prediction of coronary artery disease in type 1 diabetes. A prospective report from the Pittsburgh Epidemiology of Diabetes Complications Study. Diabetologia 2003;46:674–82.
11. O'Neal D, Harrip P. Dragicevic G, Rae D, Best JD. A comparison of LDL size determination using gradient gel electrophoresis and light-scattering methods. J Lipid Res 1998;39:2086–90.
12. Dias VC, Parsons HG, Boyd NG, Keane P. Dual-precipitation method evaluated for determination of high-density lipoprotein (HDL), HDL2 and HDL3 cholesterol concentrations. Clin Chem 1988;34:2322–7.
13. Pascot A, Lemieux I, Bergeron J, Tremblay A, Nadeau A, Prud'homme D, et al. HDL particle size: a marker of the gender difference in the metabolic risk profile. Atherosclerosis 2002;160:399–406.

DOI: 10.1373/clinchem.2004.032383

Quantitative Assessment of *PML-RARa* and *BCR-ABL* by Two Real-Time PCR Instruments: Multiinstitutional Laboratory Trial, *Pascual Bolufer,[1*] Dolors Colomer,[2] Maria T. Gomez,[3] Joaquín Martínez,[4] Silvia M. Gonzalez,[3] Marcos Gonzalez,[5] Josep Nomdedeu,[6] Beatriz Bellosillo,[7] Eva Barragán,[1] Francesco Lo-Coco,[8] Daniela Diverio,[9] Lourdes Hermosin,[10] José García-Marco,[11] Maria D. de Juan,[12] Francisco Barros,[13] Rafael Romero,[14] and Miguel A. Sanz,[15] for the Group of Molecular Biology in Hematology* ([1] Molecular Biology, Department of Medical Biopathology, Hospital Universitario La Fe, Avda Campanar 21, 46009 Valencia, Spain; [2] Hematopathology Unit, Hospital Clínic, Barcelona, Spain; [3] Molecular Biology, Hematology, Hospital Gran Canaria Dr. Negrin, Las Paslmas de GC, Spain; [4] Molecular Biology, Hematology, Hospital 12 de Octubre, Madrid, Spain; [5] Immunopathology and Molecular Biology, Hematology, Hospital Clínico Universitario, Salamanca, Spain; [6] Laboratory of Hematology, Hospital de la Santa Creu i Sant Pau, Barcelona, Spain; [7] Laboratory of Cytogenetics and Molecular Biology, Service of Pathology, Hospital del Mar, Barcelona, Spain; [8] Laboratory of Integrated Diagnosis of Oncohematologic Diseases, University Tor-Vergata, Rome, Italy; [9] Laboratorio di Diagnostica Molecolare Oncoematologica, Dipartimento di Biotecnologie Cellulari ed Ematologia, Universitá degli Studi "La Sapienza", Rome, Italy; [10] Biology, Hematology, Hospital de Jerez, Jerez de la Frontera, Cádiz, Spain; [11] Molecular Cytogenetic Unit, Servicio de Hematologia, Hospital Universitario Puerta de Hierro, Madrid, Spain; [12] Unified Laboratory, Immunology, Hospital Donostia, San Sebastian, Gupuzcoa, Spain; [13] Molecular Medicine Unit-INGO (Sergas), University of Santiago de Compostela, Hospital Clínico Universitario de Santiago, Santiago de Compostela, Spain; [14] Departamento de Estadistica e Investigación Operativa, Universidad Politécnica de Valencia, Valencia, Spain; [15] Clinical Hematology, Service of Hematology, Hospital Universitario La Fe, Hospital Universitario La Fe, Valencia, Spain; * author for correspondence: fax 34961973030, e-mail bolufer_pas@gva.es)

The recent introduction on the market of instruments for real-time PCR has prompted the development of quanti-

Table 1. Results of the *PML-RARa* and *BCR-ABL* assays (copies/μL) for the participating laboratories grouped according to the instrument.

		Laboratories										
		LC							ABI			
Assay	Samples	1	2	3	4	5	6	7	8	9	10	11
BCR-ABL	Blank	0	0	0	0	0	0	0	0	0	0	0
	1	5	1	2	1	1	1	0	1	1	3	1
	2	22 299	13 120	16 370	6204	26 430	19 503	14 300	10 667	12 455	23 353	12 691
	3	10	15	12	3	29	16	47	8	13	27	9
	4	3	2	5	1	4	2	3	1	3	5	2
	5	6	1	2	1	2	4	18	1	1	4	1
	6	12	4	5	3	6	7	13	4	4	15	5
	7	178	60	86	41	122	131	282	11	13	249	110
	8	31	11	18	8	27	27	106	65	121	43	13
	9	2	2	3	2	2	3	22	1	1	2	1

		Laboratories									
	Replicates	1	2	3	4	5	6	7	8	9	10
PML-RARa											
BCR1	Blank	0	0	0	0	0	0	0	0	0	0
	Blank	0	0	0	1	0	0	0	0	0	0
	1	858	2825	1255	1965	1536	1758	1329	919	1291	2193
	1	675	3165	1195	1892	1776	2071	1342	752	1023	2400
	2	66	241	116	125	150	138	128	76	121	218
	2	90	284	142	231	145	132	136	97	133	194
	3	13	22	20	6	13	23	11	15	16	23
	3	13	40	13	2	12	18	13	6	13	22
	4	2	4	1	2	2	5	1	1	2	1
	4	2	1	1	2	1	3	2	2	1	1
BCR3	Blank	0	0	0	0	0	0	0	0	0	0
	Blank	0	0	0	0	0	0	0	0	0	0
	5	302	349	747	378	583	427	531	444	875	493
	5	329	323	609	611	706	585	509	399	842	507
	6	31	31	57	74	42	36	44	46	100	48
	6	34	31	61	56	47	34	43	48	89	45
	7	5	3	8	4	4	5	5	4	16	5
	7	7	3	7	6	7	5	5	7	13	7
	8	1	0	1	0	1	0	1	1	2	0
	8	1	0	5	0	0	1	1	1	1	0

tative assays for the most common fusion transcripts detectable in hematologic malignancies. However, because the ABI PRISM apparatus (ABI; Applied Biosystems) was the first available instrument for real-time PCR, most of the methods developed for the ABI PRISM use TaqMan probe chemistry *(1–3)*. With the introduction of other real-time PCR instruments, such as the LightCycler (LC; Roche), other methods have been described *(4–7)*. The instruments differ in several respects, including the light sources and the approach to acquisition of fluorescence data. Few reports have compared the results obtained with different types of real-time PCR instruments *(8)*. To the best of our knowledge, no such multicenter studies with common calibrators and common methods have been reported.

In the present study we analyzed the results obtained with two of the more widely used instruments for real time PCR, i.e., the ABI and LC, for amplifying two rearrangements frequently detectable in human leukemia, the *BCR-ABL* and *PML-RARa* fusion genes. For *BCR-ABL* several quantitative methods have been established for both instruments *(3–7)*, whereas for *PML-RARa* most of the quantitative methods have been developed for the ABI PRISM *(1)*.

The quantification of *BCR-ABL* transcripts is clinically relevant for monitoring patients with chronic myeloid leukemia undergoing allogeneic hematopoietic stem cell transplantation *(4, 9)* or treatment with interferon-a or imatinib mesylate *(9–11)*. For example, low numbers of *BCR-ABL* transcripts after 2 weeks of imatinib treatment predict a good response to imatinib after 4 weeks *(9)*. With respect to *PML-RARa*, recent reports have shown that quantitative assessment of *PML-RARa* transcripts allowed efficient monitoring of minimal residual disease

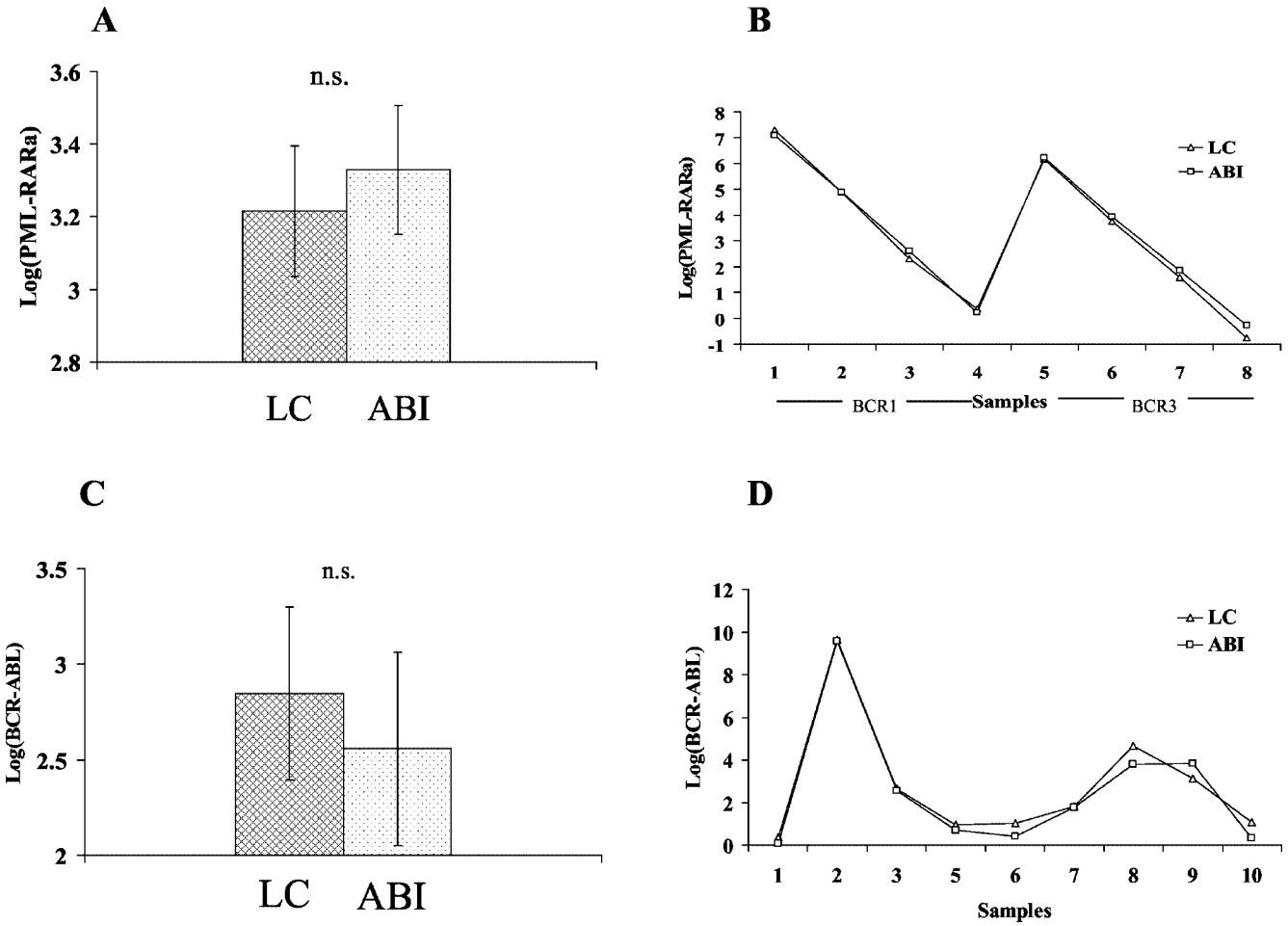

Fig. 1. Pooled means and profiles of means for the samples.

(*A*), pooled means of log(*PML-RARa*) for the LC and ABI. The *error bars* indicate 2 SD. (*B*), profiles of the means of the *PML-RARa* samples analyzed by each type of real-time PCR instrument. (*C*), pooled means of log(*BCR-ABL*) for the LC and ABI. The *error bars* indicate 2 SD. (*D*), profiles of the means of the *BCR-ABL* samples processed by each type of real-time PCR instrument. *n.s.*, not significant.

(1) and assessment of the effects of the treatment given *(12)*. Furthermore, patients who had transcription values above an empirical checkpoint after consolidation therapy had an increased risk of relapse *(13)*.

Ten laboratories participated in the trial for *PML-RARa* analysis (6 using LC and 4 ABI), and 11 laboratories were involved in the *BCR-ABL* assay (7 using LC and 4 ABI; see the list of participating laboratories in the Data Supplement that accompanies the online version of this Technical Brief at http://www.clinchem.org/content/vol50/issue6/). In the trial for *PML-RARa*, each laboratory received 20 samples: 2 reagent blanks, 4 BCR1-positive, and 4 BCR3-positive cDNA samples in two replicates. In the trial for *BCR-ABL*, the laboratories received 10 samples: 1 blank and 9 patient cDNA samples (5 B3A2-positive and 4 B2A2-positive).

The laboratories also received calibrators prepared by cloning PCR products of samples from positive patients (B3A2 isoform for *BCR-ABL*, and BCR1 or BCR3 isoforms for *PML-RARa*) into CR® II-TOPO® vector (TOPO™ Cloning® Kit). For *PML-RARa*, two sets of calibrators were prepared: one for BCR1 and the other for the BCR3 isoform. Calibrators were provided at the following concentrations: 2×10^5, 2×10^4, 2×10^2, 2×10^1, and 2 copies/μL. Samples and calibrators were shipped on dry ice by overnight courier and stored refrigerated until used. The calibrators were analyzed in duplicate and the samples in triplicate.

For *PML-RARa* quantification, the laboratories equipped with ABI used the reagents and protocol established by Gabert et al. *(14, 15)* for this instrument in the Europe Against Cancer Program (EAC Protocol April 2002). The method designed for the ABI PRISM was optimized in the LC by use of a final volume of 10 μL, including 2 μL of cDNA samples (unknowns) or 2 μL of calibrators (for the calibration curve; see the Methods file in the online Data Supplement).

For the *BCR-ABL* rearrangement the laboratories equipped with ABI used the reagents and protocol designed by Gabert et al. *(14, 15)*. The ABI method was also optimized for the LC as described (see the Methods file in the online Data Supplement).

The quantification of transcripts was carried out automatically with the software provided in each type of equipment (see the section on quantification in the Methods file in the online Data Supplement).

To compare the results among the laboratories or samples for each real-time instrument, we performed a multivariate ANOVA for laboratories and samples as described in the Statistics file in the online Data Supplement.

The efficiencies estimated from the slopes of the calibration curves for the *PML-RARa* BCR1 and BCR3 isoforms for the ABI and LC were very similar (Table 1 in the online Data Supplement). One false-positive result was detected in a BCR1 blank sample (Table 1).

All laboratories detected transcripts in the replicate of the BCR1-positive sample with the lowest number of copies, and three of the four ABI and two of the seven LC laboratories detected the replicate sample BCR3 with the lowest number of copies (Table 1). These results suggest that both instruments are capable of detecting 1–5 copies/μL of the *PML-RARa* isoforms.

We observed significant differences among global means of the *PML-RARa* results of the laboratories with LC or ABI ($P = 0.000$). However, the global means of all samples assessed with LC or ABI showed no statistical difference (Fig. 1A), as reflected in the profiles of the means of the samples processed by each real-time instrument (Fig. 1B).

We found a difference in the interaction reproducibility between the two instruments at the limits of statistical significance ($P \approx 0.05$; Table 2 in the online Data Supplement), which was attributable to the larger variance of the LC for this component.

The efficiencies estimated from the slope of the calibration curves for *BCR-ABL* were similar for the two instruments [mean (SD) 1.79 (0.04) for the LC and 1.84 (0.02) for the ABI; Table 1 in the online Data Supplement]. No false-positive results were reported for the blank controls (Table 1).

All participating laboratories except one using the LC were able to detect transcripts in the sample with the lowest amount of *BCR-ABL* transcripts (1–5 copies/μL; Table 1).

We observed significant differences among the global means of the laboratories using LC or ABI ($P < 0.001$). Conversely, we found no statistically significant differences between the ABI and LC instruments for the global means of pooled samples of the laboratories (Fig. 1C). In addition, the profiles of the means of log(*BCR-ABL*) obtained for each sample within the laboratories using an ABI or LC instrument were nearly identical (Fig. 1D).

None of the precision components differed between the ABI and LC (Table 2 in the online Data Supplement).

In summary, this multicenter study showed that the ABI and LC instruments performed similarly. As a multilaboratory trial, the results obtained can be expected to better transfer to the data reported in clinical trials than if the comparison were performed by a single laboratory. The study confirms the ability of the LC to use the TaqMan technology *(6, 16)* as an alternative to the HybProbes technology originally developed for this system *(5, 17)*.

In this study, the main statistical differences were among the pooled means of the data. These individual differences among the laboratories with the same instrument could be attributable to variability in the stability of control samples or reagents, methodologic proficiency, or instrument maintenance.

The small difference in the interaction reproducibility ($P \approx 0.05$) for *PML-RARa* could reflect a difference in sensitivity of LC to the influence of noncontrolled effects.

In conclusion, despite differences in reagents in our study, the results for the LC and ABI instruments were equivalent with respect to the means and precision, suggesting that the choice of instrument has little to do with results when laboratories use the same methods and calibrators. Standardization of quantitative real-time PCR studies in a multiinstitutional context will require adoption of common methods and calibrators. The harmonization of the results should in turn allow better comparison of data obtained in different therapeutic trials.

This study was supported financially by Roche Applied Science, Spain.

References

1. Cassinat B, Zassadowski F, Balitrand N, Barbey C, Rain JD, Fenaux P, et al. Quantitation of minimal residual disease in acute promyelocytic leukemia patients with t(15;17) translocation using real-time RT-PCR. Leukemia 2000;14:324–8.
2. van der Velden VHJ, Hochhaus A, Cazzaniga G, Szczepanski T, Gabert J, Van Dongen JJM. Detection of minimal residual disease in hematologic malignancies by real-time quantitative PCR: principles, approaches, and laboratory aspects. Leukemia 2003;17:1013–34.
3. Mensik E, Van De Loch A, Schattenberg A, Linders E, Schaap N, Van Kesssel G, et al. Quantitation of minimal residual disease in Philadelphia chromosome positive chronic myeloid leukaemia patients using real-time quantitative RT-PCR. Br J Haematol 1998;102:768–74.
4. Elmaagacli AH, Freist A, Hahn M, Opalka B, Seeber S, Schaefer UW, et al. Estimating the relapse stage in chronic myeloid leukaemia patients after allogeneic stem cell transplantation by the amount of BCR-ABL fusion transcripts detected using a new real-time polymerase chain reaction method. Br J Haematol 2001;113:1072–5.
5. Bolufer P, Sanz GF, Barragán E, Sanz MA, Cervera J, Lerma E, et al. Rapid quantitative detection of BCR-ABL transcripts in chronic myeloid leukemia patients by real-time reverse transcriptase polymerase-chain reaction using fluorescently labeled probes. Haematologica 2000;85:1248–54.
6. Eckert C, Landt O, Taube T, Seeger K, Beyermann B, Proba J, et al. Potential of LightCycler for quantification of minimal residual disease in childhood acute lymphoblastic leukemia. Leukemia 2000;14:316–23.
7. Emig M, Saussele S, Wittor H, Weisser A, Reiter A, Willer A, et al. Accurate and rapid analysis of residual disease in patients with CML using specific fluorescent hybridization probes for real time quantitative RT-PCR. Leukemia 1999;13:1825–32.
8. Exner MM, Lewinski MA. Sensitivity of multiplex real-time PCR reactions, using the LightCycler and the ABI PRISM 7700 Sequence Detection System, is dependent on the concentration of the DNA polymerase. Mol Cell Probes 2002;16:351–7.
9. Scheuring UJ, Pfeifer H, Wassmann B, Bruck P, Atta J, Petershofen EK, et al. Early minimal residual disease (MRD) analysis during treatment of Philadelphia chromosome/BCR-ABL-positive acute lymphoblastic leukemia with the Abl-tyrosine kinase inhibitor imatinib (STI571). Blood 2003;101:85–90.
10. Wang L, Pearson K, Pillitteri L, Ferguson JE, Clark RE. Serial monitoring of BCR-ABL by peripheral blood real-time polymerase chain reaction predicts the marrow cytogenetic response to imatinib mesylate in chronic myeloid leukaemia. Br J Haematol 2002;118:771–7.
11. Stentoft J, Pallisgaard N, Kjeldsen E, Holm MS, Nielsen JL, Hokland P. Kinetics of BCR-ABL fusion transcript levels in chronic myeloid leukaemia

patients treated with STI571 measured by quantitative real-time polymerase chain reaction. Eur J Haematol 2001;67:302–8.
12. Visani G, Buonamici S, Malagola M, Isidori A, Piccaluga PP, Martinelli G, et al. Pulsed ATRA as single therapy restores long-term remission in PML-RARα-positive acute promyelocytic leukemia patients: real time quantification of minimal residual disease. A pilot study. Leukemia 2001;15:1696–700.
13. Gallagher RE, Yeap BY, Bi W, Livak KJ, Beaubier N, Rao S, et al. Quantitative real-time RT-PCR analysis of PML-RARa mRNA in acute promyelocytic leukemia: assessment of prognostic significance in adult patients from intergroup protocol 0129. Blood 2003;101:2521–8.
14. Gabert J, Beillard E, Van Der Velden VHJ, Bi W, Grimwade D, Pallisgaard N, et al. Standardization and quality control studies of "real-time" quantitative reverse transcriptase polymerase chain reaction of fusion gene transcripts for residual disease detection in leukemia—A Europe Against Cancer Program. Leukemia 2003;17:2318–57.
15. Gabert J. RQ-PCR for early diagnosis of relapse risk in leukemia (Europe Against Cancer Program). http://ifrjr.nord.univ-mrs.fr/mrd_leukemia (accessed March 2002).
16. Kreuzer KA, Lass U, Bohn A, Landt O, Schmidt CHA. LightCycler technology for the quantitation of bcr/abl fusion transcripts. Cancer Res 1999;59:3171–4.
17. Barragan E, Bolufer P, Moreno I, Martin G, Nomdedeu J, Brunet S, et al. Quantitative detection of AML1-ETO rearrangement by real-time RT-PCR using fluorescently labeled probes. Leuk Lymphoma 2001;42:747–56.

DOI: 10.1373/clinchem.2003.028308

Size-Selective Extraction of Peptides from Urine for Mass Spectrometric Analysis, *Glen L. Hortin,[1*] Bonnie Meilinger,[1] and Steven K. Drake[2]* (Departments of [1] Laboratory Medicine and [2] Critical Care Medicine, Warren Magnuson Clinical Center, NIH, Bethesda, MD; * address correspondence to this author at: Department of Laboratory Medicine, NIH, Bldg 10, Room 2C-407, Bethesda, MD 20892-1508; fax 301-402-1885, e-mail ghortin@mail.cc.nih.gov)

Protein excretion in urine has been suggested as an indicator of kidney disease since the time of Hippocrates. In the early 1800s, Bright further established approaches for studying proteinuria as a marker for kidney disease *(1)*. As methods for quantitative and qualitative analysis have become more sophisticated, it has become possible to detect earlier stages of kidney disease and to differentiate different patterns of protein excretion *(1–3)*. Quantitative immunoassays of selected urinary components such as α_1-microglobulin, albumin, IgG, and α_2-macroglobulin have been shown to be useful in characterizing the nature of proteinuria *(4)*. Two-dimensional electrophoresis has provided a method for simultaneous analysis of numerous proteins in urine *(5, 6)*. Recently, a new dimension has been added to analysis of urinary components by mass spectrometric techniques, which detect many small peptide components below the size resolution of electrophoresis *(7, 8)*. The highly complex mixtures of small peptides in urine offer the potential for information-rich patterns for clinical diagnosis. Concentrations of urinary peptides serve not only as markers for kidney function but also as markers of other systemic physiologic processes. As examples, immunoassays for specific peptides provide measures of thrombosis and fibrinolysis *(9, 10)* and endocrine function *(11)*.

In the present study, we sought to identify a simple method to prepare urine specimens for the analysis of small peptide components. Sample preparation represents one of the major challenges for analysis of peptide components in urine specimens by mass spectrometry. Ideally, sample preparation needs to accomplish three tasks: (*a*) concentration of relatively dilute peptide components; (*b*) removal of salts that suppress peptide ionization in mass spectrometry; and (*c*) depletion of albumin and other high-molecular-weight components that comprise most of the total protein mass in urine. Standard methods that have been applied for protein concentration—centrifugal ultrafiltration, acetone precipitation, acid precipitation, dye precipitation, ultracentrifugation, and lyophilization—generally have drawbacks of poor peptide recovery, poorly soluble pellets, or failure to remove salts *(6)*. We examined solid-phase extraction of urinary peptides, using a polymeric sorbent with a pore size that should exclude albumin and other proteins of similar or greater size.

Urine specimens were processed in 6-mL cartridges containing 500 mg of Strata^{TM}-X polymeric sorbent (Phenomenex) on a vacuum manifold. Pore size of the sorbent was specified by the manufacturer to be 91 Å, yielding a predicted size exclusion limit of ~20 000 Da. Cartridges were primed with 4 mL of methanol followed by 4 mL of 5 g/L acetic acid before addition of urine specimens, which had been acidified with acetic acid during collection to a pH of 4–5. After extraction of urine, cartridges were washed with 8 mL of 5 g/L acetic acid, and peptides were eluted with 3-mL steps of increasing acetonitrile concentration or with 600 mL/L acetonitrile–5 g/L acetic acid. Measurements of total protein and albumin to determine the amounts of proteins eluted from the cartridges were performed by standard methods (pyrogallol red and immunoturbidimetry, respectively) on a LX-20 analyzer (Beckman-Coulter). C-Peptide was measured by competitive immunoassay with an Immulite 2000 (Diagnostics Products Corp.). Eluates from extraction cartridges were analyzed either after evaporation under nitrogen to ~2 mL or directly.

Matrix-assisted laser desorption/ionization time-of-flight (MALDI TOF) mass spectrometry was performed with an Ultraflex TOF mass spectrometer (Bruker Daltonics) in a linear positive-ion mode. Specimens were applied manually to 384-position target plates as 1-μL aliquots between layers of matrix applied as 1-μL aliquots of 10 g/L sinapinic acid in 750 mL/L acetonitrile–250 mL/L water containing 10 g/L acetic acid. Data were summed for 300 laser pulses collected from 10 positions. Measurements of mass/charge (*m/z*) were by external calibration. Calibrators and sinapinic acid were purchased from Bruker Daltonics.

Solid-phase extraction of highly proteinuric urine (Table 1) served as good example of the size selectivity and binding capacity of the extraction cartridge. We loaded 10-mL aliquots of urine successively on a single cartridge and analyzed the eluates. The albumin concentrations of flow throughs were approximately the same as the initial

Table 1. Solid-phase extraction of peptides from grossly proteinuric urine.

	Eluate concentrations (% of initial concentrations)[a]		
	Protein, g/L	**Albumin, g/L**	**C-Peptide, μg/L**
Sequential additions			
10 mL of urine	13.5 (96%)	8.7 (99%)	0.55 (1%)
10 mL of urine	14.1 (101%)	9.0 (102%)	0.87 (2%)
10 mL of urine	13.9 (99%)	8.7 (99%)	0.62 (1%)
10 mL of urine	14.1 (101%)	9.0 (102%)	0.55 (1%)
10 mL of urine	13.8 (99%)	9.0 (102%)	<0.50 (<1%)
10 mL of 5 g/L acetic acid	0.59 (4%)	0.48 (5%)	<0.50 (<1%)
3 mL of 100 mL/L acetonitrile	0.39 (3%)	0.02 (0.2%)	0.59 (1%)
3 mL of 200 mL/L acetonitrile	0.85 (6%)	0.02 (0.2%)	6.6 (12%)
3 mL of 300 mL/L acetonitrile	3.6 (25%)	0.15 (2%)	662 (1180%)
3 mL of 400 mL/L acetonitrile	3.1 (22%)	0.23 (3%)	67 (120%)
3 mL of 500 mL/L acetonitrile	0.33 (2%)	0.02 (0.2%)	3.8 (7%)
3 mL of 600 mL/L acetonitrile	0.06 (0.4%)	0.002 (0.02%)	3.0 (5%)

[a] Unprocessed urine contained 14 000 mg/L total protein, 8800 mg/L albumin, and 56 μg/L C-peptide.

concentrations, indicating very low extraction of albumin. Elution of C-peptide, which has a mass of ~3000 Da, was monitored with a quantitative immunoassay. Flow through concentrations of C-peptide were ~1% of the initial concentration even after loading of 50 mL of the proteinuric specimen, providing evidence that the capacity of the cartridge was not reached even with this large specimen load. Stepwise elution of components bound to the column by increasing concentrations of acetonitrile yielded the largest amounts of C-peptide at 300 mL/L acetonitrile. The C-peptide concentration in the 300 mL/L acetonitrile eluate was ~10-fold higher than in the initial specimen, whereas the albumin concentration was 2% of the original. The amount of C-peptide was 78% of the original for the two eluates at 300 and 400 mL/L acetonitrile compared with only 0.3% for albumin. Analysis of the C-peptide concentrations obtained for seven different 50-mL urine specimens (ranging from normal to high protein) by single-step elution with 600 mL/L acetonitrile gave mean (SD) values that were 80 (20)% of the amounts loaded on the cartridges. In analyses of 15 aliquots of a single specimen containing 1010 mg/L albumin and 32.4 μg/L C-peptide, the amounts of albumin and C-peptide eluted by acetonitrile were 2.4 (0.3)% and 106 (7)%, respectively, of the amounts loaded on the cartridges.

The low binding capacity of the cartridge for albumin (~1 mg) probably results from steric exclusion of albumin from pores of the polymeric solid-phase adsorbent. Albumin, with a molecular mass of ~67 000 Da, is well above the expected size exclusion limit for pores of the adsorbent. Therefore, low-capacity binding of albumin occurs only on the external surface of the adsorbent, and albumin binding saturates without affecting binding of small peptide components such as C-peptide; the internal surface of pores represents the major surface area for capture of small peptide components.

Extraction of urine greatly improved the ability to detect peptide components by MALDI (Fig. 1). In the *m/z* range 1250–5000, few components were apparent in unprocessed urine, and signals were very weak (Fig. 1, top). Analysis of eluates at 400 mL/L acetonitrile showed several components for the proteinuric specimen analyzed in Table 1 (Fig. 1, middle) and for a urine with a protein concentration (70 mg/L) within normal limits (Fig. 1, bottom). The proteinuric specimen had a greater number of components and yielded stronger signals, indicating greater complexity and concentration of peptides. Components detected by mass spectrometry eluted at various acetonitrile concentrations. For the six fractions that were eluted with 100–600 mL/L acetonitrile, >100 different peaks were observed for the proteinuric specimen, and 25 peaks were detected in the specimen with a low protein concentration in the *m/z* range 1200–7000 (spectra not shown). It is likely that there are thousands of peptide components in urine and that the number observed is likely to depend on the sample preparation and the sensitivity and resolution of the method of analysis *(7)*.

Results of the present study suggest that solid-phase extraction of urine with a polymeric solid phase provides a simple method for extraction of peptides for analysis by mass spectrometry. Peptides were eluted in a salt-free solution containing acetonitrile that might be concentrated further by evaporation. Elution of the greatest number of components at moderate concentrations of acetonitrile (300–400 mL/L) suggests that it should be possible to elute most components off the solid phase. Previously, solid-phase extraction has been applied as a tool for preparation of peptide mixtures, such as tryptic digests of proteins, for MALDI TOF mass spectrometry *(12–14)*. A specialized variation of solid-phase extraction that has been termed surface-enhanced laser desorption/ionization (SELDI) directly extracts peptides onto the target surface for mass spectrometry *(15)*. Typically, solid-phase extraction of peptides has involved use of octadecylsilica as the adsorbent, although some reports note that recovery of hydrophilic peptides can be increased by use of graphite particles or a mixed bed of graphite and octadecylsilica *(12–14)*. Often, sample preparation for MALDI TOF mass spectrometry has been performed in pipette tips packed with tiny amounts of adsorbent. This format provides adequate specimen for MALDI TOF mass spectrometry but not enough for other, traditional clinical laboratory techniques. In addition, octadecylsilica or graphite adsorbents are likely to lack the size selectivity observed in the present experiment because of the larger pore sizes of common adsorbents.

Polymeric adsorbents have potential advantages with respect to capacity and suitability for large volumes of aqueous specimen *(12)*. High capacity is a desirable

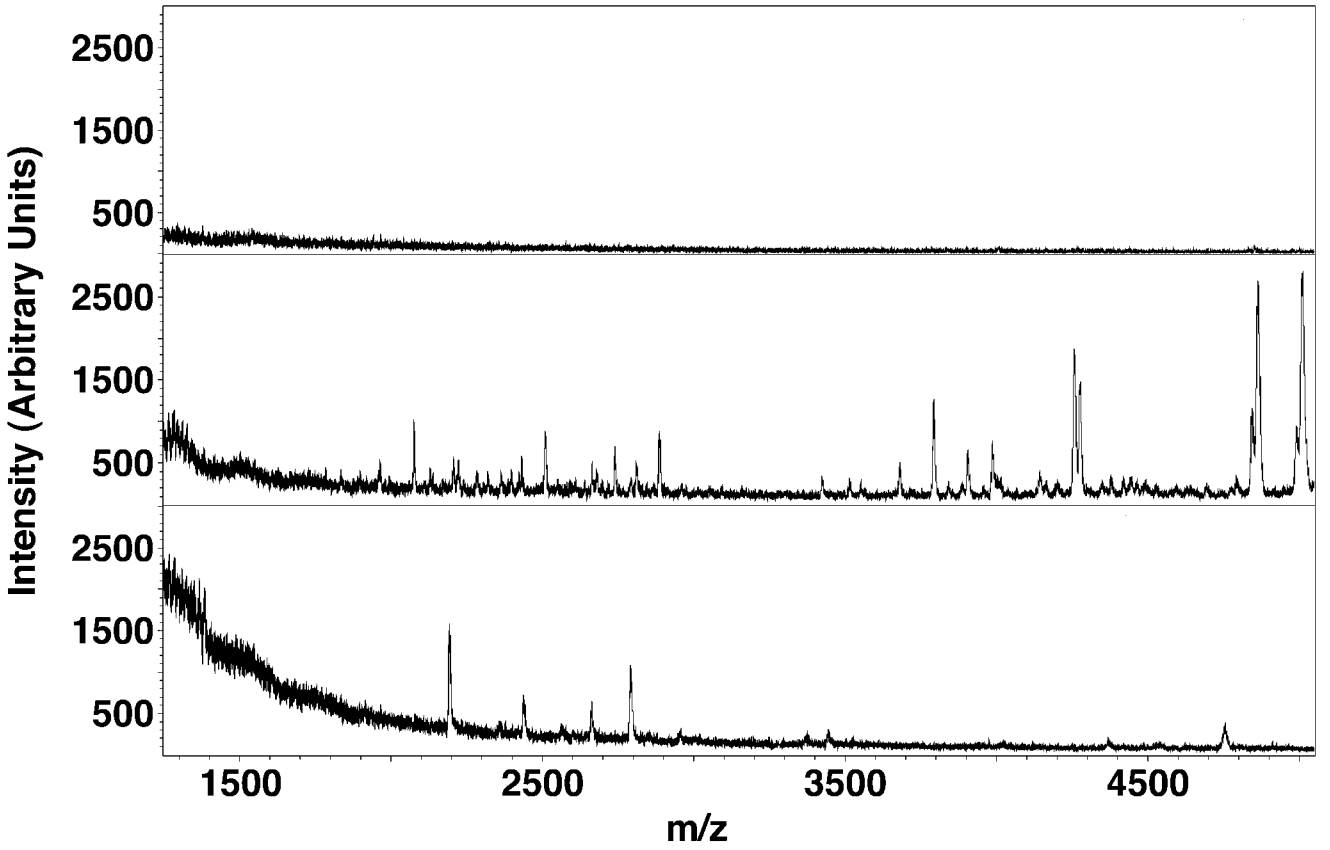

Fig. 1. Mass spectrograms of urine specimens relating signal intensity to *m/z* ratio.

(*Top*), unprocessed urine with high protein concentration (14 000 mg/L); (*middle*), eluate from solid-phase extraction of the proteinuric specimen; (*bottom*), eluate from solid-phase extraction of urine with normal protein concentration (70 mg/L).

characteristic in that it allows concentration of larger volumes of the relatively dilute peptide solutions in urine. The solid-phase extraction procedure described here permits the processing of substantial volumes of specimen and yields eluates of sufficient volume to combine mass spectrometric analysis with traditional clinical laboratory assays that can assess specimen recovery or measure components below the detection limits of mass spectrometry. Size-selective extraction of peptides may be of greatest value for fluids such as proteinuric urine or plasma, which contain high concentrations of albumin or other large proteins. For many diagnostic purposes, it may be useful to combine quantitative assays of specific components such as C-peptide with the high-resolution qualitative analysis provided by MALDI TOF mass spectrometry. The extraction technique here, which is directed at the concentration of peptide and small protein components (<20 000 Da), is complementary to the ultrafiltration techniques that are commonly used in clinical laboratories to concentrate proteins >10 000 Da in urine specimens. The size selectivity of the present extraction technique provides high enrichment of small peptide components such as C-peptide vs a protein such as albumin with a molecular mass of 67 000 Da. In the present study, we did not quantify the amounts of any proteins near the predicted size exclusion limit of ~20 000 Da. Retention of such components is likely to be affected by their molecular shape and to be intermediate in efficiency between small peptides such as C-peptide and proteins the size of albumin.

References

1. Beetham R, Cattell WR. Proteinuria: pathophysiology, significance and recommendations for measurement in clinical practice. Ann Clin Biochem 1993;30:425–34.
2. Kim MS. Proteinuria. Clin Lab Med 1988;8:527–40.
3. Glassock RJ. Proteinuria, In: SG Massry, RJ Glassock, eds. Massry & Glassock's textbook of nephrology, 4th ed. Philadelphia: Lippincott, 2001: 545–9.
4. Guder WG, Ivandic M, Hofmann W. Physiopathology of proteinuria and laboratory diagnostic strategy based on single protein analysis. Clin Chem Lab Med 1998;36:935–9.
5. Edwards JJ, Tollaksen SL, Anderson NG. Proteins of human urine. III. Identification and two-dimensional electrophoretic map positions of some major urinary proteins. Clin Chem 1982;28:941–8.
6. Thongboonkerd V, Klein E, Klein JB. Renal and urinary proteomics. In: Conn PM, ed. Handbook of proteomic methods. Totawa NJ: Humana Press, 2003:375–95.
7. Heine G, Raida M, Forssmann W-G. Mapping of peptides and protein fragments in human urine using liquid chromatography-mass spectrometry. J Chromatogr A 1997;776:117–24.
8. Hampel DJ, Sansome C, Sha M, Brodsky S, Lawson WE, Goligorsky MS. Toward proteomics in uroscopy: urinary protein profiles after radiocontrast administration. J Am Soc Nephrol 2001;12:1026–35.
9. Lind SE, Golshteyn S, Barry CP, Lindquist JR, Piergies AA, Rosen T, et al.

Assessment of coagulation system activation using spot urine measurements. Blood Coagul Fibrinolysis 1999;10:285–9.
10. Morris A, Marsh JJ, Burrows CM, Chiles PG, Konopka RG, Pedersen CA. Urine and plasma levels of fibrinopeptide B in patients with deep vein thrombosis and pulmonary embolism. Thromb Res 2003;110:159–65.
11. De Palo EF, Gatti R, Lancerin F, De Palo CB, Cappellin E, Solda G, et al. Effects of acute, heavy-resistance exercise on urinary peptide hormone excretion in humans. Clin Chem Lab Med 2003;41:1308–13.
12. Gilar M, Bouvier ESP, Compton BJ. Advances in sample preparation in electromigration, chromatographic and mass spectrometric separation methods. J Chromatogr A 2001;909:111–35.
13. Chin ET, Papac DI. The use of a porous graphitic carbon column for desalting hydrophilic peptides prior to matrix-assisted laser desorption/ionization time-of-flight mass spectrometry. Anal Biochem 1999;273:179–85.
14. Shukla AK, Shukla MM, Stover ED, Huhmer AF. Applications of mixed-mode solid-phase extraction (MMSPE) for proteomics sample preparation. Am Biotechnol Lab 2003;21:36–8.
15. Merchant M, Weinberger SR. Recent advancements in surface-enhanced laser desorption/ionization-time of flight-mass spectrometry. Electrophoresis 2000;21:1164–7.

DOI: 10.1373/clinchem.2003.030742

Haptoglobin Phenotypes in Epilepsy, *Sayed M.H. Sadrzadeh,* Yasi Saffari, and Jafar Bozorgmehr* (Department of Laboratory Medicine, University of Washington, Harborview Medical Center, Seattle, WA 98104; * author for correspondence: fax 206-731-3930, e-mail sadrzade@u.washington.edu)

Seizures occur in ~5% of people, and recur in >20% of that 5% *(1, 2)*. The etiologies of most seizures are unknown, and head trauma is implicated in only 5–10% of cases *(3)*. Blood or blood components, specifically iron, may be etiologically important; intracranial injection of hemoglobin *(4)*, lysed erythrocytes *(5)*, iron-containing proteins *(5)*, or iron salts *(6)* produced chronic focal spike activity in rodents and cats. Because microhemorrhagic events occur in the central nervous system of all people, inadequate clearance of iron-rich *(7)* hemoglobin might underlie development of some seizure disorders.

Haptoglobin binds free hemoglobin and removes it from the circulation *(8)*, thus preventing iron loss and kidney damage during hemolysis *(9)*. Haptoglobin contains β- (heavy; 40 kDa) and α- (light; α_1 = 8.9 kDa and α_2 = 16 kDa) chains. Humans are polymorphic for haptoglobin, with three major phenotypes: Hp 1-1, Hp 2-2, and the heterozygous Hp 2-1 *(10)*. The β-chains are identical in all, with variations dependent on different α-chains. Hp 1-1 expresses only the α_1-chain and is the smallest form (86 kDa). Hp 2-1 and Hp 2-2 express α_2-chains, which can form polymers of 86–300 kDa (Hp 2-1) and up to 900 kDa (Hp 2-2) *(10)*. Hp 1-1 is biologically the most effective in binding free hemoglobin and suppressing inflammatory responses associated with extracellular (free) hemoglobin *(9)*. In contrast, Hp 2-2 is the least effective *(11)*. The plasma concentrations of haptoglobin are highest in individuals with Hp 1-1 and lowest in those with Hp 2-2, with intermediate concentrations in Hp 2-1 individuals *(9)*.

Haptoglobin also has antioxidant *(12)*, angiogenic *(13)*, and antiinflammatory effects *(11, 14)*. Furthermore, haptoglobin has a role in regulation of immune responses *(15)* by suppressing release of cytotoxins from T-helper type 2 cells and regulating T-helper type 1/T-helper type 2 balance *(15)*.

If hemoglobin (or its iron) is involved in the etiology of seizures, then inadequate removal of hemoglobin (by haptoglobin) may be important. We postulated that functional differences between the haptoglobin phenotypes might be related to the severity and frequency of seizure attacks in patients with epilepsy. In this study, we investigated the serum concentrations of haptoglobin and the distribution of haptoglobin phenotypes in people with and without epilepsy and examined the relationship of haptoglobin phenotypes with C-reactive protein (CRP), which, like haptoglobin, is an acute-phase protein.

We studied 92 patients (59 men and 33 women), with a mean age of 43 (range, 21–87) years, who had one or more idiopathic seizures per month and who were treated at our medical center. Controls were 100 volunteers (62 men and 38 women), with a mean age of 44 years. No participants had intravascular hemolysis, liver disease, or trauma. The diagnosis of recurrent idiopathic epilepsy was based on clinical status and electroencephalography results. The study was approved by the local Institutional Review Board.

Phenotyping of haptoglobin was performed by gel electrophoresis followed by peroxidase staining *(16)*. Mobilities of haptoglobin in the samples were compared with authentic samples of Hp 1-1 and Hp 2-2 for phenotype identification. Concentrations of haptoglobin and CRP *(17)* were measured by fixed-time immunonephelometry with reagents and instrumentation from Dade Behring.

Data are presented as the mean (SE). We used the *t*-test with Welch's correction to assess significance of differences of means. Analysis of differences in haptoglobin phenotype distributions in patients and controls was done by χ^2 test.

Haptoglobin phenotype 2-2 was significantly associated with recurrent seizures ($P < 0.001$), being present in 67% of the patients and in only 35% of controls. Hp 2-1 and 1-1 were present in 18% and 13% of patients, respectively, and in 50% and 15% of controls. Haptoglobin was undetectable in two patients (2%). The distributions of haptoglobin types were in Hardy–Weinberg equilibrium. The association of Hp 2-2 with seizure attacks persisted when patients were compared with ethnically matched controls (Tables 1 and 2 in the Data Supplement that accompanies the online version of this Technical Brief at http://www.clinchem.org/content/vol50/issue6/; $P < 0.05$).

Haptoglobin concentrations were significantly higher ($P < 0.0001$) in patients [1.41 (0.08) g/L] than in controls [1.04 (0.04) g/L].

Serum haptoglobin concentrations in patients differed significantly from concentrations in controls when analyzed in relation to their phenotypes (Table 1).

Because haptoglobin is an acute-phase protein, we measured serum CRP in all participants. CRP was significantly higher in patients than in controls [10.1 (1.5) and 1.4 (0.3) mg/L, respectively; $P < 0.0001$]. Not only was pooled serum CRP significantly different in patients vs

Table 1. Serum haptoglobin and CRP concentrations according to haptoglobin phenotype in patients and controls.

Haptoglobin phenotype	Mean (SE) haptoglobin, g/L		Mean (SE) CRP, mg/L	
	Patients	Controls	Patients	Controls
Hp 2-2	1.31 (0.08)[a] (n = 62)	1.01 (0.09) (n = 35)	11.4 (2.1)[b] (n = 58)	2.38 (0.7) (n = 33)
Hp 2-1	1.62 (0.27)[c] (n = 11)	1.03 (0.05) (n = 50)	7.6 (1.9)[d] (n = 16)	0.93 (0.2) (n = 51)
Hp 1-1	1.71 (0.24)[e] (n = 12)	1.16 (0.1) (n = 15)	5.8 (2.1)[f] (n = 9)	0.6 (0.1) (n = 15)

[a–f] Compared with controls: [a] $P = 0.01$; [b] $P = 0.0001$, [c] $P = 0.02$; [d] $P = 0.0018$; [e] $P = 0.03$; [f] $P = 0.022$.

controls, but also in individual phenotypes (Table 1). In addition, we found statistically significant correlations between serum CRP and haptoglobin concentrations within each individual phenotype, that is, in the Hp 2-2, Hp 2-1, and Hp 1-1 groups individually ($r = 0.99$).

The role of iron and its oxidative capabilities in tissue damage is well documented *(18)*, and iron-containing proteins such as hemoglobin can initiate or enhance oxidative processes *(19)*. Increased accumulation of iron in the brain and defective antioxidant defenses have been linked to both Parkinson and Alzheimer diseases *(19)*. We previously showed that hypohaptoglobinemia was associated with high incidence and frequency of seizures in patients with idiopathic familial epilepsy *(20)*. Defective haptoglobin-mediated clearance of free hemoglobin from the central nervous system could lead to hemoglobin-dependent central nervous system damage.

The major hazard posed by iron-containing compounds is in facilitating the formation of reactive oxygen species *(21, 22)*. Hemoglobin, in the presence of a source of superoxide anions and hydrogen peroxide, can catalyze the formation of one or more reactive species resembling hydroxyl radicals *(22)*. Free hemoglobin also enhances the peroxidation of purified arachidonic acid and other polyunsaturated fatty acids within normal cell membranes *(23)*. Furthermore, purified hemoglobin or crude erythrocyte lysates, in the absence of superoxide anions or hydrogen peroxide, cause rapid peroxidation of crude murine brain homogenate *(24)*.

CRP is a marker for inflammatory processes, tissue damage, and infection *(25)*. The increase in CRP in our patients suggests that they suffered from inflammation in addition to their seizure disorders. Although we found a correlation between different haptoglobin phenotypes and serum CRP, we do not know whether there is a direct association between inflammation and the pathogenesis of seizure disorders. Haptoglobin is a marker for inflammation *(9)*, and it also was increased. We believe that identification of haptoglobin phenotypes in addition to analysis of serum haptoglobin concentrations may better identify the presence of inflammation: a Hp 2-2 phenotype may indicate the presence of an inflammatory process because Hp 2-2 is more associated with inflammation than Hp 2-1 or Hp 1-1. Indeed, Hp 2-2 type has been associated with several clinical conditions, such as atherosclerosis, cancer, infection, and neurologic disorders *(11, 26)*. In addition, Hp 2-2 complexed with free hemoglobin has a high affinity for CD 163 receptors on macrophages *(27)*. Furthermore, it has been suggested that the uptake and internalization of haptoglobin–hemoglobin complex by macrophages leads to increased oxidative stress in macrophages and, more importantly, delocalization of iron *(28)*, which can further enhance oxidative stress via generation of reactive oxygen species. Although one report denies the enhanced oxidative stress in macrophages after internalization of haptoglobin–hemoglobin complex *(29)*, most of the data in this field support the association of Hp 2-2 and inflammatory processes, and most pathologic conditions (cancer, atherosclerosis, and neurologic disorders) associated with Hp 2-2 are associated with inflammation.

In aggregate, our data clearly show an association of Hp 2-2 with the presence of seizures in patients with epilepsy. At present we do not know the mechanism for this phenomenon. We hypothesize that a defective clearing system (such as Hp 2-2), which cannot effectively remove free hemoglobin after microhemorrhagic events in the central nervous system, leads to iron accumulation and increased oxidative stress in tissue. Therefore, enhanced oxidative stress with minimum antioxidant defense can lead to tissue injury and inflammation, which may have a role in the etiology of seizure attacks in this patient population. More work is needed for better understanding of the role of haptoglobin in the pathophysiology of epilepsy.

References

1. Brodie MJ, Dichter MA. Antiepileptic drugs. N Engl J Med 1996;334:168–75.
2. Brodie MJ, Shorvon SD, Canger R, Halasz P, Johannessen S, Thompson P, et al. Commission on European Affairs: appropriate standards of epilepsy care across Europe: ILEA. Epilepsia 1997;38:1245–50.
3. Loiseau P, Jallon p. Post-traumatic epilepsy. Prog Neurol Surg 1981;10: 323–8.
4. Rosen AD, Frumin NV. Focal epileptogenesis after intracortical hemoglobin injection. Exp Neurol 1979;66:277–84.
5. Hammond EJ, Ramsay RE, Villarreal HJ, Wilder BJ. Effects of intracortical injection of blood and blood component in the electrocorticogram. Epilepsia 1980;21:3–14.
6. Willmore LJ, Sypert GW, Munson J. Chronic focal epileptiform discharges induced by injection of iron into rat and cat cortex. Science 1978;200: 1501–3.
7. FairbanksV, Beutler E. Iron metabolism. In: Beutler E, ed. Hematology, 6th ed. New York: McGraw-Hill 2000:295–305.
8. Wassell J. Haptoglobin: function and polymorphism. Clin Lab 2000;46:547–52.
9. Javid J. Human haptoglobins. Curr Top Hematol 1978;1:151–92.
10. Black JA, Dixon GH. Amino-acid sequence of α chains of human haptoglobins. Nature 1968;218:738–41.
11. Langlois MR, Delanghe JR. Biological and clinical significance of haptoglobin polymorphism in humans. Clin Chem 1996;42:1589–600.
12. Gutteridge JM. The antioxidant activity of haptoglobin towards haemoglobin-stimulated lipid peroxidation. Biochim Biophys Acta 1987;917:219–23.
13. Cid MC, Grant DS, Hoffman GS, Auerbach R, Fauci AS, Kleinman HK. Identification of haptoglobin as an angiogenic factor in sera from patients with systemic vasculitis. J Clin Invest 1993;91:977–85.
14. Bowman BH. Haptoglobin. In: Bowman BH, ed. Hepatic plasma proteins. San Diego: Academic Press, 1993:159–67.
15. Arredouani M, Matthijs P, Van Hoeyveld E, Kasran A, Baumann H, Ceuppens JL, et al. Haptoglobin directly affects T cells and suppresses T helper cell type 2 cytokine release. Immunology 2003;108:144–51.

16. Smithies O. Zone electrophoresis in starch gels: group variations in the serum proteins of normal adults. Biochem J 1955;61:629–41.
17. Ledue TB, Weiner DL, Sipe J, Poulin SE, Collins MF, Rifai N. Analytical evaluation of particle-enhanced immunonephelometric assays for C-reactive protein, serum amyloid A, and mannose binding protein in human serum. Ann Clin Biochem 1998;35:745–53.
18. Thompson KJ, Shoham S, Connor JR. Iron and neurodegenerative disorders. Brain Res Bull 2001;55:155–64.
19. Sadrzadeh SM, Graf E, Panter SS, Hallaway PE, Eaton JW. Hemoglobin. A biologic Fenton reagent. J Biol Chem 1984;259:14354–6.
20. Panter SS, Sadrzadeh SM, Hallaway PE, Haines JL, Anderson VE, Eaton JW. Hypohaptoglobinemia associated with familial epilepsy. J Exp Med 1985; 161:748–54.
21. Repine JE, Eaton JW, Anders MW, Hoidal JR, Fox RB. Generation of hydroxyl radical by enzymes, chemicals and human phagocytes in vitro: detection using the anti-inflammatory agent, dimethyl sulfoxide (DMSO). J Clin Invest 1979;64:1642–51.
22. Rosen H, Klebanoff SJ. Role of iron and ethylenediaminetetraacetic acid in the bactericidal activity of a superoxide anion-generating system. Arch Biochem Biophys 1979;208:512–9.
23. Sadrzadeh SM, Eaton JW. Hemoglobin-mediated oxidant damage to the central nervous system requires endogenous ascorbate. J Clin Invest 1988;82:1510–5.
24. Sadrzadeh SMH, Anderson DK, Panter SS, Hallaway PE, Eaton JW. Hemoglobin potentiates central nervous system damage. J Clin Invest 1987;79: 662–4.
25. Gabray C, Kushner I. Acute phase proteins and other systemic responses to inflammation [Erratum in: N Engl J Med 1999;340:1376]. N Engl J Med 1999;340:448–54.
26. Langlois MR, Martin ME, Boelaert JR, Beaumont C, Taes YE, De Buyzere ML, et al. Haptoglobin phenotype 2–2 overrepresentation in Cys282Tyr hemochromatotic patients. J Hepatol 2001;35:707–11.
27. Kristiansen M, Graversen JH, Jacobsen C, Sonne O, Hoffman HJ, Law SK, et al. Identification of the haemoglobin scavenger receptor. Nature 2001;409: 198–201.
28. Roguin A, Ribichini F, Ferrero V, Matullo G, Herer P, Wijns W, et al. Haptoglobin phenotype and the risk of restenosis after coronary artery stent implantation. Am J Cardiol 2002;89:806–10.
29. Raley MJ, Loegering DJ. Role of an oxidative stress in the macrophage dysfunction caused by erythrophagocytosis. Free Radic Biol Med 1999;27:1455–64.

DOI: 10.1373/clinchem.2003.028001

Pitfall in HPLC Assay for Urinary Metanephrines: An Unusual Type of Interference Caused by Methenamine Intake, *Hanneke W.M. van Laarhoven,[1*] Jacques J. Willemsen,[2] H. Alec Ross,[2,3] Louk V.A.M. Beex,[1] Jacques W.M. Lenders,[4] and Fred C.G.J. Sweep*[2] (Departments of [1] Medical Oncology, [2] Chemical Endocrinology, [3] Endocrinology, and [4] General Internal Medicine, University Medical Centre Nijmegen, Nijmegen, The Netherlands; * address correspondence to this author at: University Medical Centre Nijmegen, Department of Medical Oncology, PO Box 9101, 6500 HB Nijmegen, The Netherlands; fax 31-24-354-0788, e-mail h.vanlaarhoven@onco.umcn.nl)

Evaluation of a clinically inapparent adrenal mass led to tests for pheochromocytoma *(1)* with findings of increased urinary metanephrine and normetanephrine but normal plasma metanephrines and catecholamines.

A 45-year-old woman presented with pulmonary embolism and thrombosis of the left arm. Her recent medical history included removal of the right breast because of cancer with postoperative locoregional radiotherapy and chemotherapy. She had a known spina bifida and an urostoma. She took pyridoxine, oxazepam, methenamine, paracetamol, furosemide, and tamoxifen on a regular basis. On physical examination she had a normal blood pressure, no Cushing signs, and no evidence of tumor recurrence.

After treatment with fractionated heparin and acenocoumarol the patient was further evaluated for the presence of tumor recurrence or distant metastases as an explanation for her thromboembolism. Mammography showed no signs of malignancy. The computed tomography (CT) scan of the thorax showed a pulmonary embolism but no evidence of metastases. The abdominal CT scan revealed a 2.5-cm hypodense mass in the right adrenal gland, most likely an adenoma. Because the differential diagnosis of adrenal masses with low attenuation on CT includes functional tumors, especially pheochromocytoma *(2)*, the functionality of the adrenal mass was determined.

Cortisol was 0.09 and 0.07 μmol/L after a repeated 1-mg dexamethasone suppression test. The 24-h urinary excretion of cortisol was 37.9 nmol, which made the presence of glucocorticoid excess unlikely. Serum potassium was within reference values, and renin and aldosterone were not increased, which together with the normal blood pressure excluded primary aldosteronism. Urinary excretion of metanephrines, measured as described previously *(3)*, was increased on repeated occasions [normetanephrine (NMN), 36 450 nmol/24 h (reference values <2900 nmol/24 h); metanephrine (MN), 10 256 nmol/24 h (reference values <1000 nmol/24 h)], suggesting the presence of a pheochromocytoma. However, both fractionated plasma-free metanephrines, which may be preferred for the diagnosis of pheochromocytoma in high-risk patients *(4)*, and plasma catecholamines were not clearly increased [NMN, 312 pmol/L (reference values <600 pmol/L); MN, 264 pmol/L (reference values <300 pmol/L); adrenaline, 0.04 nmol/L (reference values <0.3 nmol/L); noradrenaline, 2.84 nmol/L (reference values <3.0 nmol/L)]. Because of the patient's impaired mobility and anxiety, no metaiodobenzylguanidine scan was performed.

Close inspection of the urinary chromatograms of this patient revealed, in addition to an extra peak at an unusual location, a striking decrease (10- to 15-fold) in the internal standard (4-*O*-methyltyramine) peak compared with urinary chromatograms of other patients. In contrast, the heights of the MN and NMN peaks were in the usual range. Because calculation of the concentrations of MN and NMN was based on the internal standard principle, in which a constant ratio between recoveries of the analytes to be measured and the internal standard is assumed for processed samples and calibrators *(3)*, very high estimates of MN and NMN resulted. Thus, either the recovery of MN and NMN followed that of the internal standard, meaning that the high result was correct, or the internal standard principle did not hold in this urine sample and underestimation of the procedural recovery, rather than increased MN and NMN concentrations, was responsible for the strongly increased MN and NMN values calculated from the chromatography data.

We hypothesized that interaction of a substance with the internal standard decreased the signal for the internal standard and that this substance might originate from the patient's medications. To test this hypothesis the drugs used by the patient were dissolved in the same medium that was used for addition of the internal standard (0.1 mol/L HCl) and added to the urine of a healthy person. The quantities added to the urine sample corresponded to 200%, except for methenamine (100%), of the patient's daily intake of furosemide (40 mg/day), acenocoumarol (2–3 mg/day), pyridoxine (20 mg/day), tamoxifen (20 mg/day), oxazepam (10 mg/day), and methenamine (3 g/day), distributed in a 24-h portion of urine, assuming complete clearance by the urine.

The resulting chromatograms are shown in Fig. 1A. We observed a decrease in the peak for the internal standard (Fig. 1A, peak IS) and the concomitant appearance of an extra, large peak (Fig. 1A, peak X) only in the portion of urine to which methenamine had been added. The other chromatograms were identical in all respects. The patient was asked to stop taking methenamine for a 2-week period. As shown in Fig. 1B, 2 weeks after she stopped methenamine intake, there was no evidence of an extra peak X, and the internal standard peak had resumed its expected height. Moreover, the MN and NMN peaks retained their previous heights. This virtually rules out high procedural losses of MN, NMN, and the internal standard as underlying these results, although the urine samples necessarily were obtained on different occasions.

These findings indicate that methenamine is responsible for the lowered signal for the internal standard, leading to false-positive values for urinary fractionated

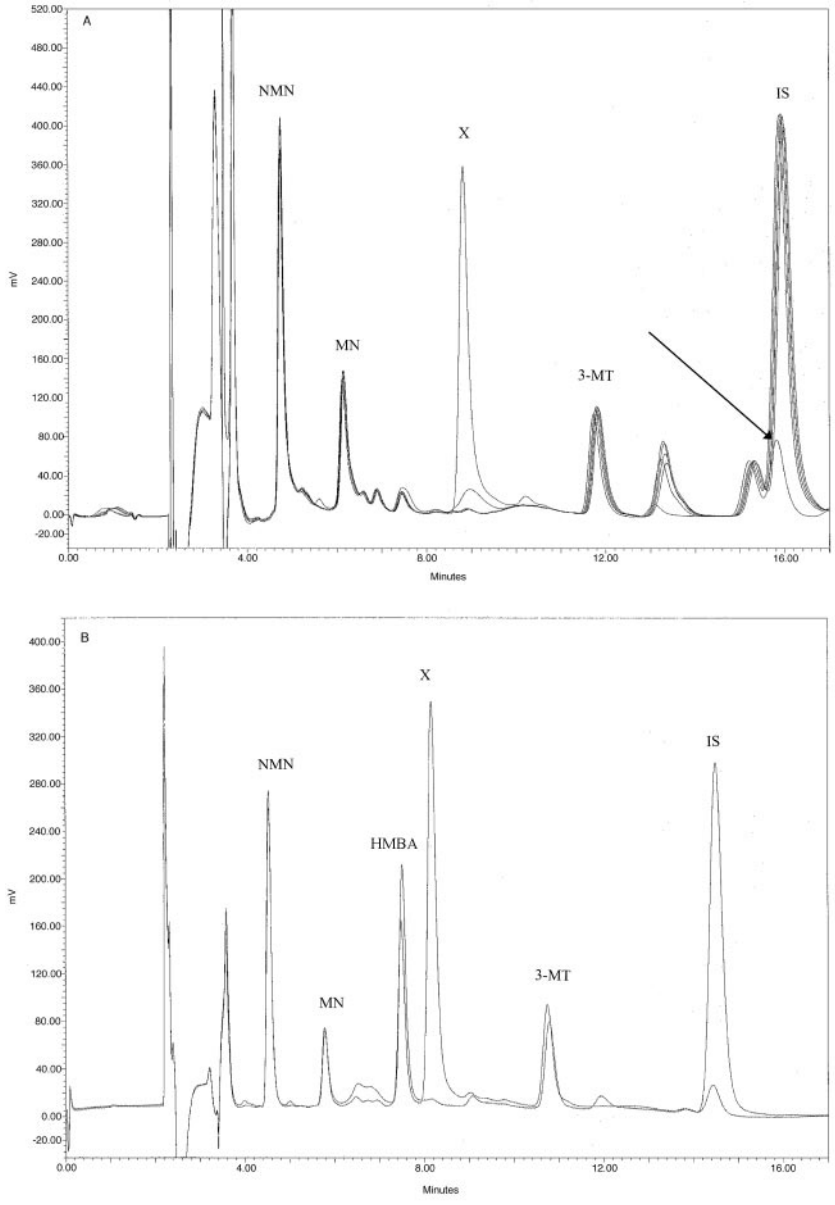

Fig. 1. Chromatograms of urine from a healthy person to which the patient's medications had been added (*A*) and the patient's urine before and after stopping methenamine (*B*).

(*A*), pyridoxine, oxazepam, methenamine, furosemide, tamoxifen, and acenocoumarol dissolved in HCl (0.1 mol/L) were added separately to the urine. The decrease in the signal for the internal standard (*IS*) after addition of methenamine is indicated by the *arrow*. The extra peak is indicated with an *X*. *3-MT*, 3-methoxytyramine. (*B*) the chromatograms are for samples taken before and 2 weeks after stopping methenamine. Two weeks after stopping methenamine, the patient's urine had no evidence of an extra peak X, and the internal standard was increased to expected values.

metanephrines. Methenamine interferes with the determination of estriol in urine when an acid hydrolysis technique is used *(5)*. However, to our knowledge, interaction with 4-*O*-methyltyramine has not been reported previously. Apart from withdrawal of methenamine medication, the use of an alternative internal standard to reliably assess urinary metanephrines in the presence of methenamine could be considered. Hydroxymethoxybenzylamine (HMBA) could be used in patients on methenamine, although methenamine affects the HMBA peak as well, but to a much lesser extent (Fig. 1B). Because small peaks are observed occasionally coeluting with HMBA (Fig. 1A), we do not recommend the use of HMBA as an internal standard.

The frequency of misleading results for urinary metanephrines may be appreciable because methenamine (Urimax, Urised, Hiprex, Uroquid-acid) is commonly used in the prevention and treatment of urinary tract infections (especially in patients with a urinary catheter or neurogenic bladder) and 4-*O*-methyltyramine is one of the reagents supplied by Bio-Rad for the assay of urinary metanephrines (UMET by HPLC). This problem is independent of whether the calibrators from this assay are used. Especially in patients who are on methenamine treatment, the diagnosis of pheochromocytoma should be considered only after repeated increased urinary fractionated metanephrines on measurement with different internal standards or after the patient has stopped taking methenamine. The diagnosis should be supported by other laboratory results (fractionated plasma free metanephrines and/or catecholamines in plasma or urine) and ultimately confirmed by histology. More generally, in cases in which lower recovery of the internal standard leads to increased values for urinary metanephrines, analysts should be aware of the possibility of unexpected interactions such as the one described.

References

1. Grumbach MM, Biller BM, Braunstein GD, Campbell KK, Carney JA, Godley PA, et al. Management of the clinically inapparent adrenal mass ("incidentaloma"). Ann Intern Med 2003;138:424–9.
2. Blake MA, Krishnamoorthy SK, Boland GW, Sweeney AT, Pitman MB, Harisinghani M, et al. Low-density pheochromocytoma on CT: a mimicker of adrenal adenoma. Am J Roentgenol 2003;181:1663–8.
3. Willemsen JJ, Ross HA, Wolthers BG, Sweep CG, Kema IP. Evaluation of specific high-performance liquid-chromatographic determinations of urinary metanephrine and normetanephrine by comparison with isotope dilution mass spectrometry. Ann Clin Biochem 2001;38(Pt 6):722–30.
4. Lenders JW, Pacak K, Walther MM, Linehan WM, Mannelli M, Friberg P, et al. Biochemical diagnosis of pheochromocytoma: which test is best? JAMA 2002;287:1427–34.
5. Touchstone JC, Stojkewycz M, Smith K. The effect of methenamine mandelate (mandelamine) on determination of urinary estriol. Clin Chem 1965; 11:1019–22.

DOI: 10.1373/clinchem.2004.032912